2012

Experimental study on the support stiffness effect on the performance of an external linear viscous damper

Jennifer Anne Fournier
University of Windsor

EXPERIMENTAL STUDY ON THE SUPPORT STIFFNESS EFFECT ON THE PERFORMANCE OF AN EXTERNAL LINEAR VISCOUS DAMPER

By

Jennifer Anne Fournier

A Thesis
Submitted to the Faculty of Graduate Studies
through the Department of Civil and Environmental Engineering
in Partial Fulfillment of the Requirements for
the Degree of Master of Applied Science at the
University of Windsor

Windsor, Ontario, Canada

Library and Archives Canada

Published Heritage Branch

395 Wellington Street
Ottawa ON K1A 0N4
Canada

Bibliothèque et Archives Canada

Direction du Patrimoine de l'édition

395, rue Wellington
Ottawa ON K1A 0N4
Canada

Your file Votre référence
ISBN: 978-0-494-88942-8

Our file Notre référence
ISBN: 978-0-494-88942-8

Experimental Study on the Support Stiffness Effect on the Performance of an External Linear Viscous Damper

By

Jennifer Anne Fournier

APPROVED BY:

Dr. N. Zamani (Outside Department Reader)
Mechanical Automotive & Materials Engineering

Dr. B. Budkowska (Department Reader)
Department of Civil and Environmental Engineering

Dr. S. Cheng (Advisor)
Department of Civil and Environmental Engineering

Dr. A. El Ragaby (Chair of Defense)
Department of Civil and Environmental Engineering

05 September 2012

Author's Declaration of Originality

I hereby certify that I am the sole author of this thesis and that no part of this thesis has been published or submitted for publication.

I certify that, to the best of my knowledge, my thesis does not infringe upon anyone's copyright nor violate any proprietary rights and that any ideas, techniques, quotations, or any other material from the work of other people included in my thesis, published or otherwise, are fully acknowledged in accordance with the standard referencing practice. Furthermore, to the extent that I have included copyrighted material that surpasses the bounds of fair dealing within the meaning of the Canada Copyright Act, I certify that I have obtained a written permission from the copyright owner(s) to include such material(s) in my thesis and have included copies of such copyright clearances to my appendix.

I declare that this is a true copy of my thesis, including any final revisions, as approved by my thesis committee and the Graduate Studies office, and that this thesis has not been submitted to any other University of Institution.

Abstract

An experimental study and a finite element analysis is conducted on a cable-damper system to study the individual and combined effects of damper stiffness and damper support stiffness on controlling stay cable vibrations. For the studied ranges of damper stiffness and damper support stiffness, the optimum damper coefficient is found to be shifted up to 22% and the modal damping ratio varies by as much as 23%. Results show that the optimum damper size increases as the damper stiffness and the damper support stiffness increase. Though the corresponding maximum attainable modal damping ratio also increases with more rigid damper support stiffness, it was found to be lower if damper stiffness increases. Approximate relations between the optimum damper size and the damper location, damper stiffness, damper support stiffness, as well as the corresponding maximum attainable modal damping ratio with these three system parameters are proposed.

Acknowledgements

I would like to thank my advisor, Dr. Shaohong Cheng, for her guidance through the entire process of creating this study and writing this thesis. It was a pleasure to learn from her and, as a result, I have greatly broadened my knowledge of structural dynamics and technical writing. I would also like to thank my thesis committee, Dr. B. Budkowska and Dr. N. Zamani for their efforts in reviewing and improving my work with their helpful insights. Lastly, I would like to thank laboratory technologists Mr. Matthew St. Louis, Mr. Lucian Pop, and Mr. Patrick Seguin for their excellent help and suggestions with the current experimental study, and computer systems administrator Mr. Mark Gryn for his help with the current numerical study.

Table of Contents

List of Figures

List of Tables

Chapter 1: Introduction

1.1 Background

Cable-stayed bridges are commonly used in civil infrastructure. Their economic design, utility, and pleasing aesthetics have led to their use over unprecedented span lengths. The main span of Sutong Bridge in China, for example, is over a kilometer long and is currently the longest in the world. As bridge spans increase, so must their stay cables, which loose rigidity with length. The longest cable on the Sutong Bridge has a length of 580 meters. Due to their low inherent damping, which is often less than 1%, and low natural frequencies, stay cables are particularly sensitive to excitations by various dynamic sources. Violent, large amplitude vibrations of stay cables have been observed on bridge sites, and are of concern both for the healthy maintenance of the structure and for the bridge users. Excessive cable vibrations may result in fatigue failure at the cable-deck or cable-tower connections and/or the deterioration of the cable corrosion mechanism. The source of stay cable vibration is an area of study that is important to ensure the safety of the bridge. To date, a number of vibration mechanisms have been identified as potentially harmful to bridge stay cables. The primary sources of vibration are from rain-wind-induced vibration, vortex-induced oscillation, high-speed vortex excitation, wake galloping, galloping of dry-inclined cables, and parametric excitation.

1.2 Types of cable excitation

Rain-wind-induced vibrations occur during periods of moderate wind and rain within a low frequency range of 1-3Hz. The amplitude of cable oscillations could reach ~ 0.25 – 1 meter and have resulted in cables hitting each other in some extreme cases. An early observation of this phenomenon was during the construction of the Meiko-Nishi

Bridge in Japan (Hikami and Shiraishi, 1988). Experimental and analytical studies as well as field monitoring programs were carried out to study the mechanisms associated with this phenomenon (Flamand, 1995; Main and Jones, 2001; Kumarasena et al., 2007; Ni et al., 2007; Taylor and Robertson, 2010; Wang and Hou, 2011). The circular cross-section of the cable is altered with respect to oncoming wind when rain water droplets rest on the cable. This results in an unstable aerodynamic force acting on the cable and, when the droplet oscillates at the natural frequency of the cable, the cable resonates and exhibits large vibrations.

Vortex-induced vibration occurs when wind is acting in the direction perpendicular to the axis of the cable. Kármán vortices shed alternatively from either side of the cable, generating an oscillating force perpendicular to the direction of the wind (towards the cable) which induces cable vibration. If this force oscillates at a frequency near the natural frequency of the cable, resonance occurs which leads to large amplitudes of cable motion. Vortex shedding can be "locked-in" to a resonant frequency for a period when excitation wind speeds have been exceeded. These vibrations generally occur at low wind speeds and have a vibration amplitude response of approximately one cable diameter (Kumarasena et al., 2007; Zuo et al, 2008).

High-speed vortex excitation has not yet been fully understood. This type of vibration is thought to result from the contribution of several modal frequencies and the interaction between Kármán vortex shedding and axial vortex shedding. This vibration has been observed to occur at higher frequencies than Kármán vortex excitation in a narrow high reduced wind speed range and has a limited amplitude (Matsumoto et al., 2001; Cheng et al., 2008a).

Wake galloping generally occurs when cables are in the wake of other structural elements such as other cables, bridge towers, and nearby buildings. When cables move in and out of a wake, they experience a change in the speed of wind and increased turbulence and they may begin to oscillate. If this oscillation frequency nears the natural frequency of the cable, resonance will occur. Wake galloping may be most easily avoided by installing cables in a properly spaced configuration so they will not be influenced by each other's wakes, as well as minimizing wakes generated from nearby construction (Kumarasena et al., 2007).

Galloping of dry inclined cables occurs in the critical Reynolds number range and has only been observed experimentally; there are no confirmed cases from the field to date. In the lab, vibration was observed when the angle between the cable axis and the wind was 60° or between 75° - 90°. It was found that the mechanism of this type of vibration can be explained by the Den Hartog criterion, but its full mechanism is still not clearly understood (Cheng et al., 2008b).

Parametric excitation occurs when bridge stay cables are forced to vibrate as a result of the motion of the bridge tower or bridge deck. Traffic live load, ground motion (earthquake), and wind are some examples of what may cause the bridge superstructure to move. This movement causes stay cable anchorage points to displace vertically (deck anchorage) or horizontally (tower anchorage), causing a fluctuation in the tension experienced within the cable. The ratio of the excitation frequency to the cable natural frequency often observed to yield large amplitude responses from parametric excitation is 2 (Hou and Wang, 2011).

1.3 Vibration mitigation techniques

To suppress unfavorable cable motions, various vibration controlling means have been proposed. They can be generally categorized as aerodynamic type and mechanical type.

The alteration of the cable casing surface has proven to be an effective measure in controlling both rain-wind-induced vibration as well as vortex-induced vibration. This vibration mitigation method is classified as an "aerodynamic" type because the surface treatments would change the aerodynamic forces that induce the cable to vibrate. The surface treatment could prevent the formation of water rivulet on the cable surface and disturb the formation and shedding of the Kármán vortices. Surface modification patterns were tested in wind tunnel studies to investigate their effectiveness. A commonly used protrusion pattern is the helical spiral, shown on the top cable in Figure 1-1, along with two other patterns that have been tested (Yeo and Jones, 2011). The U.S. Grant Bridge in Ohio, USA, uses the helical spiral type of surface protrusion. Modification of the base cylindrical cross-section of the cable casing, as shown in Figure 1-2, is a very recent area of research that is currently being tested in wind tunnels (Kleissl and Georgakis, 2011).

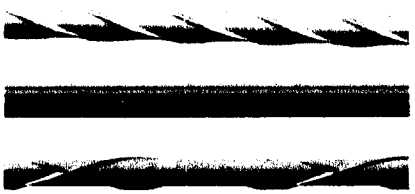

Figure 1-1: Cable casing surface protrusions (Yeo and Jones, 2011)

Figure 1-2: Cable casing cross-section alterations (Kleissl and Georgakis, 2011)

The mechanical type of vibration control includes the use of cross-ties, which would increase the in-plane stiffness and thus the natural frequency of cables; and external dampers, which would directly increase damping in the cable.

Cross-ties are transverse cable connectors that connect several stay cables together to increase the overall stiffness and damping of the entire cable network. The points of tie connection limit the motion of the stays, decreasing their effective length and increasing cable in-plane stiffness, which tends to increase the natural frequencies of the cables. Environmental cable excitation is generally most critical in the lower modes of vibration. Increased cable natural frequencies help to avoid increased dynamic response at resonance in these critical lower modes. Both experimental and numerical work (e.g. Yamaguchi and Nagahawatta, 1995; He et al., 2010; Caracoglia and Jones, 2005) have shown that flexible cross-ties are more effective than their stiff counterparts because flexibility allows for energy dissipation within the cross-ties, and that some prestress should be applied to the cross-ties when they are installed. However, segmenting the cable with the ties tends to generate intense local vibrations that are not desirable. This method of vibration mitigation has been successfully used on several bridges, for example, the Fred Hartman Bridge in Texas, USA (Caracoglia and Jones, 2005), and the Dames Point Bridge in Jacksonville, Florida, USA (Kumarasena et al., 2007).

Many external type mechanical dampers have been used in the field such as the friction damper (Myrvoll et al., 2002), high damping rubber dampers (Nakamura et al., 1998), tuned-mass dampers (Cai et al., 2006), magnetorheological (MR) dampers (Christenson and Spencer, 2001), and viscous dampers (Main and Jones, 2001). MR dampers generate resistance to control cable motion through the alignment of magnetic

particles in the damper in the direction parallel to an applied magnetic field. They have been explored primarily through semi-active control (Johnson et al., 2007), and passive control (Cho et al., 2005). A newly proposed method of vibration contol changes the boundary condition of the classic cable system: one end of the cable is no longer fixed. The support is flexible and has both stiffness and damping in the direction of cable vibration, which may reduce vibration displacement more effectively than a passive damper (Hwang et al., 2009). Viscous dampers are the most commonly used mechanical type. They are being used on the Fred Hartman Bridge in the USA, the Brotonne Bridge in France, and the Aratsu Bridge in Japan. Design tools have been proposed and developed for their application (e.g. Pacheco et al., 1993; Tabatabai and Mehrabi, 2000; Cheng et al, 2010). Improvements to the classic viscous damper have been attempted recently with adjustable fluid dampers (Xu and Zhou, 2007). They use shape memory alloy to optimize the damper performance.

Often overlooked, however, is the effect of damper and damper support stiffness in the viscous damper design. Practical design tools must include these parameters in order to predict accurately the additional damping from the damper. Without considering these factors, damping may be overestimated in design and cables in the field may not receive adequate damping as expected, which may leave the bridge structure vulnerable to dynamic excitation.

1.4 Motivations

The accurate prediction of the additional damping a viscous damper can provide for a stay cable is imperative to an efficient damper design. There is a lack of research that has been done on the effect of damper stiffness and damper support stiffness on the

performance of a viscous damper, and their combined effect has rarely been investigated. The very few existing studies which explored this issue indicated that both damper and damper support stiffness would have a sizeable effect on the accurate prediction of the system damping ratio.

The lack of study in the area of how damper stiffness and damper support stiffness would affect damper efficiency was the motivation for the current work, which included the construction of an experimental study and a finite element analysis of the dynamic behaviour of a cable-damper system while including damper and damper support stiffness properties. The impacts of these two parameters on the damper performance were investigated separately as well as in combination. This study has not only confirmed the trends currently documented, but it has extended their practicality to the actual damper design by proposing approximations for the optimum damper size and its corresponding maximum equivalent first modal damping ratio.

1.5 Objectives

The objectives of this study were thus proposed to be:

1. Design a linear viscous damper that allows for adjustable damper stiffness and support stiffness.
2. Design the calibration system for the damper.
3. Conduct cable forced vibration tests to observe the following:
    a. the effect of damper support stiffness on cable damping ratio
    b. the combined effect of damper stiffness and damper support stiffness on cable damping ratio

4. Develop a finite element model of the cable-damper system including damper stiffness and damper support stiffness. The model was developed using the ANSYS commercial software. The energy-based method proposed by Cheng et al. (2010) was used to calculate the damping ratio of the system.
5. Compare experimental and numerical results, as well as those reported in the literature.
6. Develop approximate expressions for the optimum damper size and its corresponding maximum attainable equivalent first modal damping ratio to be used in practical damper design in order to account for the influence of damper stiffness and damper support stiffness effects on its performance.

Chapter 2: Literature Review

A common simplification in the analysis of a cable-damper system has been to idealize the cable as a taut string. Therefore, cable sag (inclination) and bending stiffness are neglected. This assumption has often been used in analytical studies, such as those that use complex eigenvalue analysis to estimate the additional damping expected in different modes of vibration from a linear viscous damper.

Kovacs (1982) identified the existence of an optimum viscous damping coefficient using the semi-empirical approach and developed an analytical equation estimating its value, based on the two extremes of cable damping: no damping and a damper with infinite damping capacity, which will act as a rigid support. This research analyzed only the first mode of cable vibration, although it has the potential of being extended to higher modes.

A universal damping estimation curve was subsequently developed by Pacheco et al. (1993), also based on eigenvalue analysis using the taut cable assumption. This curve, shown in Figure 2-1, can be used for a practical range of stay cables and linear viscous dampers, and it assesses the optimal size and location of a damper needed for controlling cable vibration in a specific mode in which the maximum amount of additional damping must be provided. In addition, this curve can further estimate the additional damping to be had in other modes based on the initial damper design developed from the curve. Modal damping ratio is plotted on the y-axis and the non-dimensional damper coefficient is potted on the x-axis, where ξ_i is the modal damping ratio in the i^{th} mode of vibration, x_c is the location of the damper, L is the span length of the cable, c is the damper coefficient,

m is the mass per unit length of the cable, ω_{01} is the fundamental natural frequency of the cable, and i is the mode number. This curve can be used for the first six modes of cable vibration and it has increased usefulness over previous work because of its simplicity in application. An analytical solution representing the universal estimation curve has also been developed. It was proposed by Krenk (2000) that maximum additional damping that can be achieved from a linear viscous damper could be approximated simply as $\xi = x_c/2L$.

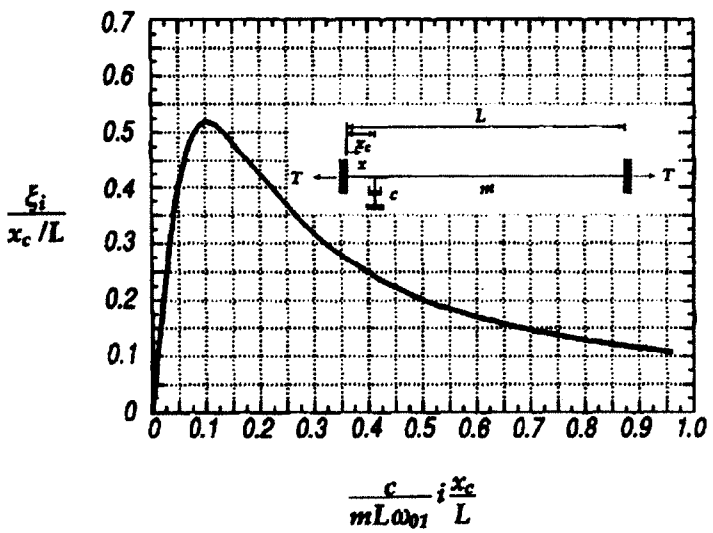

Figure 2-1: Universal damping estimation curve
(Pacheco et al., 1993)

The shortfall of linear viscous dampers is that the optimal damping coefficient can only be achieved in one specified mode of vibration. It will have an increasingly rigid effect on higher modes and an increasingly less rigid effect on lower modes. This also causes the natural frequency of the cable to shift towards that of a similar cable with a shortened length. However, the preferred mode to dampen is generally not known beforehand. In the study by Main and Jones (2001), the case of an infinitely rigid damper

was analyzed as a "clamped case" and analytically described by a clamping ratio, which was seen to increase with mode number, for a particular damping coefficient. This means that the damper acts in a more rigid manner for higher cable vibration modes, and confirms that this type of damper may only act optimally for one mode, because its effectiveness decreases for other modes. This optimal mode must be known before the damper is designed, and must be designed on a case-by-case basis for each cable in question, which may not be economically practical in design. It is worth pointing out that, though not optimal, a linear viscous damper may offer some damping effect to other vibration modes.

An analytical comparison between linear and nonlinear viscous dampers has been done by Main and Jones (2002) using the taut cable assumption. A universal damping estimation curve for a nonlinear damper was developed. The behavior of a nonlinear viscous damper can be generally described as exerting a force, proportional to the velocity of the cable, raised to some positive exponent. The use of this type of damper might be an improvement over the linear viscous damper because its efficiency is largely dependent on the amplitude of cable oscillation, and is less sensitive to mode number. The damper performs optimally in modes that experience oscillations in the vicinity of the design amplitude. Specifically, it was found that a nonlinear viscous damper with the exponent of ½ was completely independent of mode number and was equally effective at the same amplitude of vibration oscillation, regardless of the mode. This extends the design of dampers beyond a specific mode of vibration.

A mathematical model and semi-empirical design equation for nonlinear dampers was developed for high velocity applications by Jia et al. (2008). The taut string-single

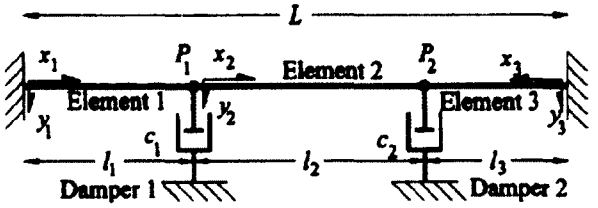

Figure 2-2: Taut string-two damper model (Caracoglia and Jones, 2007)

damper analytical model and the associated complex eigenvalue formulation have been extended to the two damper case, as illustrated in Figure 2-2. Universal damping estimation curves (comparable to the taut-string, single damper curve) were generated by Caracoglia and Jones (2007) for the two damper case as well. It was found that the modal damping of the damped cable was improved when the dampers were installed at opposite ends of the cable, but worsened when located at the same end due to their interaction. The latter would actually increase the stiffness at that end of the cable.

Tabatabai and Mehrabi (2000) studied the dynamic behaviour of a damped flexible cable by including the sagging and bending stiffness of the cable in the formulation. A notable conclusion was made that bending stiffness has a considerable effect on the obtainable damping ratio that can be achieved by a mechanical viscous damper, and that the taut cable approximation is likely to overestimate the obtainable damping ratio. Design equations / methods for damper design have been proposed which include bending stiffness but restrict damper location to the vicinity of the cable end.

Cable sag, often analytically expressed by the inextensibility parameter (λ^2) was initially proposed by Irvine and Caughey (1974). It is defined as the ratio of the stiffness of an ideal massless cable to that of an actual sagging cable. The sagging effect was found to be significant primarily in the first mode of vibration for cables with an inextensibility parameter greater than one. The universal damping estimation curve proposed by Pacheco et al. (1993) was deemed valid only for short to medium length

cables, where sag can justifiably be neglected. Xu and Yu (1998), as well as Tabatabai and Mehrabi (2000), developed curves, similar to the universal damper design curve, to determine the maximum damping ratio and the optimum damper size while considering the cable sagging effect for the first mode of cable vibration and beyond.

Energy-based methods have been explored to evaluate the additional damping provided by an attached viscous damper. Jiang (2006) used the kinetic-energy decay ratio of a freely vibrating cable, obtained from a finite element model developed using the ANSYS commercial software, and converted it into equivalent Rayleigh damping.

Cheng et al. (2010) developed a mathematical equation based on the kinetic energy decay time-history of a freely vibrating damped cable to evaluate the additional damping provided by an attached viscous damper. The time-history response was obtained from numerical simulations of a freely vibrating cable damper system developed using the ABAQUS commercial software. This work expanded on the previous studies by not only including the sag and flexural rigidity of the cable, but also lifting the restriction on the damper installation location in the application.

The dynamic behaviour of a cable-damper system has also been extensively studied experimentally. Pacheco et al. (1993) conducted tests to validate the proposed universal damping estimation curve and found that the amount of additional damping provided by a linear viscous damper did not reach the predicted optimum value. It was suggested that this could be attributed to the effects of cable sag and non-ideal linear viscous damper behavior.

Xu et al. (1999) conducted both free and forced vibration tests on a cable-damper system, with varying cable tension to simulate a range of sag conditions. The existence of an optimal damper coefficient that can reach a maximum modal damping ratio for a given damper location has been confirmed. Large-amplitude force-controlled vibration tests revealed non-linear vibration of an undamped cable, while the linearity was restored in the three lowest modes of vibration with the use of an oil damper. Out-of-plane vibration was also observed during these tests near the first in-plane natural frequency of the cable because of its proximity to its first out-of-plane natural frequency, which was thought to have generated internal resonance. In the experiment, the oil damper was found to be able to extinguish the out-of-plane vibration in the first mode, while effectively mitigating the in-plane vibration.

Field observations evaluating the performance of linear viscous dampers were conducted by Main and Jones (2001) on the Fred Hartman Bridge in Texas, USA, where two dampers were installed on two different stay cables. The dampers were found to be effective in mitigating cable vibrations that were identified to have stemmed from vortex- and rain-wind-induced excitations. After installing the dampers, not only the amplitude of cable vibration but also the acceleration of cable motions were decreased significantly. It was also observed that the damper forces were the greatest when the wind was in the same direction as the cable was declining.

Experimental research has also been extended to the use of multiple dampers attached to one cable by Sun et al. (2004). It was found that two dampers, installed at opposite ends of the cable, will increase the overall damping in the system; the sum of the additional damping provided by each damper is approximately equivalent to the overall

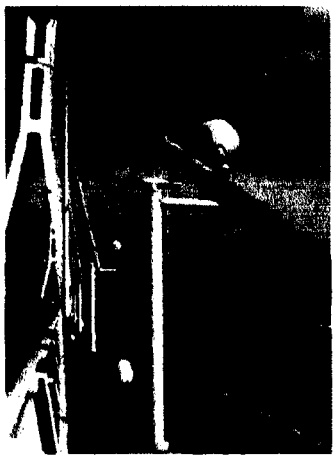

Figure 2-3: Damper support structure (Sun et al., 2004)

cable damping ratio. However, installing the two dampers at the same end of the cable will reduce the cable damping ratio.

The installation of linear viscous dampers has been to date generally restricted to the end of a cable within a few percent of the cable length for practical reasons. However, the damper will have increased effectiveness and damping capabilities if it can be moved towards the mid-span of the cable. In field applications, this may require a damper support structure to allow the damper to be installed beyond its conventional position, as shown in Figure 2-3. It is worth noting that none of the studies reviewed above considered the stiffness of the damper itself and the support in the formulation. These could have considerable impact on the efficiency of the damper.

A few studies addressed the issue of damper stiffness and damper support stiffness. Zhou (2005) used complex modal analysis to develop an equation for the optimal damper size, which included damper stiffness. It was found that as the non-dimensional damper stiffness increased, the optimal damper size would increase linearly.

Xu and Zhou (2007) developed an analytical formula using the taut cable assumption for the cable damping ratio using an adjustable fluid damper. This damper type acts as a passive fluid damper after the optimum damping coefficient is found through application. The formula represented the adjustable fluid damper using the Maxwell model, which can be described as a dashpot connected in series with a spring.

An additional spring was connected in series with the damper spring to represent support stiffness. The cable damping ratio was represented as a function of damper support stiffness; an increase in damper support stiffness increased the cable damping ratio.

Fujino and Hoang (2008) analytically derived an asymptotic formula for the modal damping of a cable, which included cable sag, flexural rigidity, and damper support stiffness. In the formula, the influencing factors were expressed as modification / reduction factors, which can be used conveniently in practical damper design. This study confirmed that, for cables with a small sag parameter, sagging effect was significant only for the 1st symmetric mode of cable vibration and that the influence of cable flexural rigidity was apparent in all modes of interest. Damper support stiffness was found to be independent of the mode of cable vibration and to have a significant effect on the maximum damping capability of the damper. With the increase of damper support stiffness, the cable damping ratio increases. Damper design equations including the damper support stiffness were proposed.

The analytical work by Huang and Jones (2011) has led to the development of universal damping estimation curves for predicting modal damping ratio of a damped cable by including the effect of damper support stiffness, although the taut cable assumption was used in their formulation. In this study, a decrease in damper support stiffness was also found to decrease additional damping from an attached linear viscous damper.

Sun et al. (2004; 2008) analytically analyzed the individual effects of damper stiffness and damper support stiffness on the maximum attainable damping ratio, based

on the taut string assumption. An increased damper stiffness and decreased damper support stiffness were each found to independently decrease the maximum obtainable cable damping ratio. Efficiency factors were proposed, which were defined as the ratio of actual additional damping from experimental results to the analytically calculated results based on ideal linear viscous damper theory.

Huang (2011) conducted an experimental work focusing specifically on the effect of damper stiffness on the efficiency of a linear viscous damper in suppressing cable vibrations. Springs were installed between a model cable and a linear viscous damper to simulate the damper stiffness. Results indicated that the existence of damper stiffness would reduce the effectiveness of a damper.

Further study needs to be undertaken to understand the effects of damper stiffness and damper support stiffness on the additional damping provided by a viscous damper. A thorough understanding of both of these parameters will help bridge designers to maximize viscous damper effectiveness in mitigating stay cable vibration. The current study has expanded on previous work by considering these two parameters both separately and in combination in an experimental study and through a finite element analysis of a cable-damper system. Approximations for the optimum damper size and its corresponding maximum achievable damping ratio have been developed for the convenience of practical damper design.

Chapter 3: Experimental Study

An experimental study was carried out to investigate the dynamic behavior of a cable-damper system. This chapter will include a detailed description of the experimental setup, the equipment, and the testing procedures that have been used, as well as the experimental results. An existing experimental setup, developed by Huang (2011), was modified to be used for the current study. This experimental study was set up in room B-19 in Essex Hall at the University of Windsor, Ontario, Canada.

3.1 Experimental setup

A steel wire cable was used to model a bridge stay cable and it was mounted horizontally between two steel columns. A sketch of the experimental setup is shown in Figure 3-1.

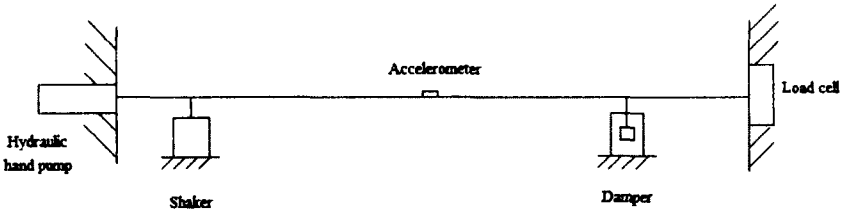

Figure 3-1: Sketch of experimental setup

One end of the cable was attached to a load cell for measuring the pretension in the cable, and the other end was attached to a hydraulic pump for applying tension in the cable. The cable had a span length of 9.33 m (mounted into position), a nominal diameter of 4.65 mm, a unit mass of 0.092 kg/m, and a nominal moment of inertia of 15.8 mm^4. The appropriate amount of pretension for this cable to achieve the desired dynamic behaviour was investigated by Huang (2011) and found to be within the range of 2500 N – 4000 N.

This range is high enough to avoid too little tension in the cable, which would cause the cable to be slack, and low enough to avoid too much tension, which would cause the vibrating cable to exhibit elliptical motion. The pretension in the cable used for this experimental study was 3200 N. The natural frequency of the model cable was lowered to approach that of an actual bridge stay cable by adding 20 evenly spaced 50 gram mass blocks to increase its unit mass. The resulting unit mass of the cable was 0.2 kg/m. The first natural frequency of a cable (f_1) can be predicted using the formula: $f_1 = 1/(2L)\sqrt{T/m}$, where L = cable length (m), T = cable pretension (N), m = cable unit mass (kg/m). The resulting natural frequency of the cable, after the addition of the mass blocks, is predicted to be 6.78 Hz. In the lab, the natural frequency of the cable was found to be approximately 7.0 Hz.

A Universal Flat Load Cell, model number FL25U-2SG, was mounted at one end of the cable to measure the applied pretension in the cable. It has a maximum capacity of 25,000 lb and it was calibrated using a universal tensile tester, which yielded a calibration constant of 5.458 kN/mV. This constant was inputted into the data acquisition system to display cable tension in kN (with a display resolution of 10 N). The load cell is shown in Figure 3-2.

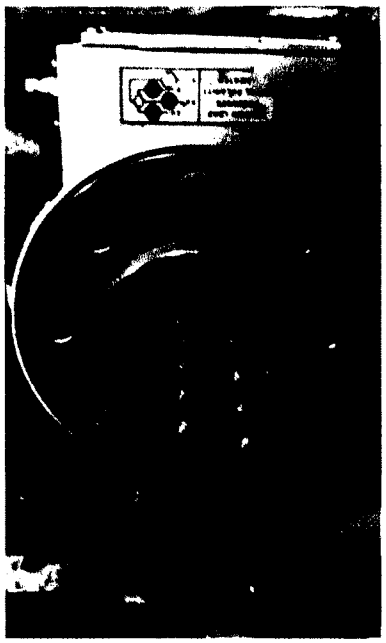

Figure 3-2: Universal Flat
Load Cell

An Enerpac hydraulic steel hand pump, shown in Figure 3-3, was installed at the opposite end of the cable from the load cell to apply pretension to the cable. The unit, model number PH-84, has a maximum pressure rating of 10,000 psi. In this experiment, the hydraulic pump was setup to exert a pretension of 3200 N to the cable. This value was measured by the load cell located at the opposite end of the cable.

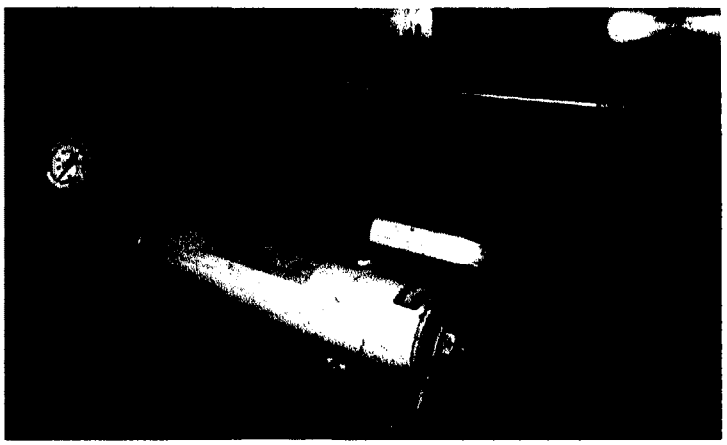

Figure 3-3: Hydraulic hand pump

An accelerometer was placed at the mid-span of the cable to monitor the first modal response of cable vibration. It was placed on the very top of the cable cross-section in order to record only the vertical motion. Real time data was collected using the Astrolink Xe data acquisition and control software. The data was monitored to make sure that the wave-form acceleration data collected was symmetric, which indicated that the unit is properly placed at the top of the cable and is receiving data from only the vertical direction of motion. The accelerometer used, model number 352A24, was purchased from Dalimar Instruments and has a testing range of 1 – 8000 Hz. The testing range used in this experimental study was 6 – 8 Hz.

An electronic dynamic Smart Shaker from the Modal Shop, Inc. was utilized for the forced vibration tests. The unit, model number K2007E01, is capable of providing up to 7 lb (31 N) of peak sine force, has a 1/2 inch (1.27 cm) stroke, and a testing frequency range of 1 – 9000 Hz. The shaker was installed at five percent of the cable length, sitting on a tripod, and directed vertically to provide excitation in only this direction, as shown in Figure 3-4. The correct installation of the damper is essential in order to receive accurate data from the accelerometer, which is installed to record vertical motion. Improper installation (non-vertical excitation) will cause unsymmetrical cable motion and thus incorrect cable damping ratio in the analysis.

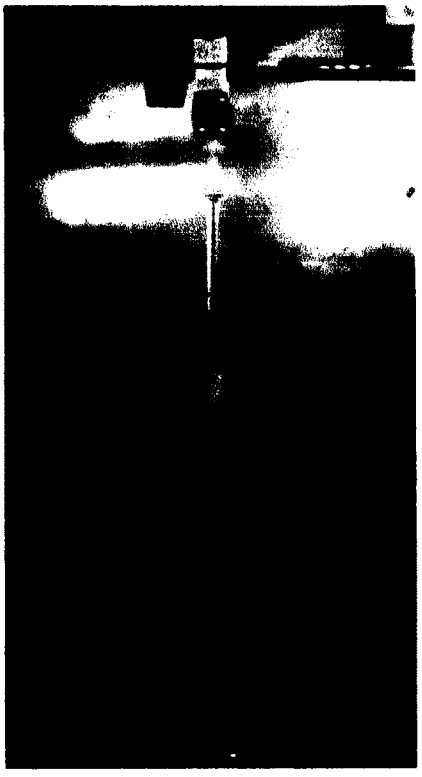

Figure 3-4: Smart Shaker

An HP signal generator, model number 33120A, was used to generate the dynamic excitation functions to control the dynamic shaker. This unit, shown in Figure 3-5, has the ability to generate many output functions including sine, square, triangle, and ramp, among others. The sinusoidal output function was used in this experiment. The signal generator can generate this output function in a frequency range of 1 – 15 MHz.

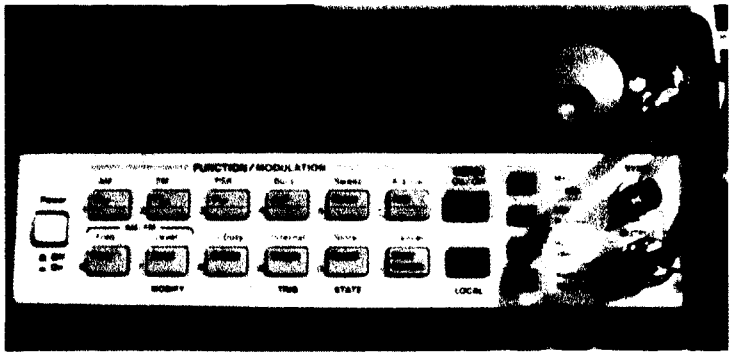

Figure 3-5: HP signal generator

The data acquisition recorder used was AstroDAQ Xe from Astro-Med, Inc. The unit, part number 22834-513, connects to a computer through a USB 2.0 interface and has eight input channels. Both the load cell and the accelerometer were connected to this data recorder, shown in Figure 3-6. The software that was used with this recorder was the AstroLINK Xe data acquisition and control software, also from Astro-Med, Inc. The software, part number 22834-514, can record data at frequencies up to 200,000 Hz. In this experiment, a sampling frequency of 1000 Hz was used. The Realtime mode in the software was used to monitor and capture real-time acceleration data from the accelerometer. The review mode in the software was used to review and save data previously captured.

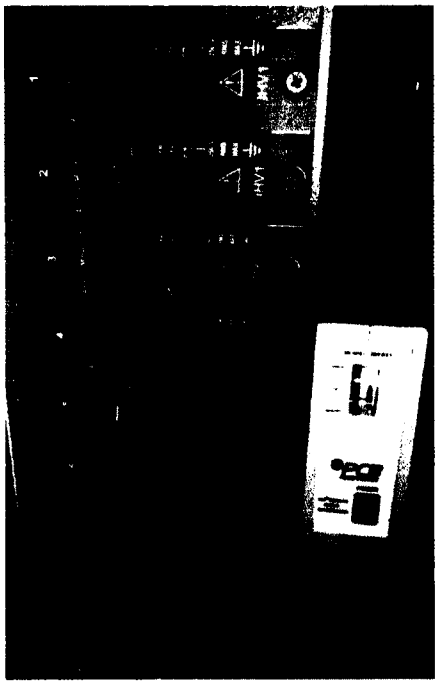

Figure 3-6: AstroDAQ XE data aquisition recorder

3.2 Damper design and calibration

A passive linear viscous damper was used in this experimental study. This damper type provides a dissipative damping force generated from the pressure difference from a piston moving through a viscous fluid. The damper used in this study was designed to have variable damper stiffness and support stiffness. It was also imperative that all energy in the system be affected only by the damper and stiffness components (no loss of energy due to friction), to result in an accurate cable damping ratio. A photograph of the damper designed for this experimental study is shown in Figure 3-7.

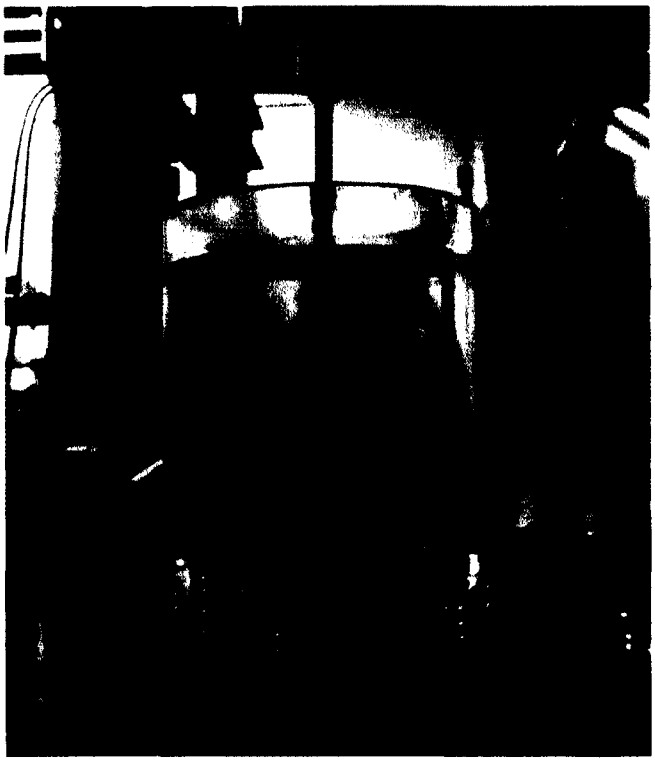

Figure 3-7: Viscous damper

The designed damper has the following main components:

1. A plastic container holds the viscous fluid. It is open at the top and it has an inner diameter of 100 mm. The bottom of the container has 12 holes carved into it to fit the support springs. Figure 3-8 shows a sketch of the damper container.

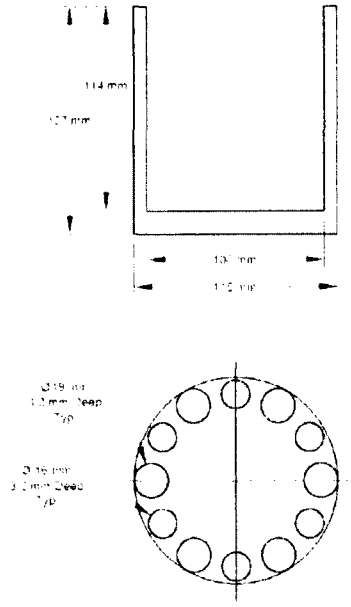

Figure 3-8: Damper container sketch

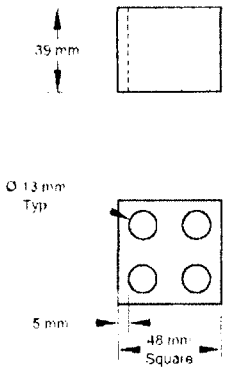

Figure 3-9: Damper block sketch

2. SYNTON PAO 100, produced by Chemtura Canada Co. and obtained from Commonwealth Oil, was used as the viscous fluid for this damper. It has a kinematic viscosity at 40°C of 1279.51 centistokes (cSt).
3. An acrylic block was designed as the piston for this damper. It has vertical holes that extend vertically and symmetrically through the block for the purpose of increasing the contact surface area with the viscous fluid to

increase the damper damping coefficient. It has a mass of 80.78 g. Figure 3-9 shows a sketch of the damper block.

4. A plastic stick connects the block to the cable. It screws into the center of the block and attaches to the cable through two aluminum pieces that fit around the cable cross-section. The stick and aluminum pieces have a mass of 26.10 g. Figure 3-10 shows a picture of the damper block connected to the stick and aluminum pieces.

Figure 3-10: Damper block,
sick, and cable attachment

5. Two sets of two springs were used to simulate the damper stiffness. They are connected to the damper container through two aluminum hooks screwed into the top surface edges of the container, directly across from each other, and they are connected to the cable directly. The stiffness of the springs was measured experimentally in the lab. The springs were obtained from McMaster-Carr and have the following properties:

Table 3-1: Damper stiffness spring properties

Spring Part No.	9654K53	9654K812
Stiffness (N/m)	140	300
Spring type	Steel Extension Spring	Steel Extension Spring

6. Two sets of six springs were used to simulate the damper support stiffness. They sit in an acrylic base plate that has holes carved out to fit their cross-section. The base of the plastic damper container rests on the springs. It has holes carved out of its base to fit the springs. The stiffness of the springs was measured experimentally in the lab. The springs were obtained from McMaster-Carr and have the following properties:

Table 3-2: Damper support stiffness spring properties

Spring Part No.	9434K147	9434K135
Stiffness (N/m)	5780	7880
Spring type	Music wire precision compression spring, zinc-plated	Music wire precision compression spring, zinc-plated

7. An acrylic base plate was designed to accompany the damper and allow for varying support stiffness. It has two sets of six holes carved into it symmetrically. Each set of six holes accommodates one set of support stiffness springs. The two sets of support stiffness springs can be used either independently or in combination. The base plate can also be directly attached to the damper to simulate an infinitely stiff support.

A damper calibration system was designed to measure the damping coefficient of the damper. An LVDT was used to measure the linear displacement of the piston (acrylic

block and stick) as it moves through the damper viscous fluid under constant applied forces. The LVDT cylinder was placed on the lid of an acrylic structure, shown in Figure 3-11, which has an opening in its side to allow for the raising and releasing of the damper piston.

Figure 3-11: Acrylic calibration unit

The top of the LVDT stick fits into the damper cylinder and its base is screwed into the aluminum top plate of the plastic damper stick, which is also connected to the acrylic damper block at its bottom end. The two aluminum pieces of the damper stick, used to attach to the cable during testing, hold rectangular prism mass blocks during calibration. The different mass blocks are used as the constant applied forces on the piston. The mass was applied in 25 g increments. The LVDT was connected to the AstroDAQ Xe data recorder to display the velocity of the LVDT in volts per second using the AstroLINK Xe software. The conversion factor for the displacement of the LVDT stick is 1 volt = 2.5 mm. It was used to convert its velocity into meters per second. The damper coefficient

has a unit of Ns/m. The applied force during calibration includes the weight of the damper acrylic block, the plastic stick and the attached aluminum pieces, the mass blocks used, the screws to attach the aluminum pieces together, and the LVDT stick. As the damper piston is released, each time with different mass blocks installed, the data acquisition software records the velocity of the LVDT stick. The relation between the applied force and the damper piston velocity, illustrated in Figure 3-12, was produced from calibration results and linear regression analysis. The slope of this force-velocity curve is the damper coefficient with the unit of Ns/m. The damper in this experimental study had a damping coefficient of 32.2 Ns/m.

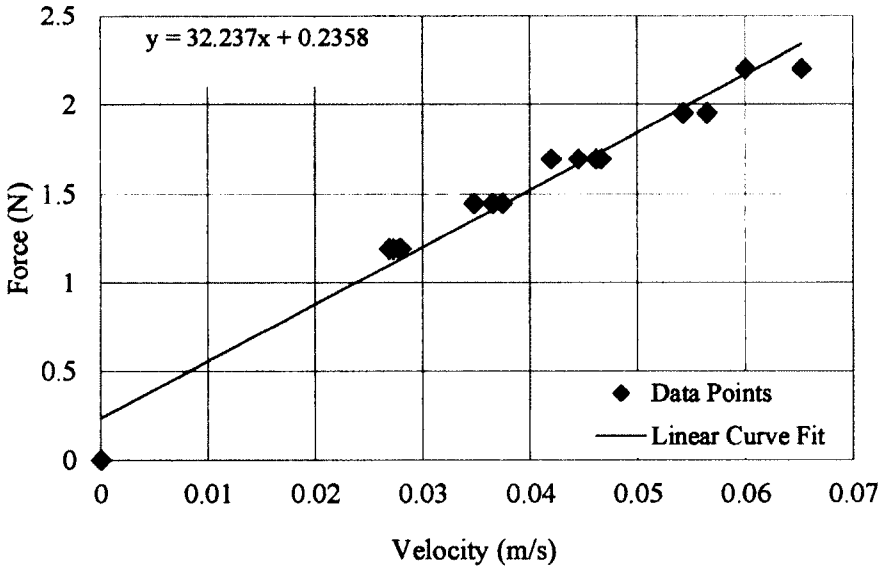

Figure 3-12: Force vs. Velocity calibration graph

3.3 Forced-vibration tests

Forced-vibration tests were performed to observe vertical cable motion under varying excitation frequencies. The combinations of damper stiffness and damper support stiffness that were tested are described in Table 3-3.

Table 3-3: Damper–stiffness combinations

Damper coefficient (Ns/m)	32.2								
Damper support stiffness (N/m)	Infinite			82000			47300		
Damper stiffness (N/m)	0	280	600	0	280	600	0	280	600

The following describes the experimental testing procedures that were followed:

1. Find the first natural frequency of the cable (to the nearest 0.05 Hz) by adjusting the excitation frequency of the shaker through the signal generator. The maximum cable response from the accelerometer data can be captured in the Realtime mode of the AstroLINK Xe software (i.e. resonance). The experimental value of the first natural frequency of the cable will be slightly higher than that estimated theoretically because the installation of the shaker decreases the effective length of the cable.
2. Create a file name for the current test and select the sampling frequency (1000 Hz was used) in the AstroLink Xe software.
3. Set the signal generator to a frequency of 0.5 Hz less than the experimental natural frequency and record the acceleration data. This data file may be subsequently reviewed (in the Review mode) and saved as a Microsoft Excel file.
4. Increase the signal generator frequency by 0.05 Hz for each test, up to $(f_1 + 0.5)$ Hz. Each damper-stiffness combination will therefore be tested at 20 frequency values.

A Butterworth Filter, which can filter higher modes out of the experimental data, leaves only data from the first mode of vibration. This filter used a band pass of $(f_1 -$

$0.6\,Hz) - (f_1 + 0.6\,Hz)$ and had a filter order of two. The acceleration data was subsequently converted to displacement data using a Fourier Transform and the Matlab commercial software. With this displacement data, the half-power method was used to determine the cable-damping ratio of the tested system by plotting the frequency-response curve.

A sample data set will be presented to fully illustrate the experimental procedure. The sample data set will have the damper located at 10% of the cable length, with a damper stiffness of 280 N/m and a damper support stiffness of 47300 N/m.

First, a pretension of 3200N was applied to the cable using the hydraulic hand pump. The value of pretension was measured by the load cell, which was connected to the AstroDAQ Xe data acquisition system, and observed in the Realtime mode of the AstroLINK Xe software. The shaker was installed at 5% of the cable length, at the opposite end from the load cell. It was set to its maximum amplitude and connected to the signal generator. The signal generator was set to a sinusoidal output function. The accelerometer was installed at the mid-span of the cable, on the top of the cable cross-section. It was also connected to the data acquisition system.

The damper was subsequently installed at 10% of the cable length, at the same end as the load cell (and the opposite end from the shaker). First, the acrylic damper base plate was secured onto a steel base, which can be adjusted to raise the damper up to the height of the cable. The six support springs with stiffness of 7880 N/m are placed in their respective holes in the base plate (the springs are placed alternatively in the holes such that each spring has an empty hole adjacent to it). The support springs are installed in

parallel and their combined stiffness is a direct addition of each spring stiffness, which results in a damper support stiffness of 47300 N/m. The damper container is filled with the viscous fluid, SYNTON PAO 100, and the container is placed on the support springs. The top of the support springs fit into the holes in the damper container base. The damper block is attached to the plastic stick and placed in the damper container. The plastic stick is connected to the cable through its attached aluminum pieces, which are screwed together with the cable in between them. The two damper stiffness springs, each with a stiffness of 140 N/m, are installed in parallel. The bottom of each spring is attached to an aluminum hook, on each side of the container. The top of each spring is hooked directly onto the cable. Their combined stiffness is 280 N/m.

The fundamental frequency of the cable is then found in the experiment by adjusting the output frequency on the signal generator. The fundamental frequency is found to be approximately 7.20 Hz by qualitatively observing the maximum cable response at this excitation frequency. The shaker and damper attachments caused the fundamental frequency to increase slightly. The testing frequency range was 0.5 Hz below the fundamental frequency to 0.5 Hz above it, therefore 6.70 – 7.70 Hz. The signal generator was set to 6.70 Hz. The sampling frequency was set to 1000 Hz. The AstroLINK Xe software was used to capture the data over a time period of 12 seconds. The data was then reviewed in the Review mode and saved an excel file for further processing. The signal generator output frequency was increased by 0.5 Hz and the data was once again captured, reviewed, and saved. This was repeated up to at frequency of 7.70 Hz. This concluded testing for this sample.

The following details the data processing of the sample data set. The acceleration data from the first data file (6.70 Hz) was brought into Matlab; it was represented by the variable "b". The Butterworth filter was designed in Matlab using the "Filter Design & Analysis Tool". It was of Bandpass response type and a filter order of two. The filter was represented by the variable "Hd". An M-file, designed by Huang (2011) and included in Appendix A, was subsequently used to process the data. This file applies the Butterworth filter to remove higher modes of vibration from the experimental data and it applies Fourier Transform to convert acceleration time-history data to displacement time-history data. The M-file produces a graphical output of the displacement time-history data, shown in Figure 3-13. The maximum displacement is found using the "Data Cursor" tool, which displays data values interactively. The maximum displacement value for this data set was found to be 0.6133 cm.

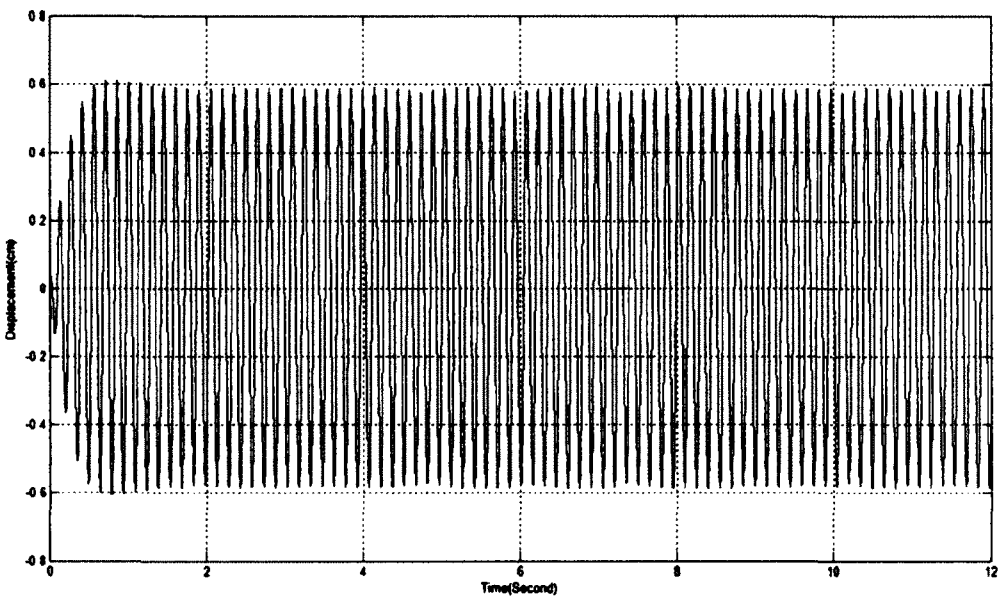

Figure 3-13: Displacement vs. Time output

Table 3-4: Maximum displacement values for each tested excitation frequency

Excitation frequency (Hz)	Maximum displacement (cm)
6.70	0.6133
6.75	0.6905
6.80	0.8046
6.85	0.9372
6.90	1.090
6.95	1.254
7.00	1.409
7.05	1.545
7.10	1.585
7.15	1.545
7.20	1.444
7.25	1.317
7.30	1.191
7.35	1.065
7.40	0.9495
7.45	0.8478
7.50	0.7586
7.55	0.6841
7.60	0.6178
7.65	0.5622
7.70	0.5108

The maximum displacement for each data file was subsequently found. These values are presented in Table 3-4. A variable was created for the excitation frequency (F) and the maximum displacement (D) in Matlab. The Curve Fitting Tool was used to plot maximum displacement (D) in centimeters versus excitation frequency (F) in Hz. The data was fitted with a cubic spline, interpolant type of fit, shown in Figure 3-14. The fitting curve was analyzed using the Analysis Tool, and the displacement was interpolated at each 0.001 Hz along the fitting curve. The maximum displacement (D_{max}) may then be found with the precision of 0.00001 Hz. In this data set, the maximum displacement was 1.58517 cm.

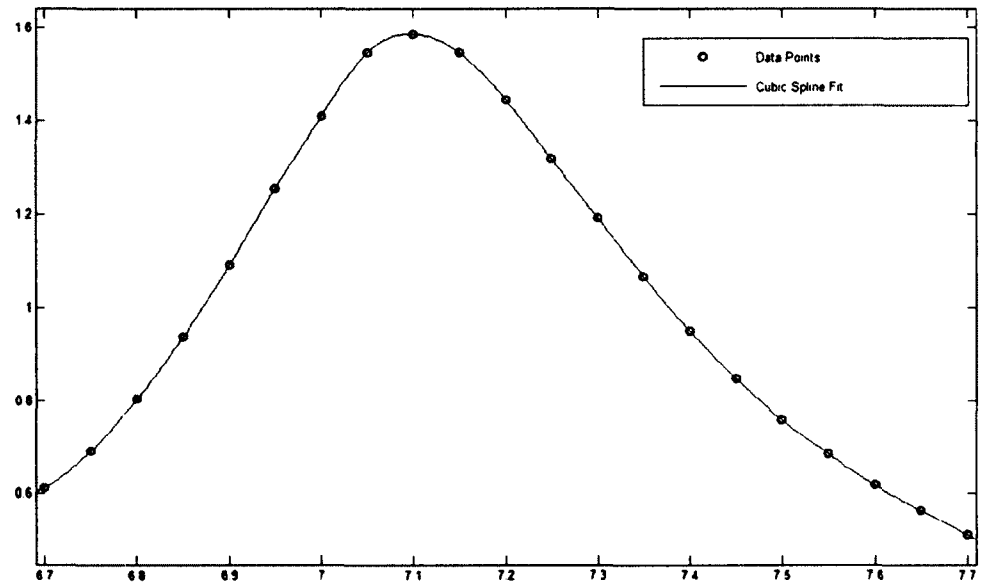

Figure 3-14: Maximum displacement (cm) vs. Excitation frequency (Hz)

The half-power method was subsequently used to calculate the experimental cable-damping ratio. The steps are listed below and a summary of the sample data set is presented in Table 3-5.

1. The maximum displacement was divided by the square-root of two to calculate the half-power points:

$$\frac{D_{max}}{\sqrt{2}} = \frac{1.58517 \text{ cm}}{\sqrt{2}} = 1.120884 \text{ cm}$$

2. The excitation frequencies (on each side of the peak displacement) that correspond to this displacement value were found to be:

$$R_1 = 6.910 \text{ Hz}$$

$$R_2 = 7.328 \text{ Hz}$$

3. The damping ratio was calculated using the following formula:

$$\xi = \frac{R_2 - R_1}{R_2 + R_1} = \frac{7.328\text{Hz} - 6.910\text{Hz}}{7.328\text{Hz} + 6.910\text{Hz}} = 0.02936 = 2.936\%$$

Table 3-5 Summary of the sample experimental data set

Damper location L_d	10% L
Damping coefficient c (Ns/m)	32.2
Damper stiffness k_d (N/m)	280
Damper support stiffness k_s (N/m)	47300
Damping ratio ξ (%)	2.936

3.4 Experimental results

Table 3-6 summarizes the combinations of damper stiffness and damper support stiffness that have been tested. The damper was installed at 4%*L*, 6%*L*, and 10%*L*. The experimental results for each damper location are presented graphically in Figures 3-15, 3-16, and 3-17, respectively.

Table 3-6: Tested stiffness combinations

Damper damping coefficient c (Ns/m)	32.2								
Damper support stiffness k_s (N/m)	Infinite			82000			47300		
Damper stiffness k_d (N/m)	0	280	600	0	280	600	0	280	600

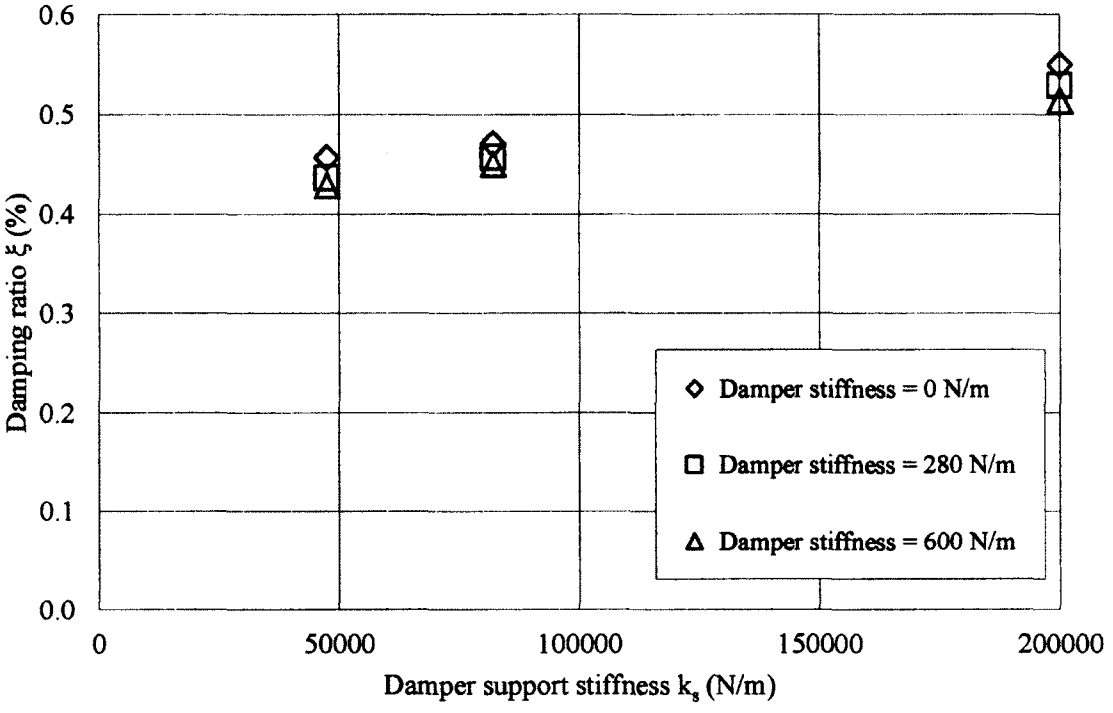

Figure 3-15: Experimental results (4%L)

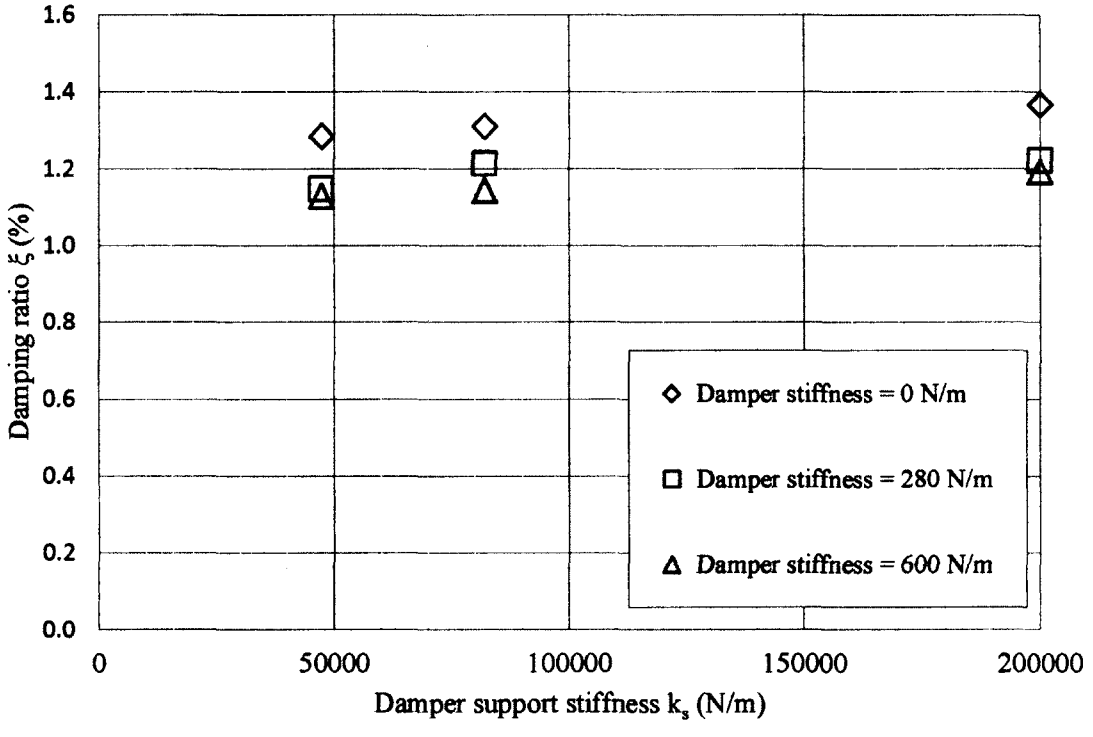

Figure 3-16: Experimental results (6%L)

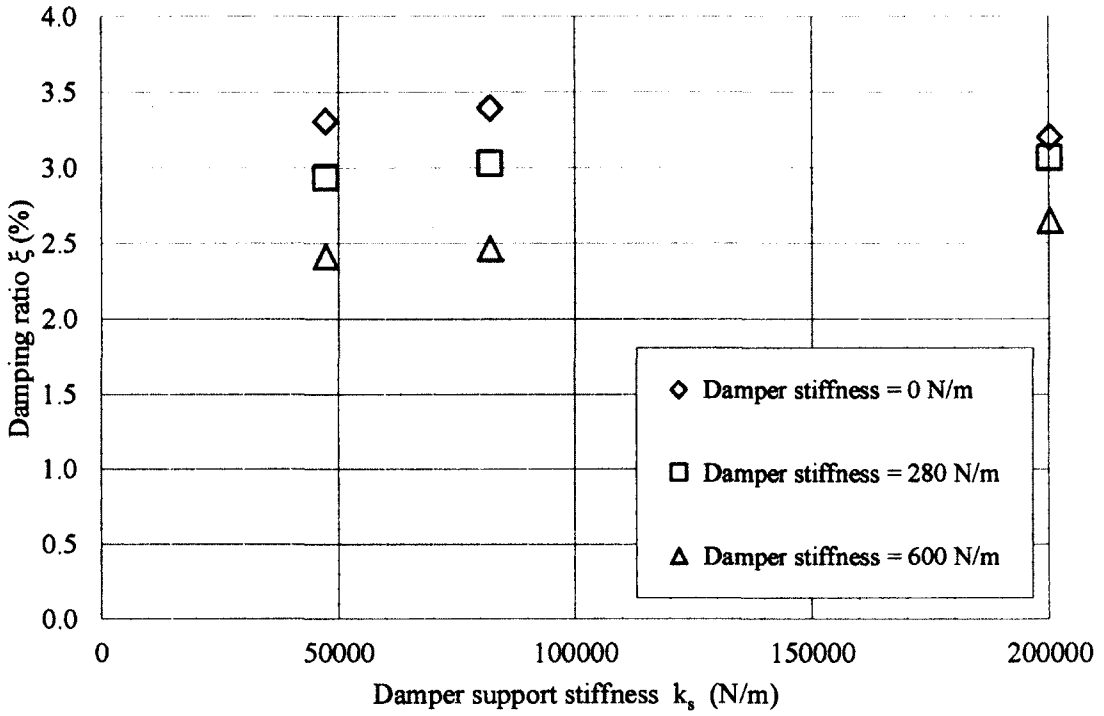

Figure 3-17: Experimental results (10%L)

The experimental results given in Figures 3-15, 3-16, and 3-17 show that the effects of damper support stiffness and damper stiffness on the performance of a linear viscous damper are similar at all three tested damper locations. It can be observed from these three figures that the modal damping ratio of the cable-damper system increases as damper support stiffness increases. This is the same trend that has been observed in previous studies (Xu and Zhou, 2007; Fujino and Hoang, 2008; Huang and Jones, 2011). The reason for this behaviour may be attributed to difference in damping force that the damper exerts when it has a rigid support (Figure 3-18) compared to when it has a support with finite stiffness (Figure 3-19). The damping force exerted by the damper may be expressed by the following:

$$F_d = c(V_A - V_B) \tag{3.1}$$

where F_d is the damping force exerted by the damper on the cable (N), c is the damping coefficient of the damper (Ns/m), V_A is the velocity of the node where the damper connects to the cable (m/s), and V_B is the velocity of the node where the damper connects to its base support (m/s). Nodes A and B are illustrated in both Figures 3-18 and 3-19. In Figure 3-18, a sketch of a damper with a rigid support is shown. For this case, the velocity of node B (V_B) in Eq. (3.1) would be zero because the rigid support is not in motion. When this is inserted into Eq. (3.1), the value of the damping force becomes the following:

$$F_d = cV_A \tag{3.2}$$

In Figure 3-19, a sketch of a damper with a support of finite stiffness is shown. The velocity of node B (V_B) in this case would be a nonzero value. This results in a smaller damping force than in the case where the damper has a rigid support. Therefore, a damper with a finite support provides less damping than that with a rigid support.

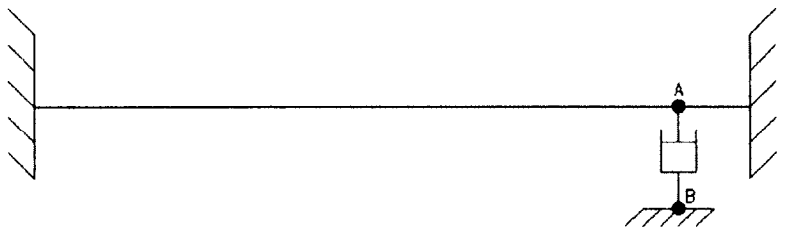

Figure 3-18: Sketch of a damper with a rigid support

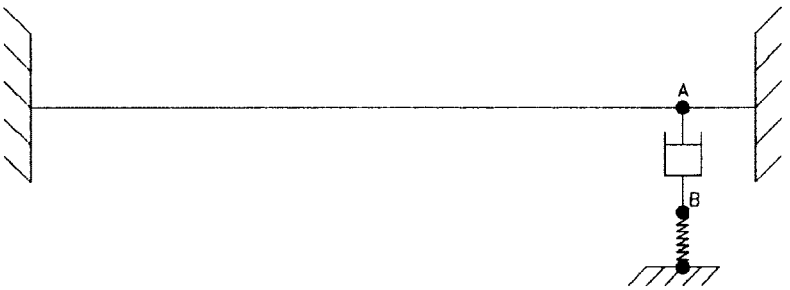

Figure 3-19: Sketch of a damper with a support of finite stiffness

The experimental results also show that the modal damping ratio decreases as the damper stiffness increases. This trend, observed by Zhou (2005) and Huang (2011), is reasonable because the existence of the damper stiffness reduces the efficiency of the damper by absorbing part of the energy and converting it to elastic energy. Without damper stiffness, this part of energy would otherwise be transferred to the damper and be dissipated through its damping mechanism. This set of data implies that to achieve the maximum efficiency of a linear viscous damper, preferably, it should be supported on a rigid base, and the stiffness of itself should be negligible.

The experimental results obtained have been compared with the existing literature to confirm their accuracy. The studies conducted by Xu and Zhou (2007), Fujino and Hoang (2008), and Huang and Jones (2011) have produced analytical formulae that predict the value of the modal damping ratio of a cable-damper system while including the effect of damper support stiffness. However, the effect of damper stiffness was not considered in these works. These formulae will therefore be used to compare with the zero damper stiffness cases of the current study. The study conducted by Zhou (2005) produced a damper efficiency reduction factor that accounts for the effect of damper stiffness only. The degradation of damper performance caused by the presence of damper stiffness observed in the current experimental study will be compared with the reduction factor calculated using the formula developed by Zhou (2005).

The equation developed by Xu and Zhou (2007) is based on the Maxwell model, i.e. a damper in series with a spring, and has the following form:

$$\frac{\xi_i}{x_c/L} \cong \frac{\pi^2 k_i}{1 + (\pi^2 k_i + i\lambda\omega_{01})^2} \tag{3.3}$$

where ξ_i is the nondimensional modal damping ratio of the cable-damper system in the i^{th} mode of vibration, x_c is the location of the damper, L is the length of the cable, ω_{01} is the undamped circular frequency of a taut cable in the first mode of vibration, k_i is the nondimensional damping parameter in the i^{th} mode of vibration, calculated based on the following:

$$k_i = \frac{c}{mL\omega_{01}} i\left(\frac{x_c}{L}\right) \tag{3.4}$$

where c is the damper coefficient. The damper support stiffness is included in the term λ, which is defined as the total relaxation time constant and is a component of the Maxwell model upon which these equations are based. This term may be calculated using the following formula:

$$\lambda = c/k_d + c/k_s \tag{3.5}$$

where k_d is the damper stiffness in series with the damper, and k_s is the support stiffness in series with both the damper and the damper stiffness. For the purpose of comparison with the current results, which only had the damper support stiffness in series with the damper (damper stiffness was in parallel with the damper), the term c/k_d was taken as zero. In order to utilize Eq. (3.3) to compare with the results of the current study, x_c/L was taken as 0.04, 0.06, and 0.10 for the 4%L, 6%L, and 10%L damper locations, respectively. The values of c, m, L, and ω_{01} were taken as 32.2 Ns/m, 0.2 kg/m, 9.33 m, and 42.59 radians/s, respectively. The value of k_s was varied from 6,300 N/m to 200,000 N/m. The value of damper support stiffness used to represent a rigid support was taken as 200,000 N/m. This is appropriate because this value is significantly larger than the values used for the finite support stiffness. The formula developed by Xu and Zhou (2007) uses

the taut cable assumption. Therefore, cable sag and bending stiffness were neglected. The dashed line in Figures 3-20 to 3-22 portrays the results by Eq. (3.3).

The equation developed by Fujino and Hoang (2008) for evaluating the amount of damping provided by an external linear viscous damper to suppress cable vibrations while considering the damper support stiffness is the following:

$$\frac{\xi_n}{x_c/L} = R_{sn}R_f\frac{\bar{k}^2 n_f n_{sn} n_n}{\bar{k}^2 + \left(1+\bar{k}n_f\right)^2 n_{sn}^2 n_n^2} \tag{3.6}$$

where $\bar{k} = x_c k/H$ is the dimensionless damper support stiffness, x_c is the location of the damper, k is the damper support stiffness, H is the chord tension of an inclined cable, and L is the length of the cable. The terms n_f and n_{sn} are the modification factors due to cable flexural rigidity and sag, respectively, and n_n is a modification factor that includes the dimensionless damper damping coefficient and its location along the cable length. The values for these modification factors were calculated using the formulae proposed in the study. For example, when the damper is located at 4%L, n_f and n_n are calculated to be 0.874 and 0.160, respectively. The value of n_{sn} was calculated to be equal to one (this factor is not dependent on the location of the damper). The terms R_{sn} and R_f are the reduction factors due to the influence of cable sag and flexural rigidity, respectively. The former was calculated to be 1.0 (it is not dependent on the location of the damper) and the latter was calculated to be 0.960 when the damper is located at 4%L. This equation was applied to the cable used in this experiment and the damper support stiffness parameter was again varied from 6,300 N/m to 200,000 N/m. The solid line in Figures 3-20 to 3-22 portrays the results of Eq. (3.6). The equation developed by Fujino and Hoang (2008) included not only the damper support stiffness, but also the cable bending stiffness and

sag. Since the damper stiffness was not included in this formula, only the experimental data points that have zero damper stiffness were used for comparison.

The universal curve equation proposed by Huang and Jones (2011) predicts the modal damping ratio of a cable-damper system by including a flexibility coefficient that takes into account the damper support stiffness. The equation has the form of the following:

$$\frac{\xi_i}{x_c/L} \cong \frac{\pi^2 k}{1+(\pi^2 k)^2 \zeta^2} \tag{3.7}$$

where k is the nondimensional damping coefficient, which can be expressed as:

$$k = \frac{c}{mL\omega_{01}} i\left(\frac{x_c}{L}\right) \tag{3.8}$$

and ζ is the effective flexibility coefficient expressed as:

$$\zeta = 1 + \frac{1/\chi}{x_c/L} \tag{3.9}$$

The effective flexibility coefficient includes a nondimensional spring stiffness parameter χ which is expressed as:

$$\chi = \frac{kL}{H} \tag{3.9}$$

where k is the damper support stiffness, L is the cable length, and H is the cable tension force. The universal curve equation, Eq. (3.7), was applied to the cable used in this experiment with the damper support stiffness parameter varied in the same range as was done for the two previous studies described. The dotted line in Figures 3-20 to 3-22

portrays the results by Eq. (3.7). This equation uses the same taut cable assumption as that developed by Xu and Zhou (2007), and therefore cable sag and bending stiffness were neglected. Damper stiffness was not included in this formula. Thus, the experimental data that have zero damper stiffness will be used for comparison.

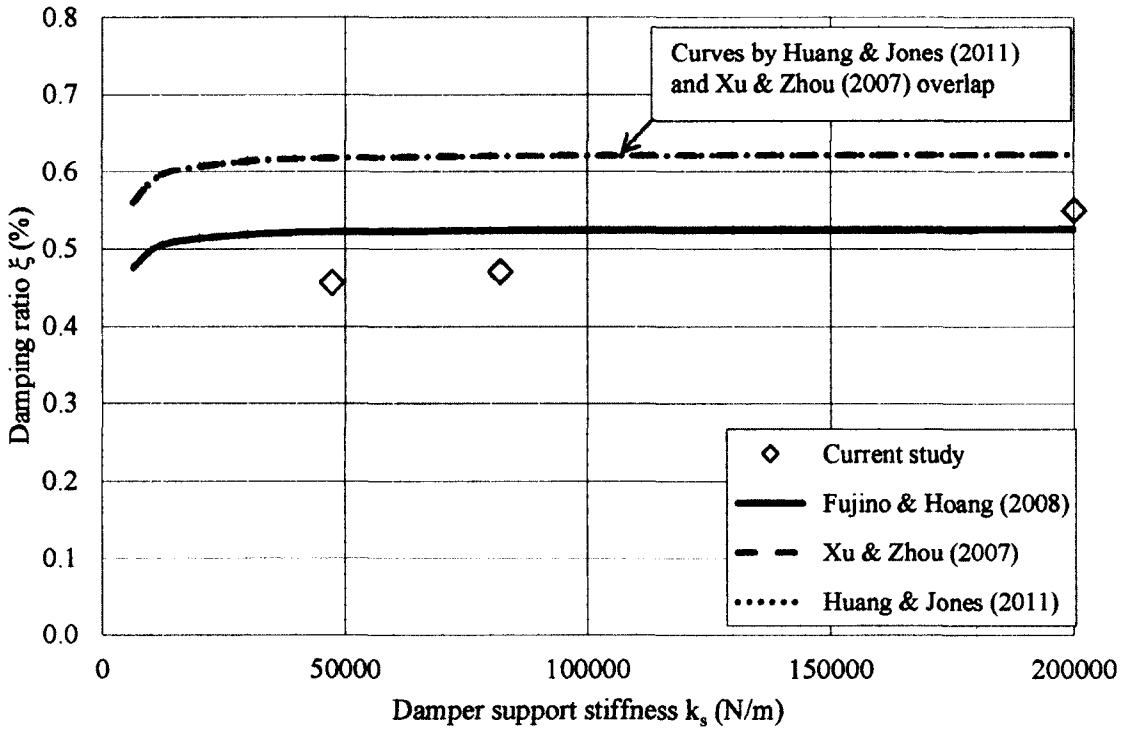

Figure 3-20: Experimental results (4%L)

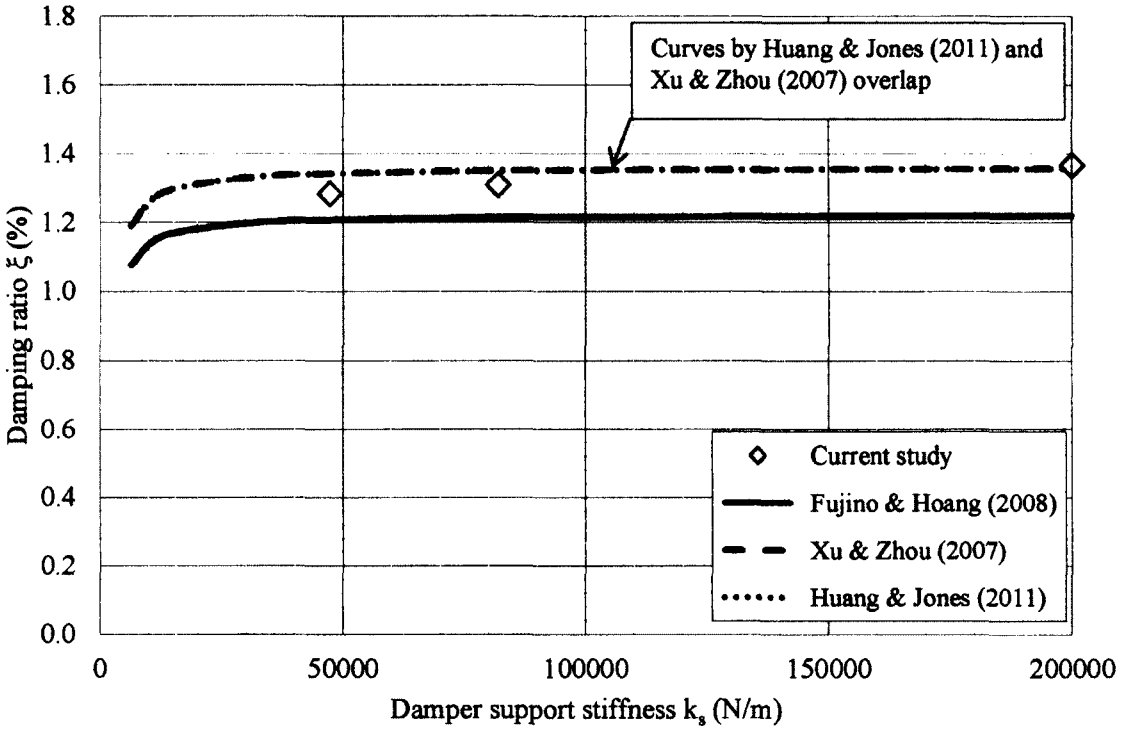

Figure 3-21: Experimental results (6%L)

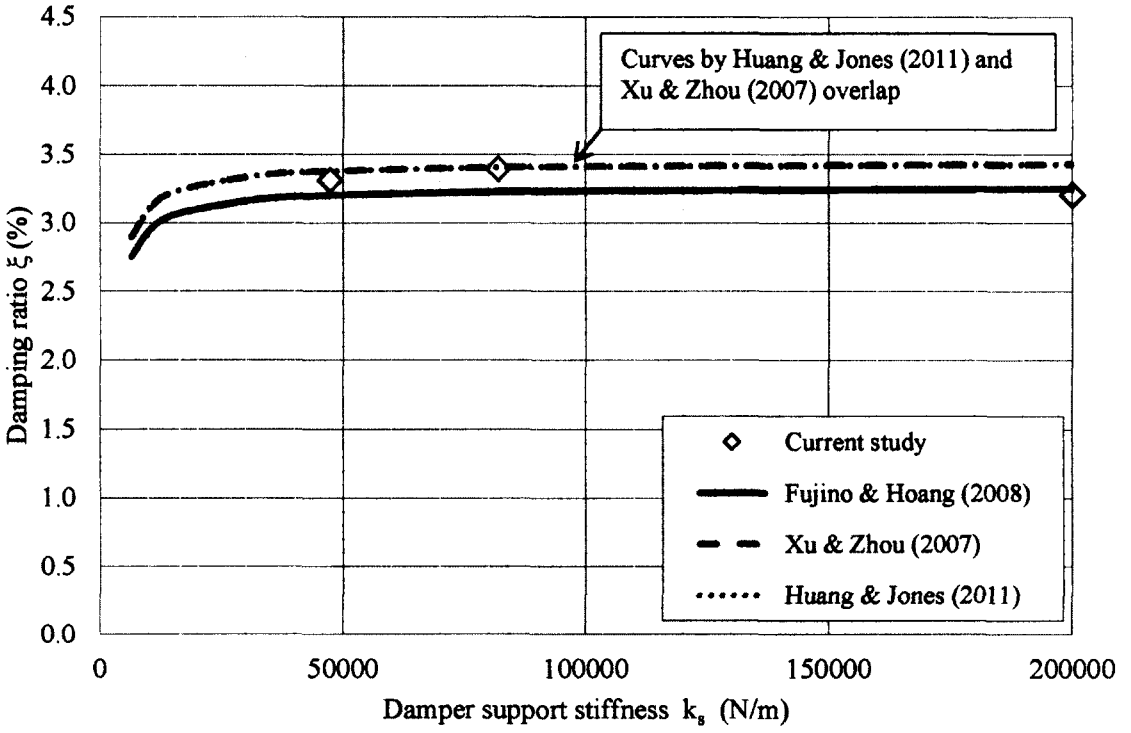

Figure 3-22: Experimental results (10%L)

In Figures 3-20 to 3-22, it may be seen that the damping ratio of the experimental results (and the modal damping ratios from literature) increase as the damper location is moved towards the mid-span of the cable. This pattern is well documented in literature (e.g. Cheng et al., 2010). As the damper is installed closer to the mid-span of the cable, the transverse displacement undergone by the cable at the location of damper installation increases. This is the same displacement that the damper piston will be subjected to while attached to the cable at this location. The work W done by the damper on the cable may be simply expressed as $W = F_d d$, where F_d is the damper force and d is the cable displacement at the damper attachment point (point A in Figure 3-18). The damper force acts in the opposite direction as the displacement of the cable, therefore the work done by the damper is negative (or rather, dissipative). The negative work done by the damper on the cable increases as the displacement undergone at the cable-damper attachment point increases. Therefore, a greater amount of oscillation energy is removed from the cable as the damper location is closer to the mid-span of the cable. Work W may also be expressed as the net change in the kinetic energy KE, i.e. $W = \Delta KE$. An increase in negative work is equivalent to a larger negative change in kinetic energy in the cable at the point of damper installation. Therefore, when the damper is installed closer to the cable mid-span, more kinetic energy (or oscillation energy) is removed from the cable, resulting in a greater modal damping ratio.

The experimental results at the 4%L damper location, as given in Figure 3-20, are slightly below the damping ratio predicted using the formulae developed by Xu and Zhou (2007), Fujino and Hoang (2008), and Huang and Jones (2011). In the 6%L and 10%L damper locations, however, the current experimental data points lie in between the

damping ratio predictions of the formulae found in the literature (Figures 3-21 and 3-22). This discrepancy in the pattern of measured data may be attributed to small differences in the damper installation location, the shaker installation location, and the setting of cable pretension in different testing cases. The entire experimental setup of the cable-damper system was torn down and re-built between tests at each damper location. Although great care was taken to ensure uniform experimental practices during each testing session, small variations in damper location and cable tension, primarily, may have a noticeable effect on the resulting modal damping ratios.

Table 3-7 summarizes the values of modal damping ratio obtained experimentally in the current study as well as the values of modal damping ratio obtained using the formulae from literature using the same damper support stiffness. Table 3-8 summarizes the absolute percent difference between the modal damping ratios obtained in the current experimental study with those calculated using the equations from literature.

Table 3-7: Summary of modal damping ratios (%)

k_s (N/m)	Damper location											
	4%L				6%L				10%L			
	Current study	Fujino & Hoang (2008)	Xu & Zhou (2007)	Huang & Jones (2011)	Current study	Fujino & Hoang (2008)	Xu & Zhou (2007)	Huang & Jones (2011)	Current study	Fujino & Hoang (2008)	Xu & Zhou (2007)	Huang & Jones (2011)
47,300	0.457	0.522	0.618	0.618	1.284	1.208	1.342	1.342	3.312	3.200	3.377	3.377
82,000	0.471	0.524	0.620	0.620	1.311	1.215	1.351	1.351	3.397	3.227	3.407	3.407
Rigid	0.550	0.525	0.622	0.622	1.367	1.220	1.357	1.357	3.207	3.249	3.431	3.431

Table 3-8: Absolute percent different between current study results and those from literature (%)

k_s (N/m)	Damper location								
	4%L			6%L			10%L		
	Fujino & Hoang (2008)	Xu & Zhou (2007)	Huang & Jones (2011)	Fujino & Hoang (2008)	Xu & Zhou (2007)	Huang & Jones (2011)	Fujino & Hoang (2008)	Xu & Zhou (2007)	Huang & Jones (2011)
47,300	12.4	26	26.0	6.3	4.4	4.4	3.5	1.9	1.9
82,000	10.1	24.1	24.1	7.9	2.9	2.9	5.3	0.3	0.3
Rigid	4.7	11.6	11.6	12.1	0.7	0.7	1.3	6.5	6.5

The study conducted by Zhou (2005) proposed a formula that predicts the reduction in modal damping ratio attributed to damper stiffness. This reduction factor is inversely proportional to the nondimensional damper stiffness, indicating that the damper loses efficiency as damper stiffness increases. This formula neglects both cable sag and bending stiffness. The equation developed is the following:

$$R_{max} = \frac{1}{1 + \frac{kx_c}{H}} \tag{3.10}$$

where k is the damper stiffness (N/m), x_c is the damper location (m), and H is the cable pretension (N). R_{max} is the reduction factor to show how much modal damping ratio is reduced when considering damper stiffness. This equation makes no consideration for damper support stiffness. Only the change in modal damping ratio due to the existence of damper stiffness, with a rigid damper support, can be used for comparison. Therefore, the damper efficiency reduction due to damper stiffness observed in the current study was calculated and compared with the reduction factor computed from Eq. (3.10) by Zhou (2005). The reduction factors for the current study were calculated by using the following formula:

$$R = \frac{\xi_{k_d \neq 0}}{\xi_{k_d = 0}} \tag{3.11}$$

where R is the reduction factor, $\xi_{k_d=0}$ is the damping ratio of a testing case where no damper stiffness existed, and $\xi_{k_d \neq 0}$ is the damping ratio of a testing case of non-zero damper stiffness. Both of these damping ratios corresponded to a rigid damper support. For example, the testing case with the damper located at 4%L and damper stiffness of 0

and 280 N/m, the modal damping ratios obtained from the current experimental study are given in Table 3-9:

Table 3-9: Experimental modal damping ratios (%) (4%L, k_s = rigid)

Damper stiffness k_d (N/m)	Modal damping ratio ξ (%)
0	0.550
280	0.529

The damper efficiency reduction factor due to the existence of damper stiffness as 280 N/m can be computed from:

$$R = \left[\frac{0.529}{0.550}\right] = 0.962$$

The reduction factor was calculated for each combination of damper location and damper stiffness tested and the results are listed in Table 3-10 along with the reduction factor calculated using the formula proposed by Zhou (2005). The two sets of results are found to agree well with each other. The error is less than 6.5%. They are also presented graphically in Figures 3-23 and 3-24 for the convenience of comparison.

Table 3-10: Modal damping reduction factor comparison

Damper location	Damper stiffness (N/m)	R_{max} Current study	R_{max} Zhou (2005)	Error (%)*
4%L	280	0.962	0.968	0.62
	600	0.934	0.935	0.11
6%L	280	0.893	0.953	6.30
	600	0.872	0.905	3.65
10%L	280	0.955	0.924	3.35
	600	0.828	0.851	2.70

*Use Zhou (2005) as reference base

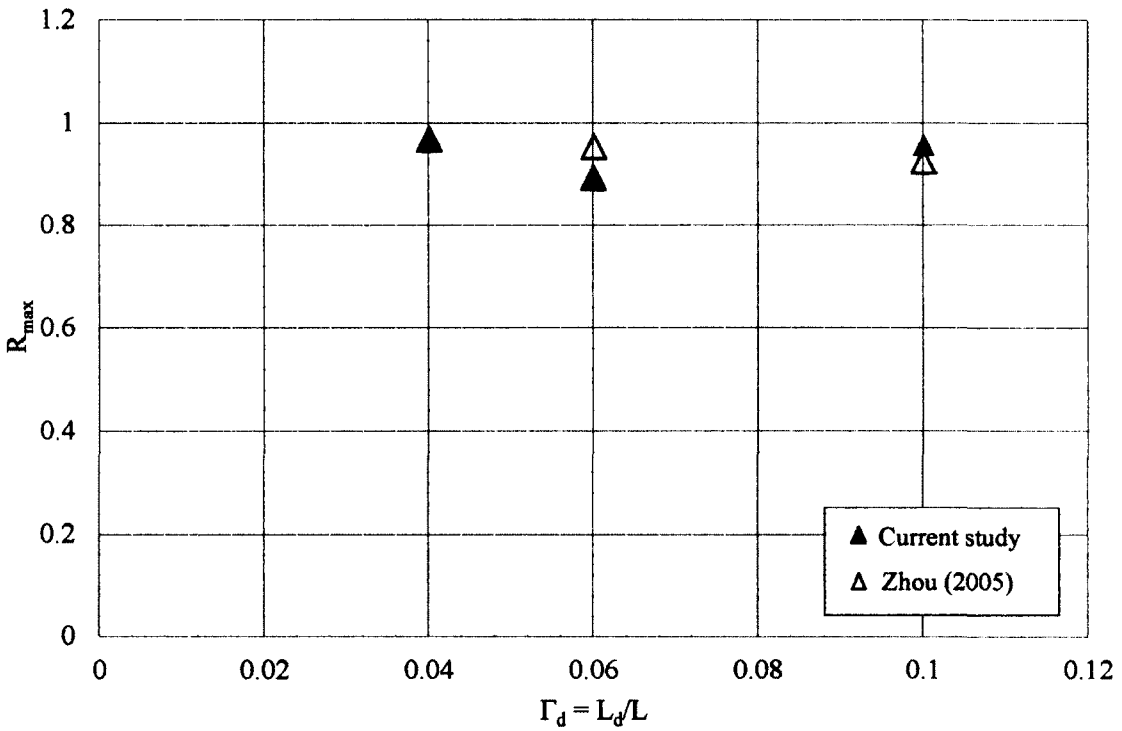

Figure 3-23: Reduction factor comparison (k_d = 280 N/m)

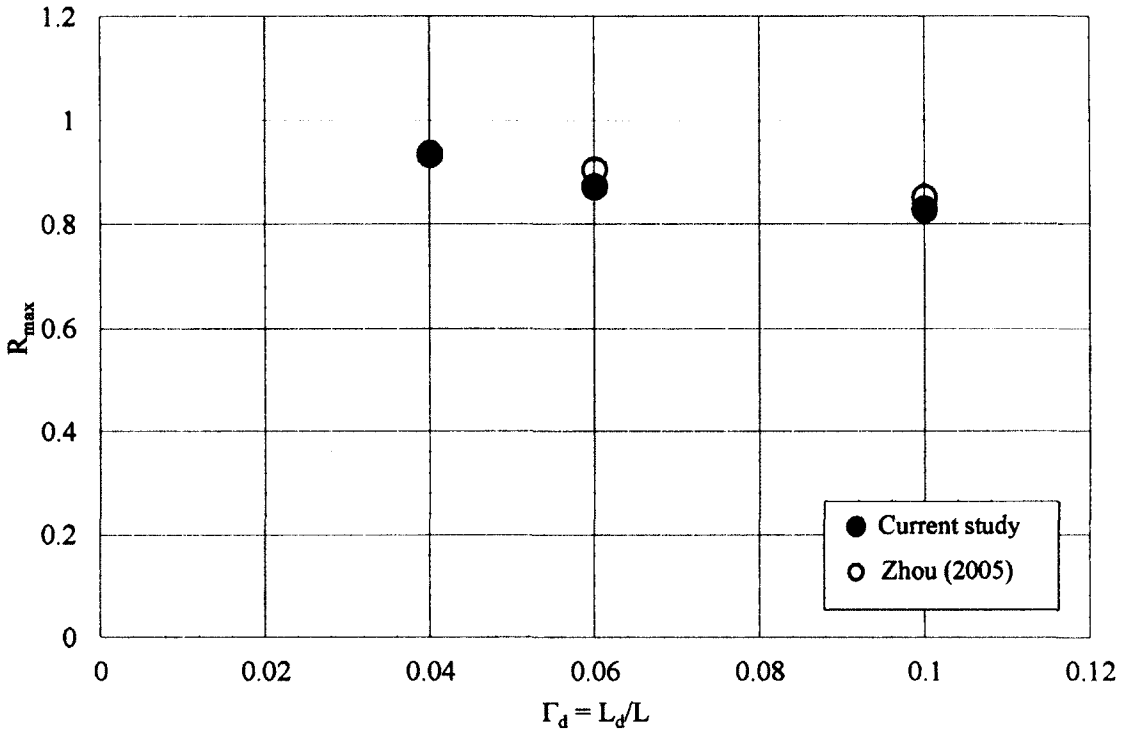

Figure 3-24: Reduction factor comparison (k_d = 600 N/m)

Chapter 4: Numerical Simulation

4.1 Finite element model

A 2D finite element model of the studied cable-damper system was analyzed using the ANSYS 14.0 commercial software. The model used was developed by Jiang (2006) and subsequently modified in the current study to include the damper stiffness and the damper support stiffness.

The cable was modeled using the element type PIPE59, which is an Immersed Pipe or Cable element type. This is a uniaxial element with six degrees-of-freedom at each node (both translation and rotation in the X, Y, and Z axes), as illustrated in Figure 4-1.

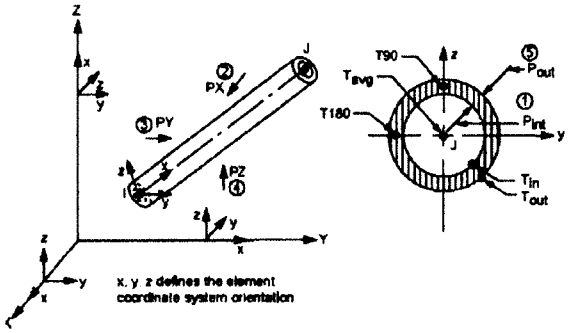

Figure 4-1: PIPE59 Element Geometry
(ANSYS 14.0 Documentation)

It is possible to use this element in tension, compression, torsion, and in bending, and it has stress stiffening and large deflection capabilities. The Real Constant No. 11, which is the initial strain in the axial direction, was utilized to apply the cable pretention of 3200 N. The initial strain was calculated using the formula relating the linear stress and strain, i.e. $\sigma = E\varepsilon$, where σ = axial stress (Pascal), E = Young's Modulus of the cable (Pascal), ε = strain (dimensionless). The axial stress may be calculated from the formula $\sigma = F/A$,

where F = cable pretention (N) and A = cable cross-sectional area (m^2). The material of the element was steel with a Young's Modulus of 200 GPa and the cable was modeled as solid by inputting a pipe wall thickness equal to the radius of the cable cross-section. The cable was fixed at both ends.

A sensitivity analysis was carried out for the purpose of selecting the optimum number of elements for the cable. A modal analysis of the cable-damper system was repeated, with the ANSYS software, using a different number of elements ranging from 50 to 500. The results are shown in Figure 4-2. A transient analysis of the cable-damper system was also repeated, with the ANSYS software, using a different number of elements ranging from 100 to 350 elements. The resulting equivalent modal damping ratio obtained through each transient analysis (the cable is divided into a different number of elements in each analysis) was compared with the equivalent modal damping ratio obtained using the formula developed by Fujino & Hoang (2008) (refer to Eq. (3.6)). The absolute percentage difference between the numerical simulation results and that obtained from the formula developed by Fujino & Hoang (2008) are shown in Figure 4-3.

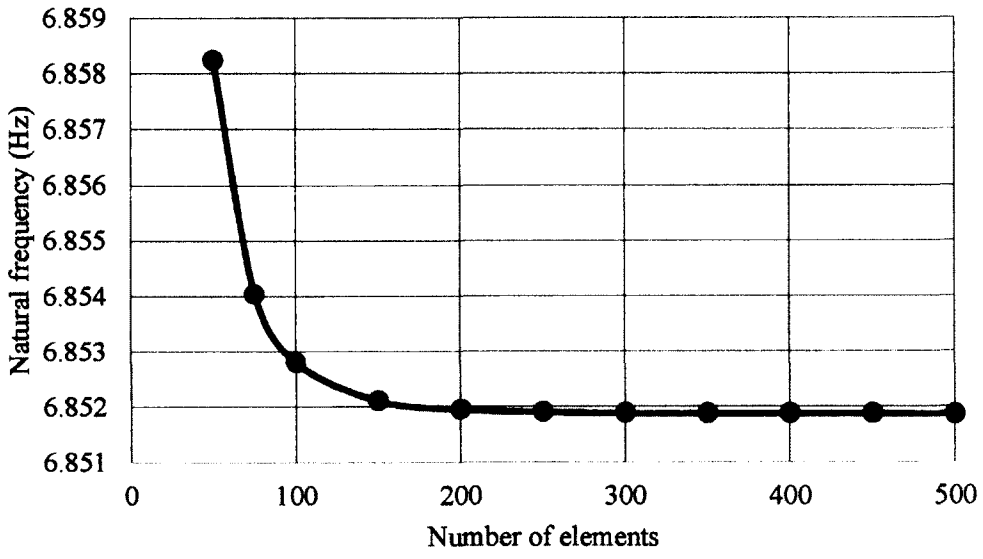

Figure 4-2: Natural frequency (Hz) vs. Number of elements graph

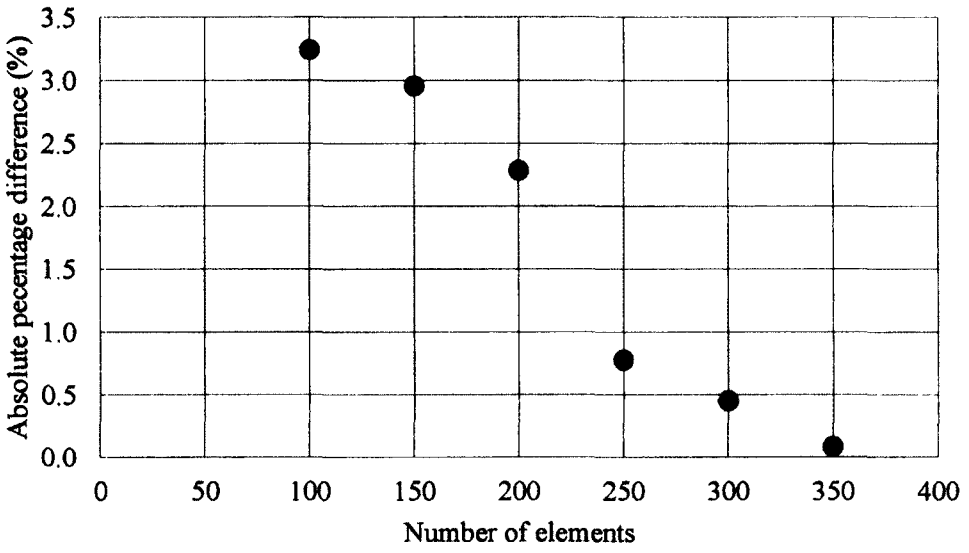

Figure 4-3: Absolute percentage difference vs. Number of elements graph

It can be seen from Figure 4-2 that the natural frequency of the cable approaches a constant value of 6.8519 Hz as the number of elements increase. This constant value is within 1.06% of the predicted theoretical value of 6.78 Hz, as was calculated previously from the formula: $f_1 = 1/(2L)\sqrt{T/m}$. The number of elements selected for this study was 200 because the natural frequency of the cable becomes constant at this value. It can be seen from Figure 4-3 that the absolute percentage difference between the damping ratio of the cable-damper system obtained from numerical simulation and the value obtained using the asymptotic formula developed by Fujino & Hoang (2008) decreases as the number of elements increase. When the number of elements is 200, the percentage difference between the two sets of data is less than 2.5%, which is acceptable. Therefore, considering both the accuracy requirement and computation time, it is decided to use 200 elements to simulate the cable in the numerical analysis.

The damper was modeled using the COMBIN14 Spring-Damper element type. This massless element was used as a longitudinal spring-damper (it has torsional spring-damper capabilities as well) connected transversely to the cable. This is a uniaxial tension-compression element with three degrees-of-freedom at each node (translation in the X, Y, and Z axes). COMBIN14 is a damper in parallel with a spring, as illustrated in Figure 4-4.

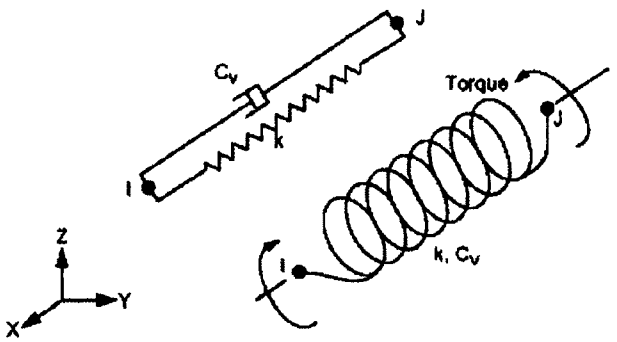

Figure 4-4: COMBIN14 Element geometry
(ANSYS 14.0 Documentation)

The damper coefficient is inputted with units of (force x time / length), or Ns/m if base units are used throughout (as was used in this study). The spring in this element is used to simulate the damper stiffness. The spring stiffness is inputted with units of (force / length), or N/m if base units are used throughout. A value of zero stiffness was used to simulate zero damper stiffness case and a nonzero value was used to simulate a specified damper stiffness. This element was modeled as fixed at its base node for simulations with infinite damper support stiffness and connected to a spring element (described subsequently) when simulating finite damper support stiffness.

The damper support stiffness was modeled as a spring in series with the damper and fixed to the ground at its base. A COMBIN14 element was used for this spring by

removing the damping property from the element, i.e. to input a very small value for the damping coefficient (<<1).

4.2 Numerical simulation

A modal analysis of the cable-damper system was conducted (developed by Jiang, 2006) to find the free vibration characteristics of the model cable, including its natural frequencies and the visualization of the corresponding mode shapes. This was done to verify that the cable properties were correctly inputted. The natural frequencies yielded from numerical simulations were compared to those calculated with the formula: $f_n = n/(2L)\sqrt{T/m}$. The mode shapes were visualized as being different from the ideal mode shapes of a vibrating string. This difference was caused by the attachment of the damper which holds the cable at its point of attachment. Figure 4-5 illustrates the deformed mode shapes that resulted from modal analysis of the cable-damper system. The damper in this figure is attached at 45% of the cable length to see the altered mode shape with greater ease. The modal analysis input file can be found in Appendix B.

a)

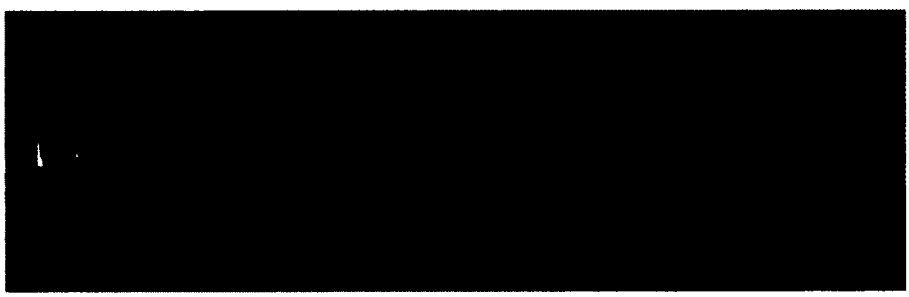

b)

Figure 4-5: Resulting mode shapes
a) Mode 1, b) Mode 2
(Damper located at 45%L, c = 133 Ns/m, rigid support, no damper stiffness)

A time-history (transient dynamic) analysis of the cable-damper system (developed by Jiang, 2006, and modified in this study) was performed to determine the dynamic response of the cable undergoing free vibration. To excite the first mode, the mid-span of the cable is displaced vertically downwards by 30 cm and the motion of the cable is recorded using an automatically generated time step (on the order of 10^{-3} seconds). The kinetic energy time-history of the mid-span node of the cable was outputted in a text file and subsequently copied into Microsoft Excel for further analysis. A sample of the data output is portrayed in Figure 4-6. The transient analysis input file can be found in Appendix C.

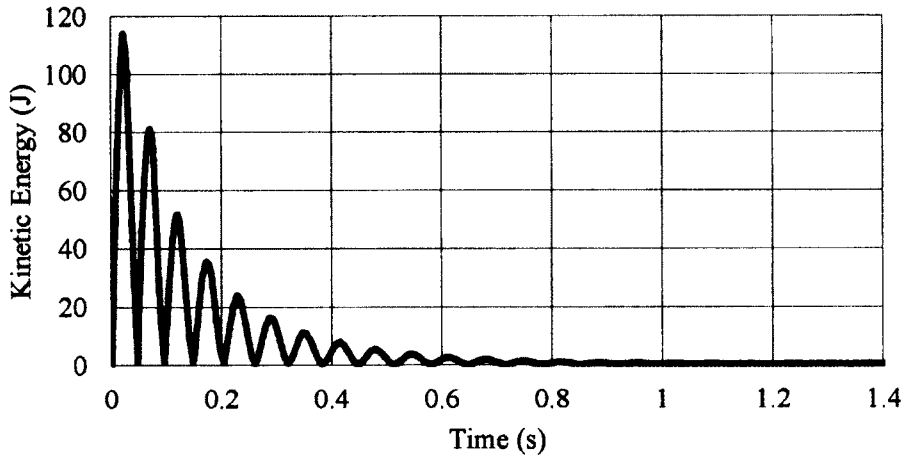

Figure 4-6: Sample kinetic energy time-history output
(Damper located at 10%L, c = 90 Ns/m, rigid support, no damper stiffness)

The energy-based approach for a linear viscous damper design, developed by Cheng et al. (2010), was used to calculate the cable damping ratio. The kinetic energy time-history output from the ANSYS finite element simulation is used in the calculation. The n^{th} modal damping ratio of a cable may be found using the following formulae:

$$\xi_n = -\frac{\ln(1-d_n)}{4\pi} \tag{4.1}$$

and

$$d_n = \frac{1}{j}\sum_{i=1}^{j} \frac{(E_{ki,n})_{max} - [E_{k(i+1),n}]_{max}}{[E_{ki,n}]_{max}} \tag{4.2}$$

where ξ_n is the damping ratio of the n^{th} mode, d_n is the kinetic energy decay ratio, and $E_{ki,n}$ is the maximum kinetic energy in the i^{th} cycle of the n^{th} modal vibration. There are two kinetic energy peaks within each vibration cycle. The first peak within each vibration cycle is selected as $E_{ki,n}$. Microsoft Excel is used to calculate Eq. (4.2) to yield the first modal damping ratio of the cable.

A sample data set will be presented to fully illustrate the procedure of the numerical simulation and the processing of the results. The sample data set presented has a damper with a damping coefficient of 90 Ns/m, located at 10% of the cable length from the cable end, with a damper stiffness of 0 N/m and a damper support stiffness of 200,000 N/m.

The system properties (damper coefficient, damper location, damper stiffness, and damper support stiffness) are first inputted into the time-history (transient analysis) command file (Appendix C). The simulation time must also be specified in the file. This command file was written in a text editor and saved with the filename extension ".inp". The ANSYS software is launched and the input file can be read directly by the software (File → Read input from...). The simulation begins immediately.

When the simulation is complete, the data results may be located. The kinetic energy time-history is automatically written to a file entitled "kinetic.txt", which will be located on the same hard drive that the program was launched on. This file contains two adjacent columns. The left column is the time (from zero to the simulation time specified in the input file). The right column is the corresponding kinetic energy of the node at the mid-span of the cable. These columns are copied into a Microsoft Excel file for processing.

The kinetic energy time history data is plotted in Microsoft Excel as a scatter plot with smooth lines, as shown in Figure 4-7. The peaks of the curve, marked with "X" on Figure 4-7, are found using an "IF" statement to display a kinetic energy value if it is greater than both the values that precede and follow it, for example

IF(AND(B3>=B4,B3>=B2),B3,NA()). These results are filtered using the Sort & Filter tool in the Data menu. This is to remove blank cells and cells that contain the #N/A error value, leaving the peak values as well as some non-peak values that also satisfy the IF statement. These are filtered manually. The peak kinetic energy values are listed in Table 4-1.

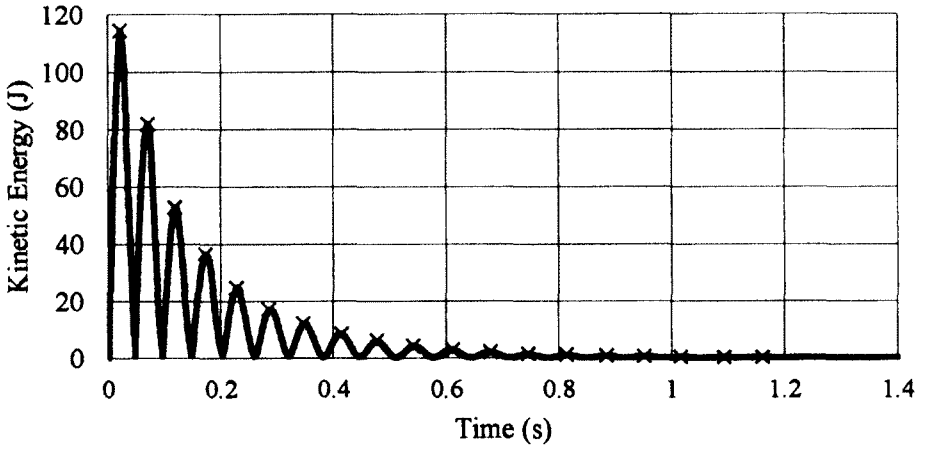

Figure 4-7: Kinetic energy time history

Table 4-1: Peak kinetic energy values

Cycle No.	Time (s)	Kinetic energy (J)
Cycle 1	0.022033	114.487
	0.070633	81.951
Cycle 2	0.118602	52.797
	0.172833	36.577
Cycle 3	0.227494	24.993
	0.285925	17.158
Cycle 4	0.346197	11.982
	0.414098	8.438
Cycle 5	0.476658	5.991
	0.540973	4.252
Cycle 6	0.611124	3.031
	0.67778	2.225
Cycle 7	0.745522	1.674
	0.812967	1.232
Cycle 8	0.884121	0.958
	0.951216	0.753
Cycle 9	1.015813	0.641
	1.092529	0.487
Cycle 10	1.160843	0.444

Each vibration cycle has two kinetic-energy peaks: kinetic energy is maximum when cable passes through its point of zero displacement (velocity is maximum) both when its velocity is positive directed upwards and positive directed downwards. The first peak of each vibration cycle is used in the energy-based approach developed by Cheng et al. (2010). The kinetic energy decay ratio (d_n) associated with the first mode (fundamental mode) of the damped cable is calculated, using Eq. (4.2), followed by the determination of the first modal damping ratio (ζ) based on Eq. (4.1), i.e.

$$d_1 = \frac{1}{9}\left[\frac{114.487 - 52.797}{114.487} + \frac{52.797 - 24.993}{52.797} + \frac{24.993 - 11.982}{24.993} + \frac{11.982 - 5.991}{11.982} + \frac{5.991 - 3.031}{5.991} + \frac{3.031 - 1.674}{3.031} + \frac{1.674 - 0.958}{1.674} + \frac{0.958 - 0.641}{0.958} + \frac{0.641 - 0.444}{0.641}\right]$$

$$= 0.454791486$$

and $\xi_1 = -\ln(1 - d_1)/4\pi$

$= -\ln(1 - 0.454791486)/4\pi$

$= 0.04827$ or 4.827 %

The first modal damping ratio (ξ) of this sample case is determined to be 4.827 %.

4.3 Numerical results

Table 4-2 summarizes the values of the damper damping coefficient, the damper stiffness, the damper support stiffness, and the damper location that have been simulated. Numerical simulations for each damper location were subdivided into four cases, which are summarized in Table 4-3. The results of the 6%*L* damper location will be presented in this section. The results of the 4%*L* and 10%*L* damper locations can be found in Appendix D.

Table 4-2: Parameter values used in the numerical study

Parameter	Tested Values							
Damper damping coefficient c (Ns/m)	18.4	32.2	46.7	70.3	90	164.8	275.5	500
Dimensionless damping coefficient Ψ	0.73	1.27	1.85	2.79	3.56	6.51	10.89	19.76
Damper location L_d	4%L, 6%L, 10%L							
Damper stiffness k_d (N/m)	0, 280, 600							
Dimensionless damper stiffness K_d	4%L: 0, 0.03, 0.07 6%L: 0, 0.05, 0.10 10%L: 0, 0.08, 0.17							
Damper support stiffness k_s (N/m)	47300, 82000, 100000, 200000, 300000, rigid							
Dimensionless damper support stiffness K_s	4%L: 5.5, 9.6, 11.7, 23.3, 35.0, rigid 6%L: 8.3, 14.3, 17.5, 35.0, 52.5, rigid 10%L: 13.8, 23.9, 29.2, 58.3, 87.5, rigid							

Table 4-3: Numerical simulations cases

Testing Case	k_s	k_d
1	rigid	0
2	not rigid	0
3	rigid	$\neq 0$
4	not rigid	$\neq 0$

a) Testing case 1: k_s = rigid, $k_d = 0$

The first numerical simulation case has a rigid damper support stiffness and a negligible damper stiffness. This is therefore an ideal cable-damper system assumed in the majority of the existing studies. The numerical simulation results for the 6%L damper

location are shown in Figure 4-8, along with three other curves based on formulae proposed in literature, i.e. the formula developed by Huang & Jones (2011), the asymptotic formula developed by Fujino & Hoang (2008), and the formula developed by Xu & Zhou (2007). The rigid damper support stiffness condition is applied to all three formulae. These curves are used to compare with the numerical simulation results to verify both the pattern and accuracy. It can be seen from Figure 4-8 that the numerical results obtained from the current study agree well with the three analytical curves. All plots are displayed in terms of nondimensional quantities. The nondimensional damping parameter (Ψ) is calculated using the formula $\Psi = (\pi c)/(mL\omega_{1s})$, where $\omega_{1s} = (\pi/L)\sqrt{H/m}$ is the fundamental modal frequency of a taut string equivalent to the cable. The nondimensional damper location (Γ_d) is calculated using the formula $\Gamma_d = x_c/L$. The nondimensional damper stiffness (K_d) and the nondimensional damper support stiffness (K_s) can be calculated using the formulae $K_d = x_c k_d/H$ and $K_s = x_c k_s/H$.

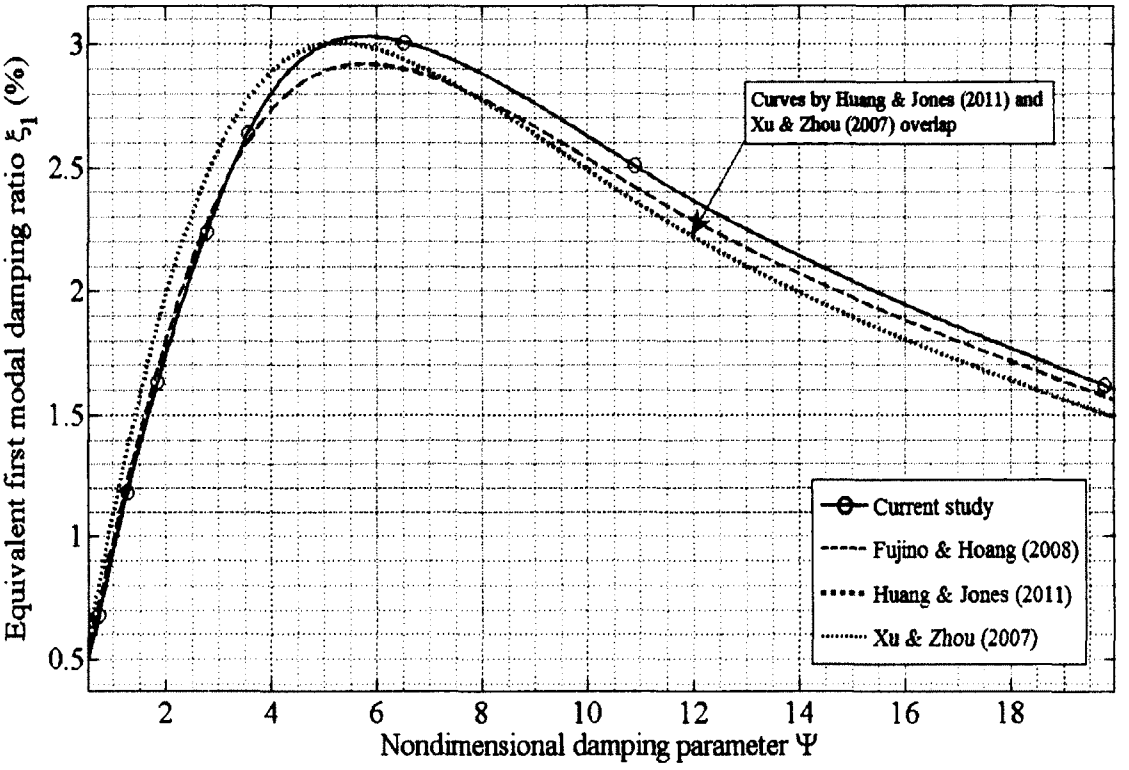

Figure 4-8: Relation between equivalent first modal damping ratio and damper size at Γ_d= 0.06 (Rigid damper support and no damper stiffness)

b) Testing case 2: $k_s \neq$ rigid, $k_d = 0$

The second testing case investigates the effect of damper support stiffness on the performance of an external linear viscous damper. In this case, the damper support stiffness is changed in each simulation using the values listed in Table 4-2, whereas the damper stiffness remains zero. The results are portrayed in Figure 4-9, with each curve corresponding to one specific damper support stiffness. For comparison, results of the rigid damper support are also shown in the same figure. The trend seen in the numerical simulation results is that if dampers of the same size (damping coefficient) but different damper support stiffness were attached to the same cable at the same location, the modal damping ratio of the cable-damper system would increase as the damper support stiffness increases. This trend is the same as that reported in previous studies (Xu and Zhou, 2007;

Fujino and Hoang, 2008; Huang and Jones, 2011). This effect is a result of the influence that the damper support has on the damping force exerted by the damper. The damping force (F_d) that a linear viscous damper can generate is equal to the damper coefficient (c) multiplied by the relative velocity between the damper-cable connection (V_A) and the damper base (V_B) (refer to Eq. (3.1)). In the case of a rigid support (refer to Figure 3-18), the base of the damper is immobile. Therefore, the velocity of the damper base is zero and the damping force is maximized. Conversely, a finite damper support (refer to Figure 3-19) would result in a decreased damping force because the motion of the damper base is not zero and the relative motion between the two damper extremities is decreased. This indicates that to install a linear viscous damper on a cable-stayed bridge closer to the cable mid-span, better cable vibration control effect can be achieved by using a more rigid supporting structure.

The resulting curves also show that the optimum nondimensional damping parameter changes as the damper support stiffness varies. An increase in damper support stiffness results in a higher value of the optimum nondimensional damping parameter. In other words, when the damper installation location is determined, to achieve the best effect of suppressing cable vibrations, the optimum size of a linear viscous damper would be larger if it will be attached to a more rigid damper support. For example, for the 6%L damper location, the tested variation in damper support stiffness resulted in a range of optimum damper coefficients from 128 Ns/m (when k_s = 47,300 N/m) to 146 Ns/m (when k_s was rigid). This trend is the same as that found in using the formula developed by Fujino and Hoang (2008) when varying the damper support stiffness.

In order to examine the accuracy of the numerical simulation results, each curve in Figure 4-9 was compared separately with the analytical formulae developed by Xu & Zhou (2007), Fujino and Hoang (2008), and Huang and Jones (2011), as was done for the first testing case. These plots are shown in Figures 4-10 to 4-14. Comparison of the four sets of data presented in these five figures show that all of the numerical simulation results agree well with the analytical ones. The results from the current study are most similar to those produced using the asymptotic formula developed by Fujino & Hoang (2008) (refer to Eq. (3.1)). This formula includes the effects of cable sag, flexural rigidity, as well as damper support stiffness, and therefore most closely resembles the parameters that have been considered in the current study. The results produced using the formulae developed by both Xu and Zhou (2007) as well as Huang and Jones (2011) predict a slightly higher equivalent first modal damping ratio in the lower range of damper coefficients, and a slightly lower equivalent first modal damping ratio in the higher range of damper coefficients. This may be attributed to the taut cable assumption that these formulae are based on, of which cable sag and bending stiffness have been neglected when deriving these formulae. It is reasonable that the curves produced by these two formulae, which are based on the same assumptions, overlap.

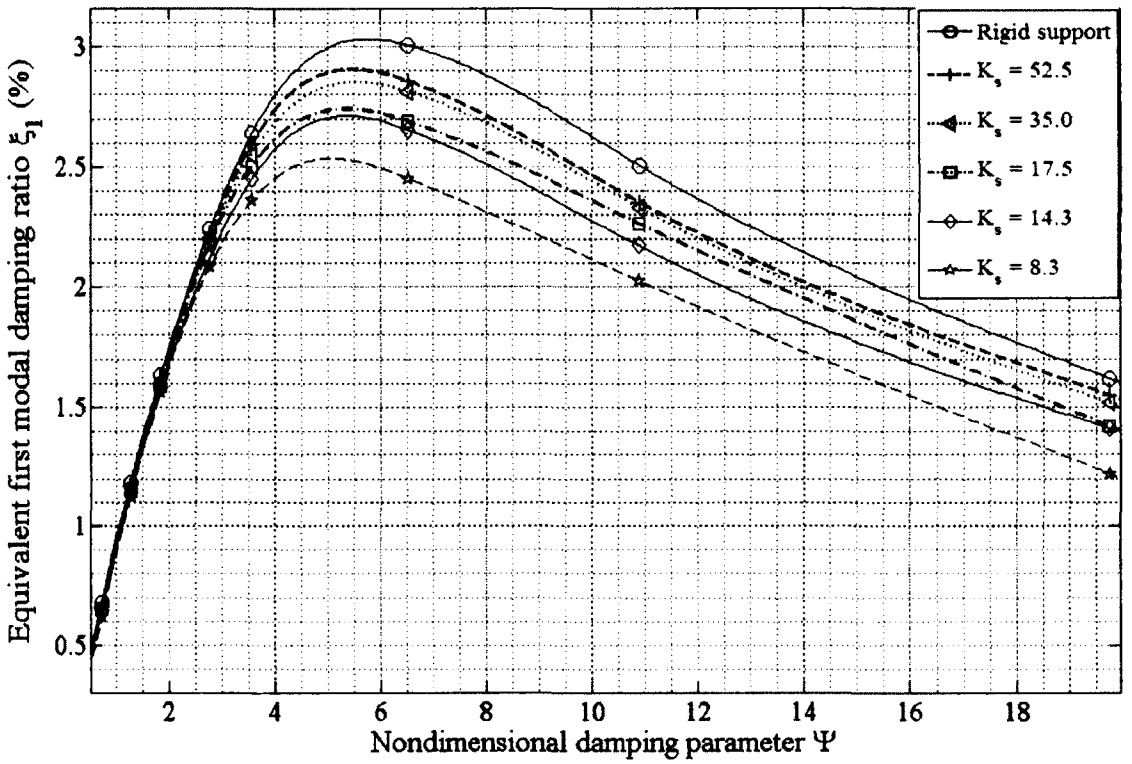

Figure 4-9: Effect of damper support stiffness ($\Gamma_d = 0.06$)

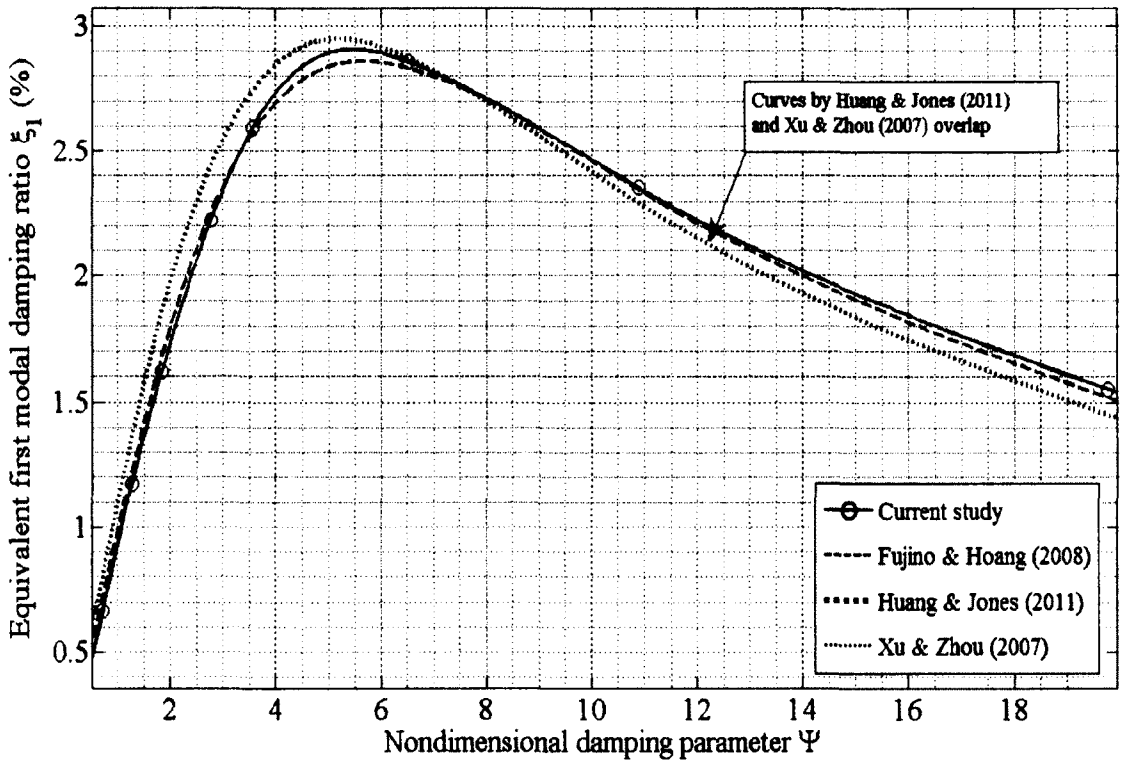

Figure 4-10: Effect of damper support stiffness ($K_s = 52.2$, $\Gamma_d = 0.06$)

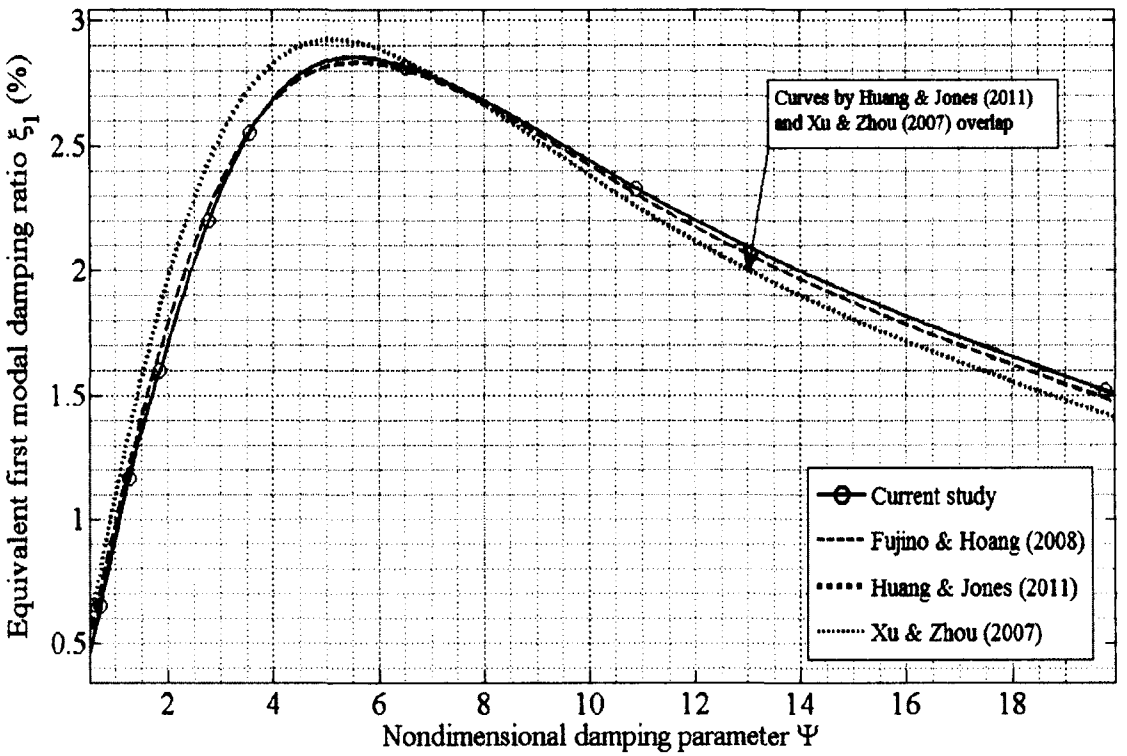

Figure 4-11: Effect of damper support stiffness ($K_s = 35.0$, $\Gamma_d = 0.06$)

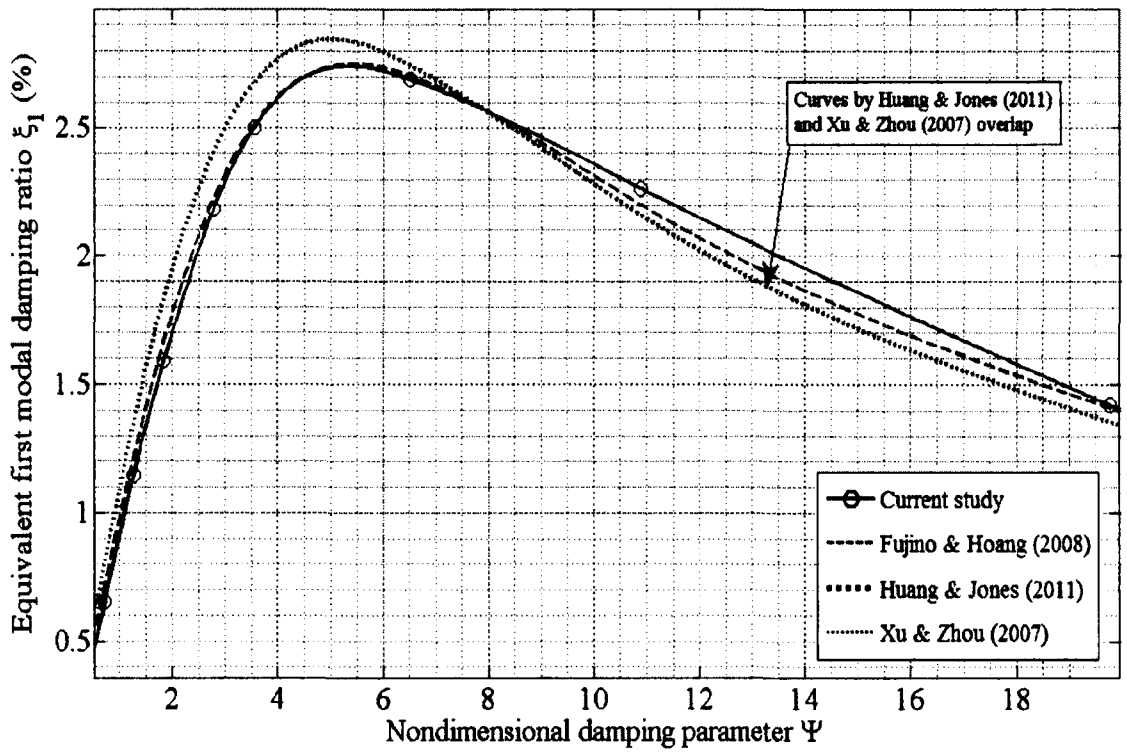

Figure 4-12: Effect of damper support stiffness ($K_s = 17.5$, $\Gamma_d = 0.06$)

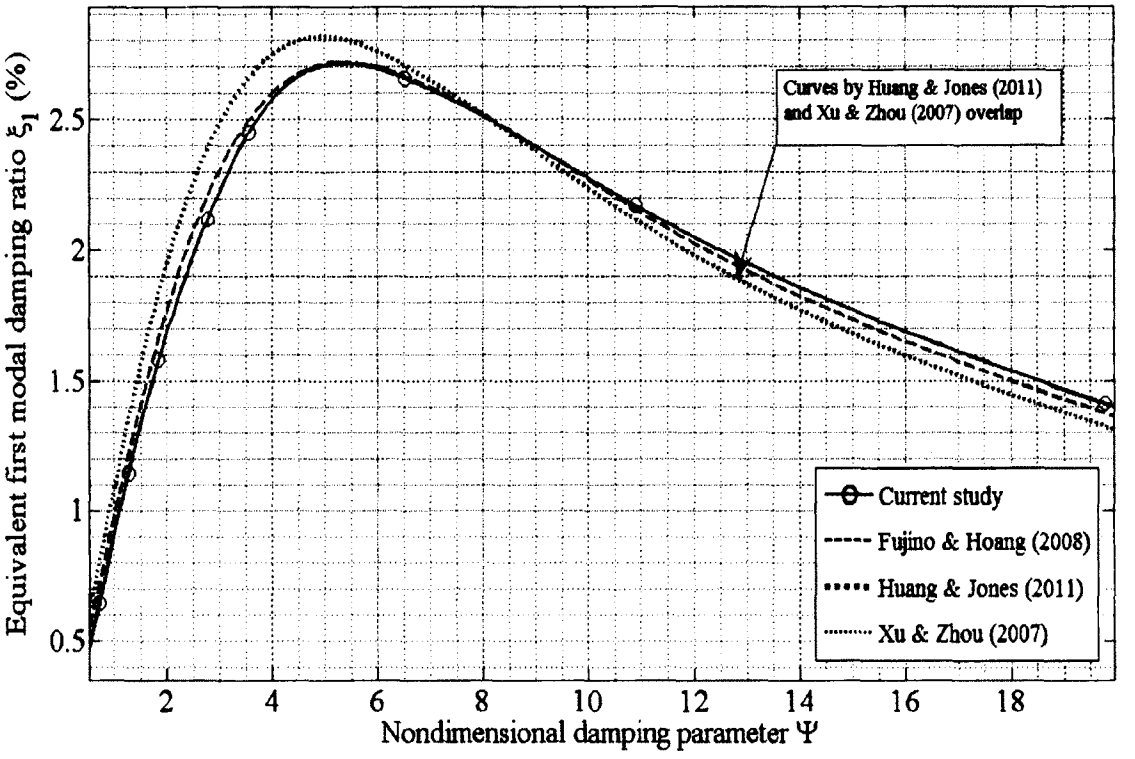

Figure 4-13: Effect of damper support stiffness ($K_s = 14.3$, $\Gamma_d = 0.06$)

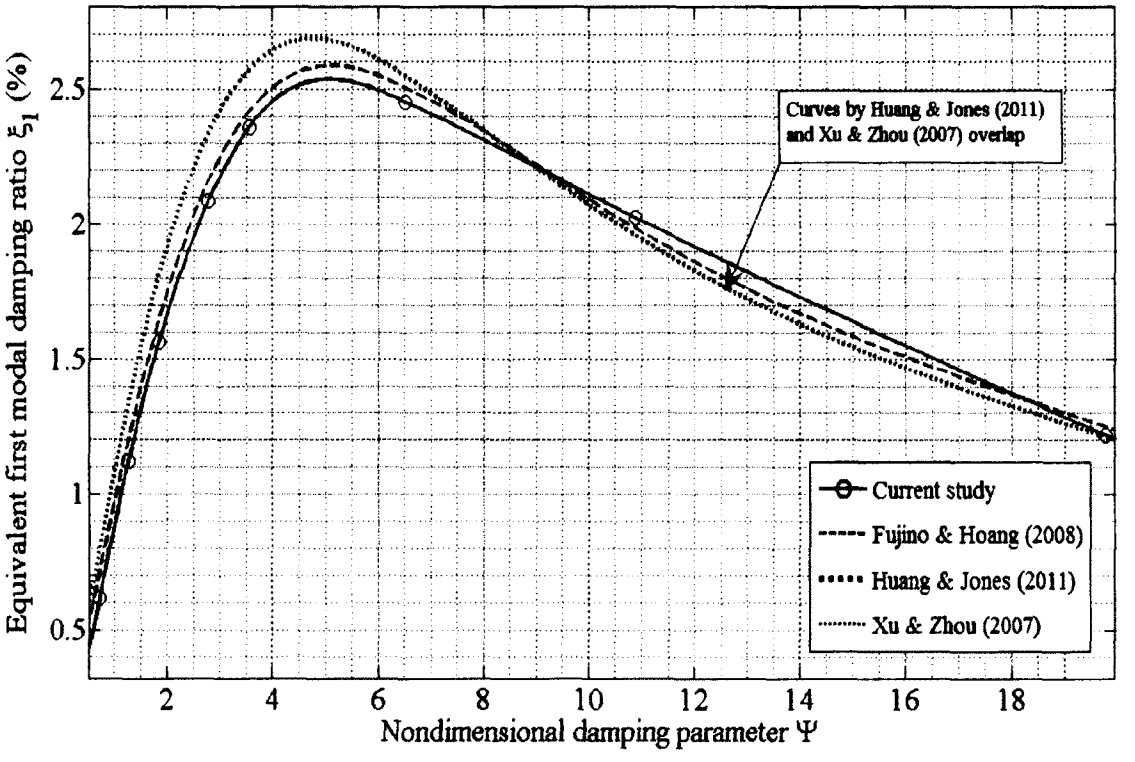

Figure 4-14: Effect of damper support stiffness ($K_s = 8.3$, $\Gamma_d = 0.06$)

c) Testing case 3: k_s = rigid, $k_d \neq 0$

The third testing case investigates the effect of damper stiffness on the performance of an external linear viscous damper. In this case, the different values of damper stiffness listed in Table 4-2 are used in each simulation, whereas the damper support stiffness remains rigid. The resulting curves corresponding to each damper support stiffness are displayed in Figure 4-15, along with the results of the rigid support stiffness case from the first testing case. The numerical simulation results suggest that the modal damping ratio would decrease if the damper stiffness increases. This trend is consistent with that reported in previous studies (Zhou, 2005; Huang, 2011). Conceptually, this case is similar to that of the second numerical simulation testing case. The existence of damper stiffness will reduce the efficiency of a damper because part of the energy that transferred from the oscillating cable to the damper will be converted to elastic energy through damper stiffness and feed back to the cable during the periodical motion of the cable-damper attachment point. Without the existence of damper stiffness, this fraction of energy would have otherwise been more efficiently dissipated through the damping mechanism of the damper. Therefore, a damper without damper stiffness will provide better control of stay cable vibrations compared to a damper with certain damper stiffness.

The resulting curves also show that the optimum nondimensional damping parameter varies as the damper stiffness changes. In Figure 4-15, the optimum nondimensional damping parameters of the three curves shown are 5.76, 6.21, and 6.29 for the nondimensional damper stiffness' of 0, 0.05, and 0.10, respectively. In other words, at the damper location of 6%L, the damper sizes of 145.7 Ns/m, 157.1 Ns/m, and 159.1

Ns/m were found to be optimum when the damper had stiffness' of 0 N/m, 280 N/m, and 600 N/m. An increase in damper stiffness results in a higher value of the optimum nondimensional damping parameter. This means that a damper of a larger size will be required for optimal performance when the stiffness of a damper is increased. The formula for predicting the optimum damping parameter proposed by Zhou (2005) gives the same trend.

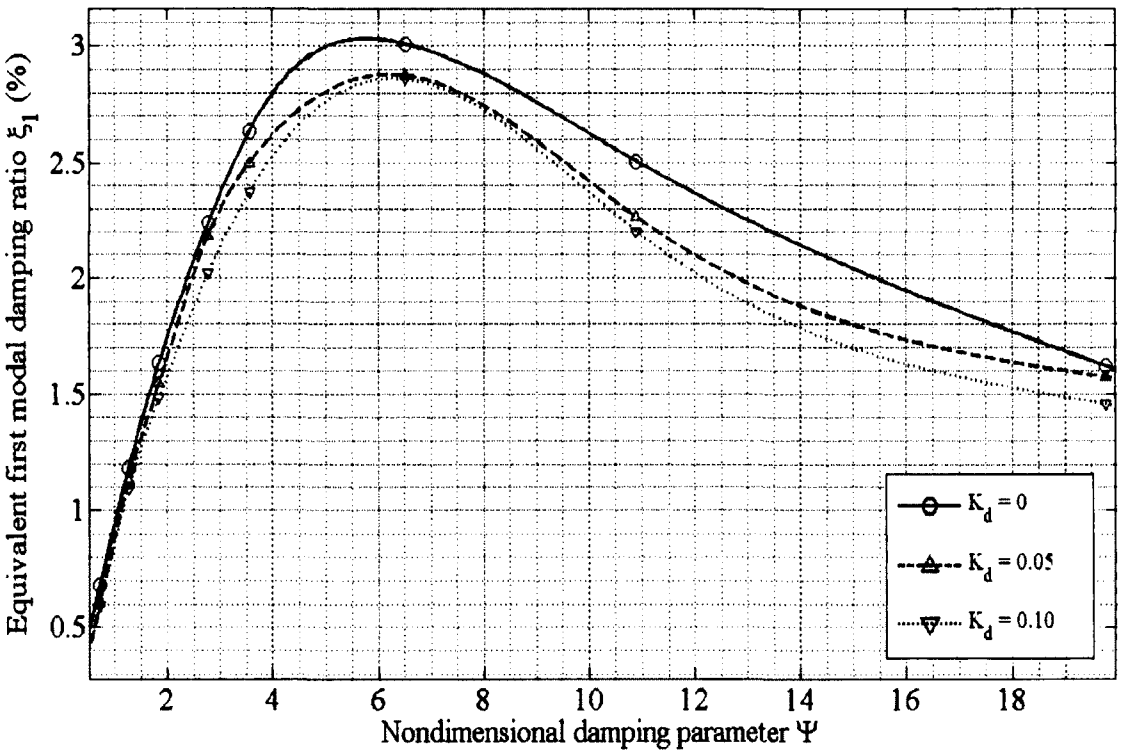

Figure 4-15: Effect of damper stiffness ($\Gamma_d = 0.06$)

In order to confirm the accuracy of the numerical simulation results, the modal damping ratio reduction factors computed from the simulated data sets were compared to the reduction factors calculated using the formula proposed by Zhou (2005) (refer to Eq. (3.2)). The following formula was used to calculate the reduction factor for a simulated set of results from the current study:

$$R = \frac{1}{8}\sum_{i=1}^{8}\frac{\xi_{i,k_d\neq 0}}{\xi_{i,k_d=0}} \tag{4.3}$$

where R is the reduction factor of a set of results at a particular damper stiffness value. The ratio between the modal damping ratio of the non-zero damper stiffness condition ($\xi_{i,k_d\neq 0}$) (the third testing case) and that of the zero damper stiffness condition ($\xi_{i,k_d=0}$) (the first testing case) is calculated for each of the eight damper damping coefficients listed in Table 4-2. The average of these eight ratios is taken, yielding the reduction factor corresponding to a specific damper stiffness to be compared with the formula proposed by Zhou (2005). A sample calculation for the reduction factor based on the results of the current study at a damper stiffness of 280 N/m (K_d = 0.05) will be presented here. The simulated modal damping ratios for the first testing case as well as those for the third testing case (k_d = 280 N/m, K_d = 0.05) are listed in Table 4-4.

Table 4-4: Current study modal damping ratios ($\Gamma_d = 0.06$)

Damping coefficient c (Ns/m)	$\xi_{k_d=0}$ (%)	$\xi_{k_d=280\ N/m}$ (%)
18.4	0.679	0.606
32.2	1.182	1.130
46.7	1.635	1.546
70.3	2.240	2.186
90	2.637	2.500
164.8	3.007	2.873
275.5	2.506	2.263
500	1.620	1.572

The reduction factor calculation for the case of damper stiffness of 280 N/m when the damper was located at 6%*L* from the cable end is the following:

$$R = \frac{1}{8}\left[\frac{0.606}{0.679} + \frac{1.130}{1.182} + \frac{1.546}{1.635} + \frac{2.186}{2.240} + \frac{2.500}{2.637} + \frac{2.873}{3.007} + \frac{2.263}{2.506} + \frac{1.572}{1.620}\right] = 0.943$$

This value was compared with the reduction factor calculated using the formula proposed by Zhou (2005) using the same damper stiffness (280 N/m) and damper location (6% of the 9.33 m long cable, which is a distance of 0.5598 m):

$$R_{max} = \frac{1}{1 + \frac{kx_c}{H}} = \frac{1}{1 + \frac{(280\frac{N}{m})(0.5598\ m)}{3200\ N}} = 0.953$$

Table 4-5 compares the reduction factors corresponding to the simulated damper stiffness with those calculated using the formula developed by Zhou (2005). It can be seen that the two sets of results agree well with each other.

Table 4-5: Comparison of modal damping ratio reduction factor

Dimensionless damper stiffness (K_d)	Reduction factor		
	Current study	Zhou (2005)	Absolute percentage difference (%)*
0.05	0.943	0.953	1.05
0.10	0.904	0.905	0.11

*Use Zhou (2005) as reference base

d) Testing case 4: $k_s \neq$ rigid, $k_d \neq 0$

The fourth testing case investigates the combined effects of damper stiffness and damper support stiffness on the performance of an external linear viscous damper. In this case, both the damper stiffness and the damper support stiffness are varied. Results corresponding to the case of damper stiffness $K_d = 0.05$ and varying damper support stiffness are displayed in Figure 4-16, and those plotted for the damper stiffness of $K_d = 0.10$ and varying damper support stiffness are shown in Figure 4-17. Both of these two plots manifest a similar pattern as to how the optimum damping coefficient and the corresponding maximum achievable damping ratio vary as the studied parameters change. When considering both k_s and k_d, the curves in Figures 4-16 and 4-17 have the same pattern as the ideal case when no damper stiffness exists and the damper support stiffness is rigid. At each damper location, an optimum damper size exists, which can provide the maximum achievable damping ratio for that damper location. The values of optimum

damping parameter and their corresponding maximum achievable damping ratios obtained from the simulations for the current study for the fourth testing case are listed in Tables 4-6 and 4-7, respectively.

Table 4-6: Optimum nondimensional damping parameters (testing case 4 of the current study)

Dimensionless damper support stiffness K_s	$K_d = 0$	$K_d = 0.05$	$K_d = 0.10$
8.3	5.07	4.89	5.18
14.3	5.36	5.15	5.75
17.5	5.35	5.46	5.85
35.0	5.54	5.62	6.15
52.5	5.47	6.20	5.73
rigid	5.76	6.21	6.29

Table 4-7: Maximum achievable damping ratio (%) (testing case 4 of the current study)

Dimensionless damper support stiffness K_s	$K_d = 0$	$K_d = 0.05$	$K_d = 0.10$
8.3	2.54	2.48	2.33
14.3	2.71	2.60	2.42
17.5	2.74	2.64	2.5
35.0	2.85	2.67	2.6
52.5	2.91	2.76	2.66
rigid	3.03	2.88	2.86

The results in Table 4-6 show the general pattern of how the optimum damper size is affected by the change in both damper stiffness and damper support stiffness. Observing from left to right across the table, it can be seen that an increase in damper stiffness generally causes an increase in the optimum damper size. Observing from top to bottom down the table, results show that an increase in damper support stiffness also causes an increase in the optimum damper size. These individual effects of damper stiffness and damper support stiffness on the optimum damper size are the same as those seen in the previous two testing cases. The same combined effects of damper stiffness and damper support stiffness are also seen in the cases of 4%L and 10% L damper locations, the graphs of which can be found in Appendix D.

With respect to the maximum achievable damping ratio, observing from left to right across Table 4-7, an increase in damper stiffness is found to result in a decreased maximum achievable damping ratio. Observing from top to bottom down the same table shows a trend where increased damper support stiffness leads to a higher maximum achievable damping ratio. This is a reasonable trend, reflecting both the individual effects of damper stiffness and damper support stiffness. Both of these two parameters, an increase in the former and a decrease in the latter, cause a decrease in damping ratio individually. Therefore, it is reasonable that their combined effect follows the same trend.

In order to maximize damper performance when damper stiffness exists, a larger damper size may be required in order to have a larger damping force to counteract the effects of damper stiffness. This may account for the trend observed when damper stiffness exists. When damper support stiffness increases, the damping force is

maximized due to the more rigid condition of the damper base (point B in Figure 3-18), causing a larger velocity difference between the top and the base of the damper. A larger damper force as damper support stiffness increases will yield a larger damping ratio. This ability to maximize damping force through the means of damper size and relative velocity between the two extremities of the damper may explain the trend of an increased optimum damper size with an increasingly rigid damper support. From the above observation, it can be concluded that to have the maximum possible cable vibration control when using a linear viscous damper, the damper stiffness should be minimized and the damper support stiffness should be maximized.

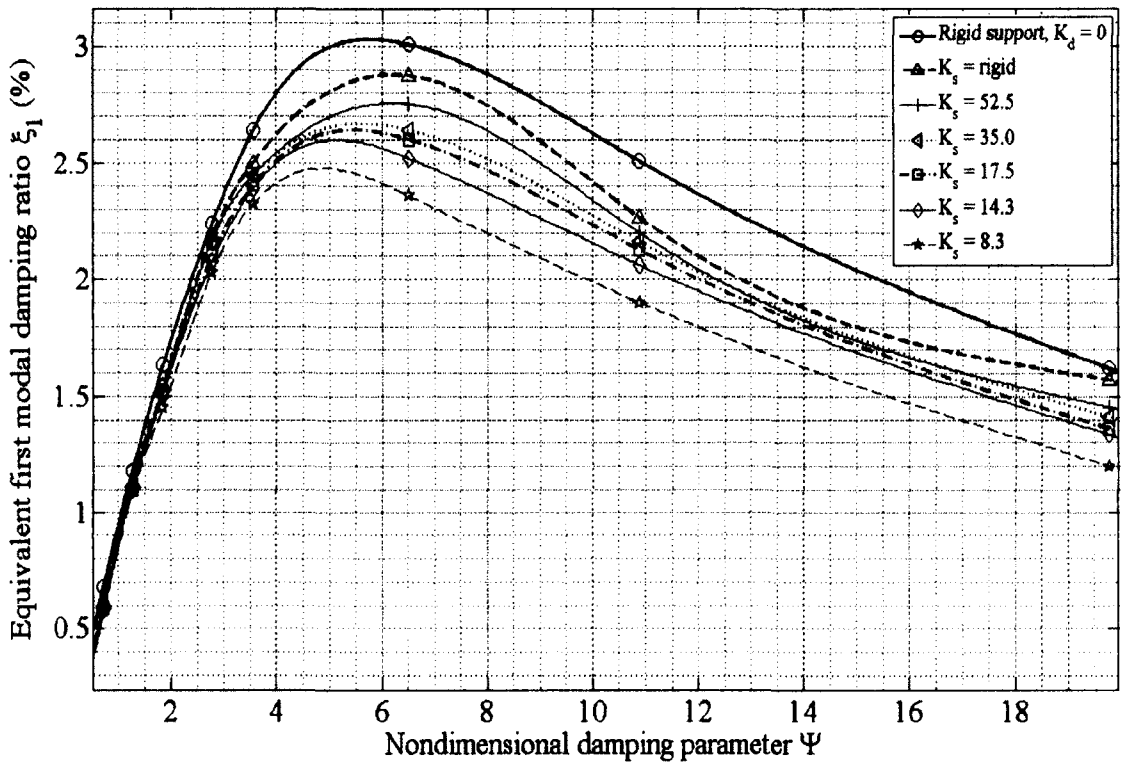

Figure 4-16: Combined effect of damper stiffness and damper support stiffness ($K_d = 0.05, \Gamma_d = 0.06$)

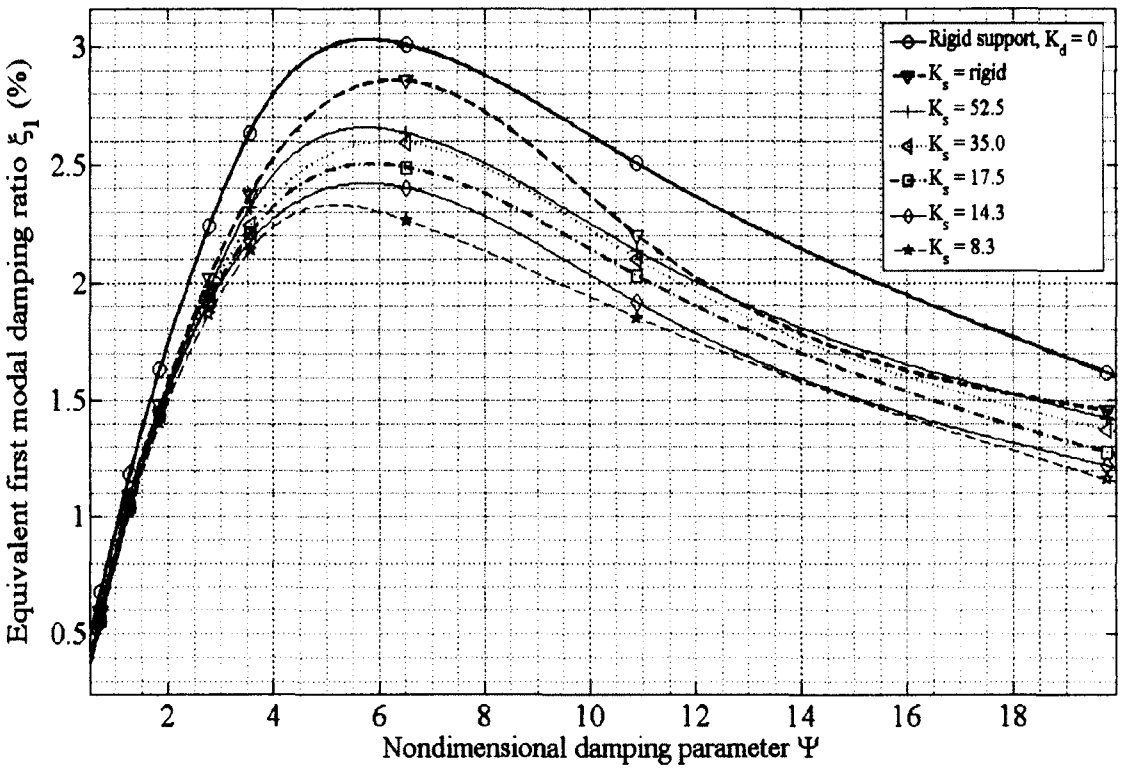

Figure 4-17: Combined effect of damper stiffness and damper support stiffness ($K_d = 0.10$, $\Gamma_d = 0.06$)

The numerical simulation results for the damper locations of 4%L and 10%L are given in Appendix D. The same trend with respect to the effects of damper stiffness and damper support stiffness on the damper size and the corresponding maximum achievable damping ratio can also be observed.

Chapter 5: Further Discussion on Results

5.1 Comparison of experimental and numerical results

The results from the current experimental study will be compared with those from the numerical simulations. Since, in the physical tests, only one damper size of c = 32.2 Ns/m was used, only the numerical simulation results with the same damper size will be used for comparison. Figures 5-1 to 5-3 show the experimental and numerical results under the conditions of damper size c = 32.2 Ns/m, zero damper stiffness, and respective damper location at 4%L, 6%L, and 10%L. In these figures, the results for the same cable-damper system condition using the formulae developed by Xu and Zhou (2007), Fujino and Hoang (2008), and Huang and Jones (2011) are also displayed for the convenience of comparison (refer to Section 3.4 for formulae usage details). As can be seen from these three figures, the experimental results are similar to those from the numerical study. They are most representative of the numerical simulation results when the damper is located closer to the end of the cable. A damper installation location within a few percent of the cable length is practiced most commonly on actual cable-stayed bridges. The numerical simulation results are accurate within a few percent to the solid line curve displaying the results using the formula developed by Fujino and Hoang (2008), which includes both damper support stiffness and cable bending stiffness. The curves depicting the results based on the formulae developed by Xu and Zhou (2007), and Huang and Jones (2011), which overlap with each other, overestimate the attainable damping ratio in the damped cable. This overestimation is attributed to the taut cable assumption used in the development of these formulae, where the effects of cable bending stiffness and cable sag were ignored.

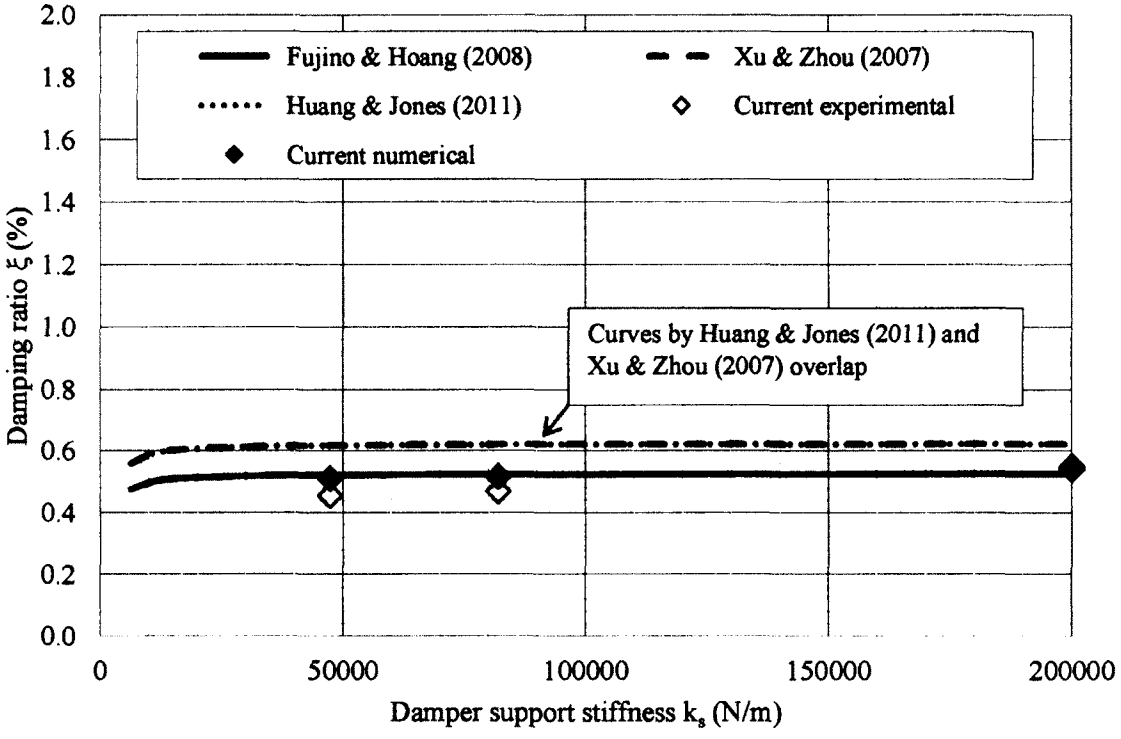

Figure 5-1: Experimental and numerical results (4%L, $k_d = 0$)

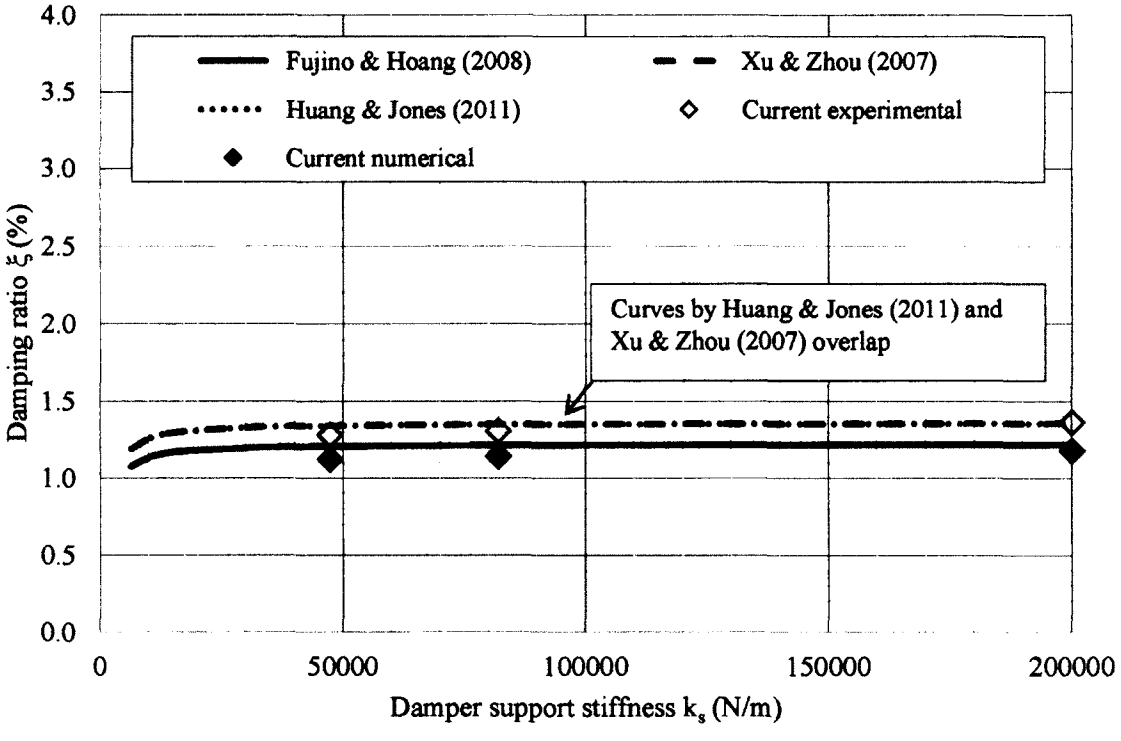

Figure 5-2: Experimental and numerical results (6%L, $k_d = 0$)

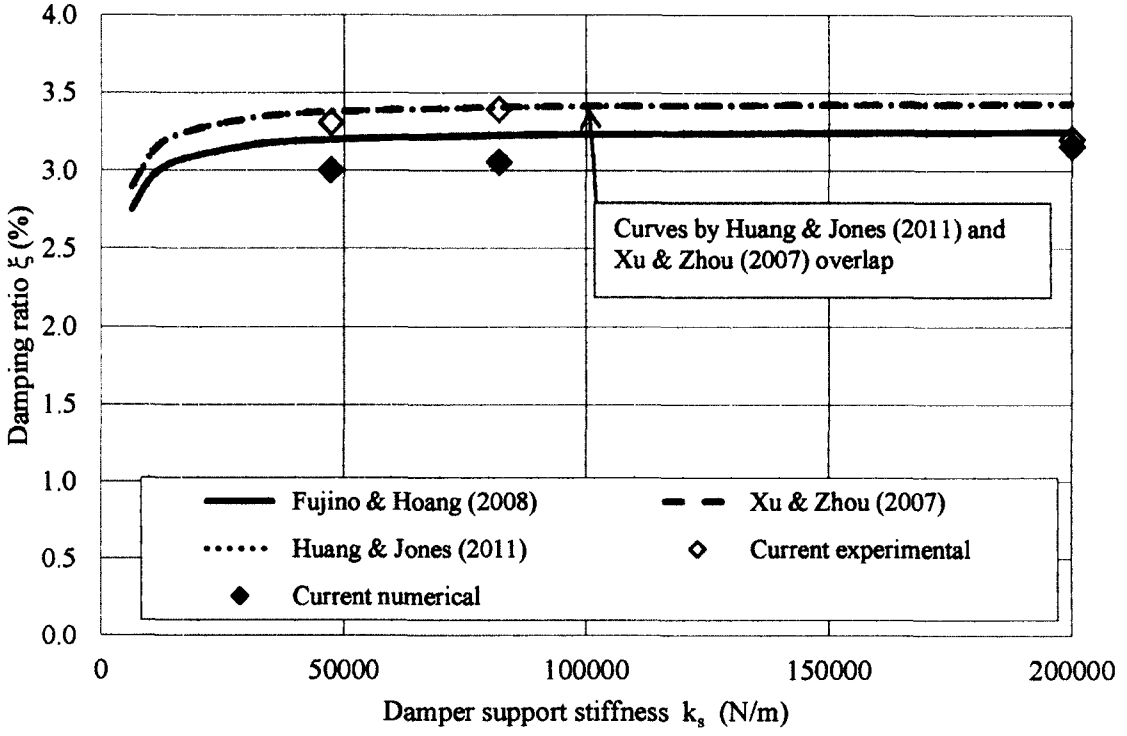

Figure 5-3: Experimental and numerical results (10%L, $k_d = 0$)

Figures 5-4 to 5-6 show the comparison between the experimental and the numerical results for the non-zero damper stiffness conditions at the 4%*L*, 6%*L*, and 10%*L* damper installation locations, respectively. Since no study is available in the literature that can predict the equivalent damping ratio of a cable-damper system while considering both the damper support stiffness and the damper stiffness effects, no reference curve is given in these three figures. The experimental results are found to agree well with the numerical results in all cases.

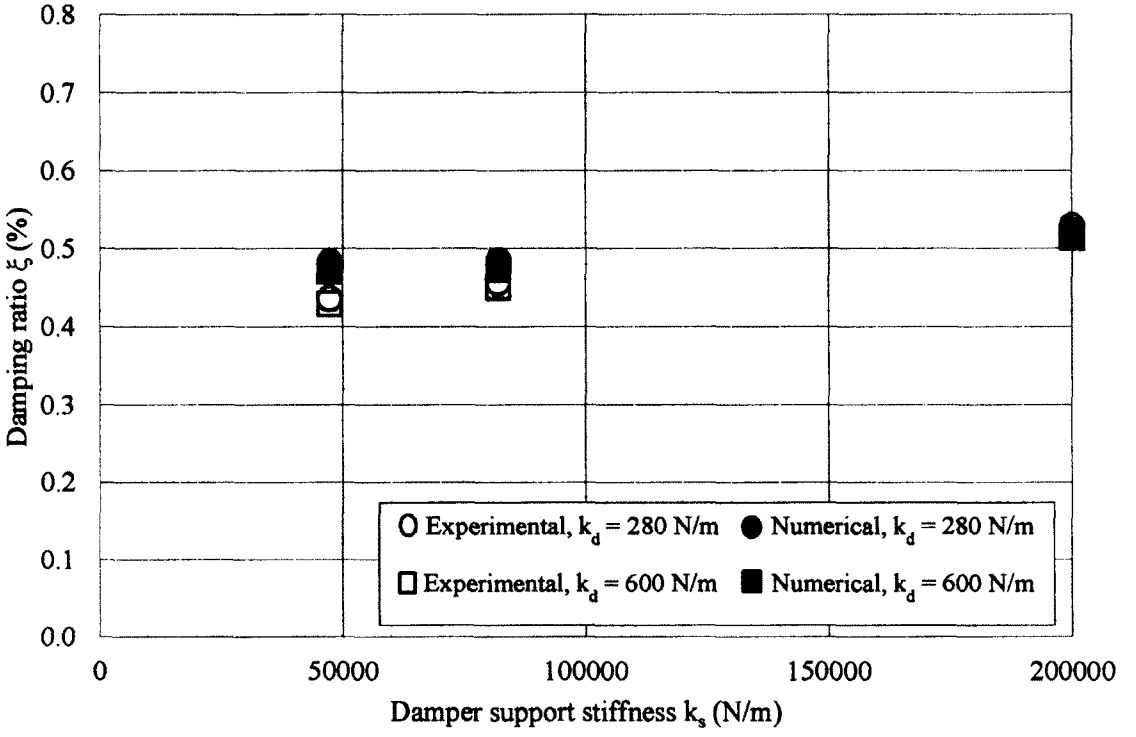

Figure 5-4: Experimental and numerical results (4%L, $k_d \neq 0$)

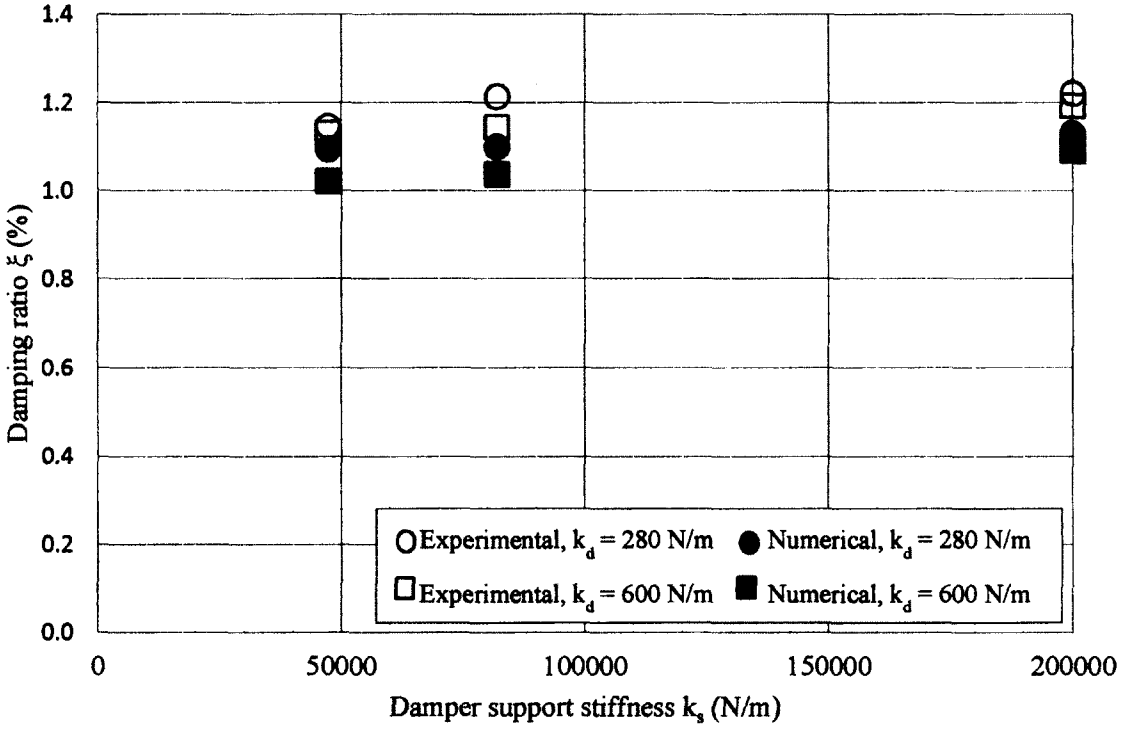

Figure 5-5: Experimental and numerical results (6%L, $k_d \neq 0$)

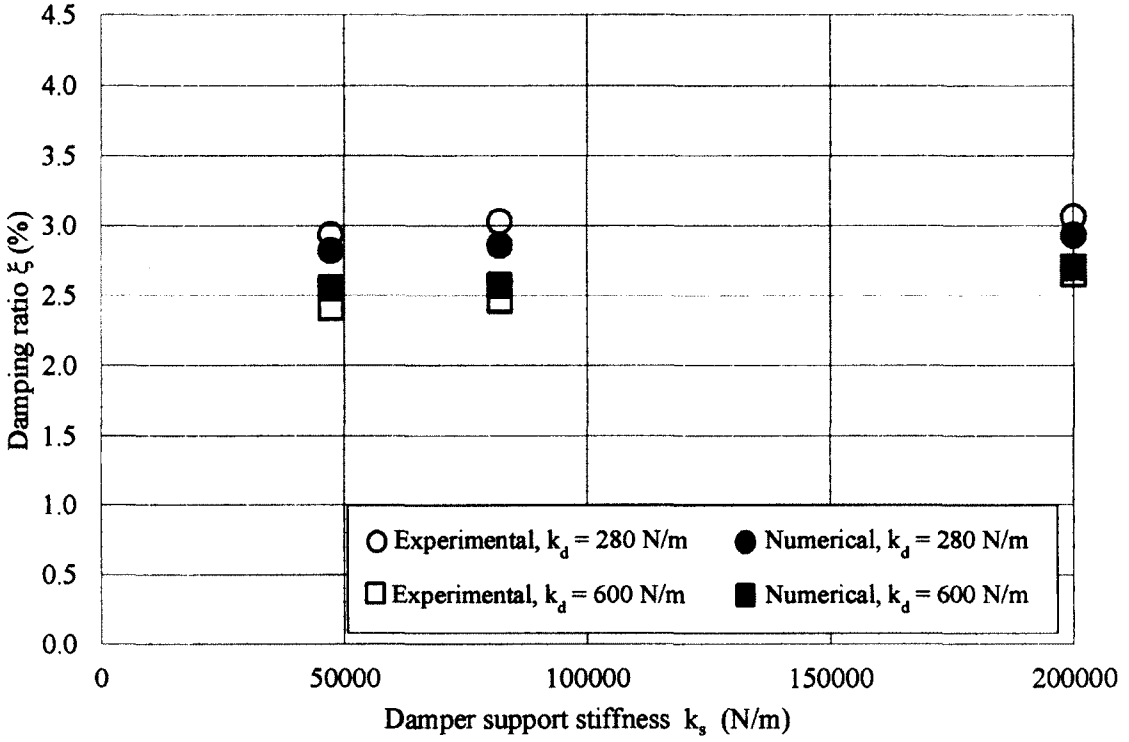

Figure 5-6: Experimental and numerical results (10%L, $k_d \neq 0$)

In Sections 3.4 and 4.3, the damper efficiency reduction factor due to the existence of damper stiffness was computed respectively based on the experimental and numerical simulation results. They are shown together in Figures 5-7 and 5-8 along with the set determined based on Zhou's formula (2005) for comparison. As can be seen from the figures, all three sets of results show the same trend and agree well with each other.

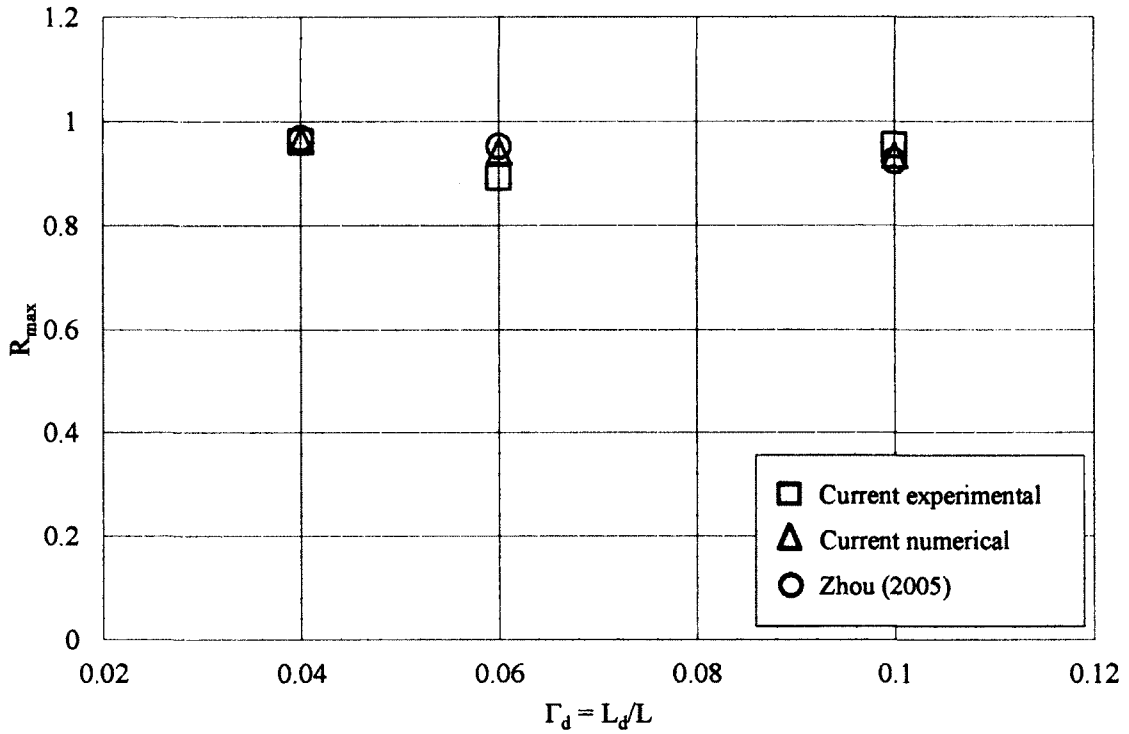

Figure 5-7: Reduction factor comparison (k_d = 280 N/m)

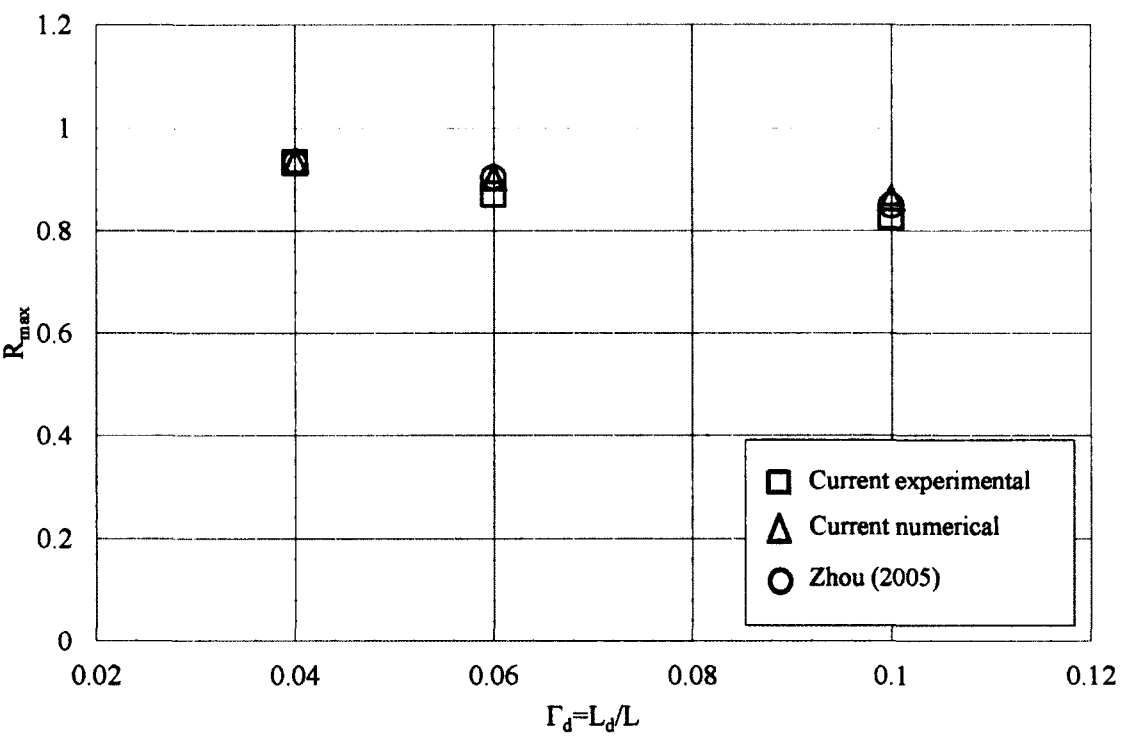

Figure 5-8: Reduction factor comparison (k_d = 600 N/m)

5.2 Estimation of optimal damper size and maximum achievable damping ratio

Regression analysis was applied to the results obtained from the current numerical study to develop an approximate relation between the optimum damper size Ψ_{opt} and the nondimensioanl system parameters of damper location Γ_d, damper stiffness k_d, and damper support stiffness k_s. The same exercise was done for the maximum achievable damping ratio. The expressions of these two approximate relations are given in Eqs. (5.1) and (5.2).

$$\Psi_{opt} = 1.309178 + 0.062143[\ln(\Gamma_d)]^4 + 0.068345\ln(K_s) + 2.239942K_d \quad (5.1)$$

$$\xi_{max} = -0.00205 + 0.465924\Gamma_d + 0.0005\ln(K_s) - 0.0295K_d \quad (5.2)$$

where Ψ_{opt} is the optimum nondimensional damping parameter, ξ_{max} is the corresponding maximum achievable equivalent first modal damping ratio, Γ_d is the nondimensional damper location, K_s is the nondimensional damper support stiffness, and K_d is the nondimensional damper stiffness. The coefficient of determination associated with the preceding approximations in Eqs. (5.1) and (5.2) are 0.977 and 0.990, respectively.

These approximations are useful in designing the linear viscous dampers to suppress cable vibrations on cable-stayed bridges. In particular, in the preliminary design stage, multiple design schemes are proposed. The availability of a convenient yet reliable tool that can quickly predict the controlling effect of different schemes will be very advantageous to the designers. To the knowledge of the author, these are the first of such approximate equations that include the effect of both damper support stiffness and damper stiffness in a simple form for the purpose of linear viscous damper design. The regression data analysis tool in Microsoft Excel was used to obtain these approximations.

Equation (5.1) is plotted in Figure 5-9 against the nondimensional damper support stiffness for the same combinations of damper location, damper stiffness, and damper support stiffness as were used in the numerical study. Three groups of curves are presented in Figure 5-9 which correspond to the damper locations of 4%L, 6%L, and 10%L, respectively. Every group contains three curves, with each representing a specific nondimensional damper stiffness case. As can be seen from the figure, the optimum damper size is highly dependent on the damper location, but is not sensitive to the nondimensional damper support stiffness, especially in the case of a more rigid support. The change in damper stiffness would affect the optimum damper size. This impact is more obvious when the damper is installed closer to the cable mid-span.

The significance of different system parameters in affecting the optimum damper size can also be deduced from Eq. (5.1). The optimum damper size Ψ_{opt} is proportional to the natural logarithm of the nondimensional damper location Γ_d to the fourth exponent, which renders Ψ_{opt} most sensitive to the variation in Γ_d. Since the nondimensional damper location is always less than one, the result of the term $(ln(\Gamma_d))^4$ decreases as the nondimensional damper location increases. In other words, the optimum damper size decreases as the damper is installed closer to the cable mid-span. A simplified explanation for this occurrence is presented here. The damper damping force F_d may be represented by $F_d = cV$, where c is the damper size and V is the cable velocity at the damper connection point (refer to Eq. (3.2)). From basic mechanics, force F may be represented by $F = W/d$, where W is the work done by the force F and d is the displacement in the direction of the force. By equating these two equations representing force, damper size may be expressed in terms of the displacement at the cable-damper

attachment point as $c = W/(Vd)$. In this manner, it can be seen that a smaller damper size is required to generate the same force when there is a greater displacement at the cable-damper attachment point. This would occur if the damper were located more towards the cable mid-span.

The form of Eq. (5.1) suggests that the nondimensional damper support stiffness K_s has a marginal effect on the optimum damper size. The natural logarithm of K_s, which increases slowly as the damper support becomes more rigid, is multiplied by a fractional constant. Therefore, as the nondimensional damper support stiffness increases, though the optimum damper size would increase as well, this amount will be very small. On the other hand, the increasing rate of the natural logarithm decreases as the damper support stiffness increases; this explains why a relatively larger increase exists at lower damper support stiffness, whereas its impact at a higher K_s range is negligible, as can be observed in Figure 5-9.

Compared to K_s, the nondimensional damper stiffness K_d has a more sizeable effect on the damper size. In the approximate relation expressed by Eq. (5.1), Ψ_{opt} varies linearly with K_d with a linear constant greater than 2. Therefore, an increase in the nondimensional damper stiffness will require a larger damper size to achieve the optimum performance. The results from the experimental and numerical studies (refer to Chapters 3 and 4, respectively) have shown that an increase in damper stiffness results in a decrease of the maximum attainable cable-damping ratio. Thus, a larger damper size is required when larger damper stiffness is present in order to counteract the effect of damper stiffness and maximize the attainable damping ratio. Again, the damping force may be expressed as $F_d = cV$. However, if damper stiffness exists, then an associated

elastic force $F_s = -k_d d$ also exists, where k_d is the damper stiffness and d is the displacement in the direction of the force. Therefore, the resulting force offered by the damper to the cable would be a function of F_d and F_s, i.e. $F_d = f(cV, -k_d d)$. If isolating the damper size c, it can be seen that it is a function of the damper damping force, the positive damper stiffness multiplied by the displacement at the cable-damper attachment point, and the inverse of velocity at this point, i.e. $c = f(F_d, k_d d, 1/V)$. In this manner, it can be seen that, for the same damper damping force, an increase in the nondimensional damper stiffness would result in a greater optimum damper size.

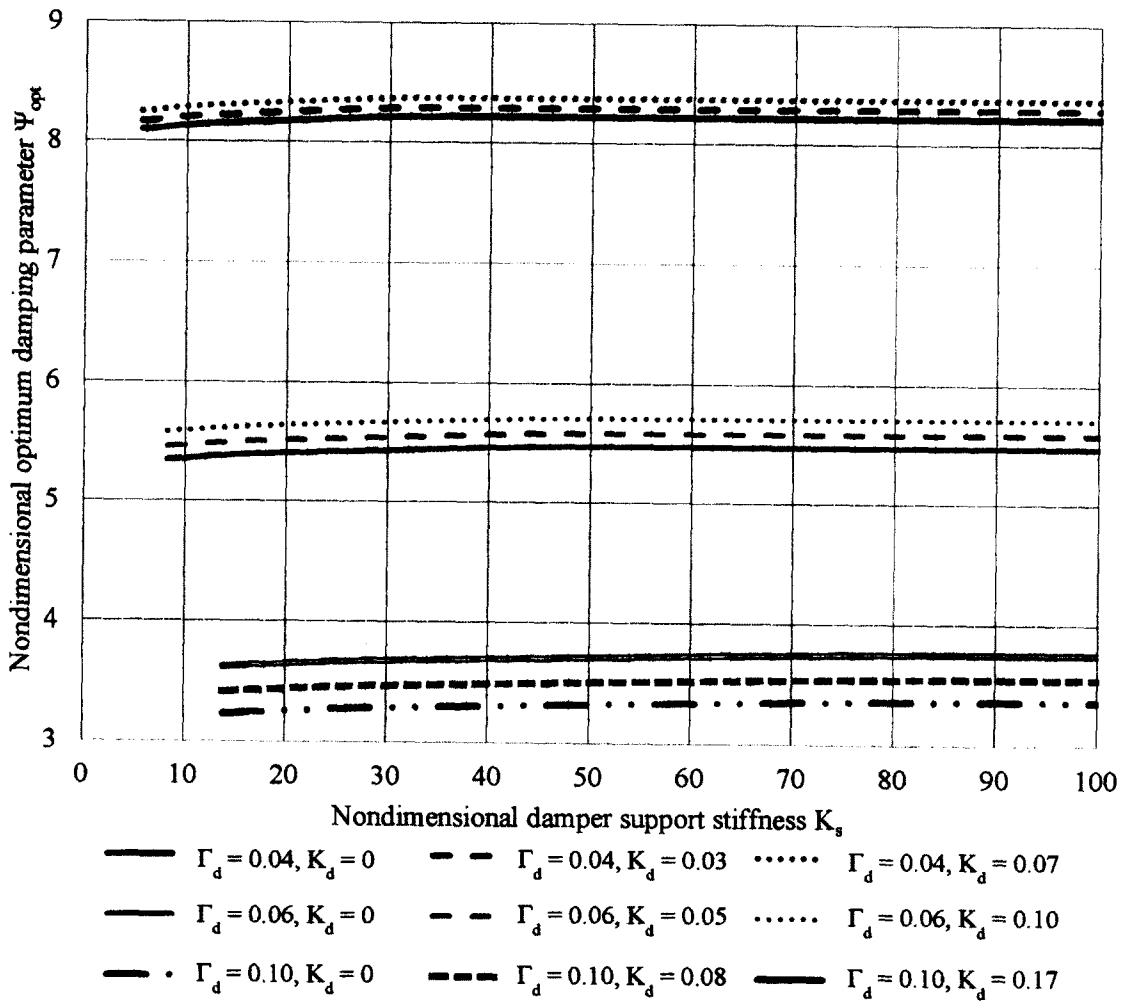

Figure 5-9: Graphical representation of Eq. (5.1)

The optimum damper sizes obtained from the current numerical study are compared with those estimated by the approximate relation represented by Eq. (5.1). The comparisons are shown graphically in Figures 5-10 to 5-18. Each figure collects results of the cases that have the same damper location and same damper stiffness. For the zero damper stiffness condition, the results from the formulae proposed by Xu and Zhou (2007), Fujino and Hoang (2008), and Huang and Jones (2011) are also displayed (refer to Section 3.4 for formulae usage details). Again, the results by Xu and Zhou (2007) and Huang and Jones (2011) overlap. As is indicated by the specified coefficient of determination of 0.977, the numerical simulation data points correlate well with the regression approximation.

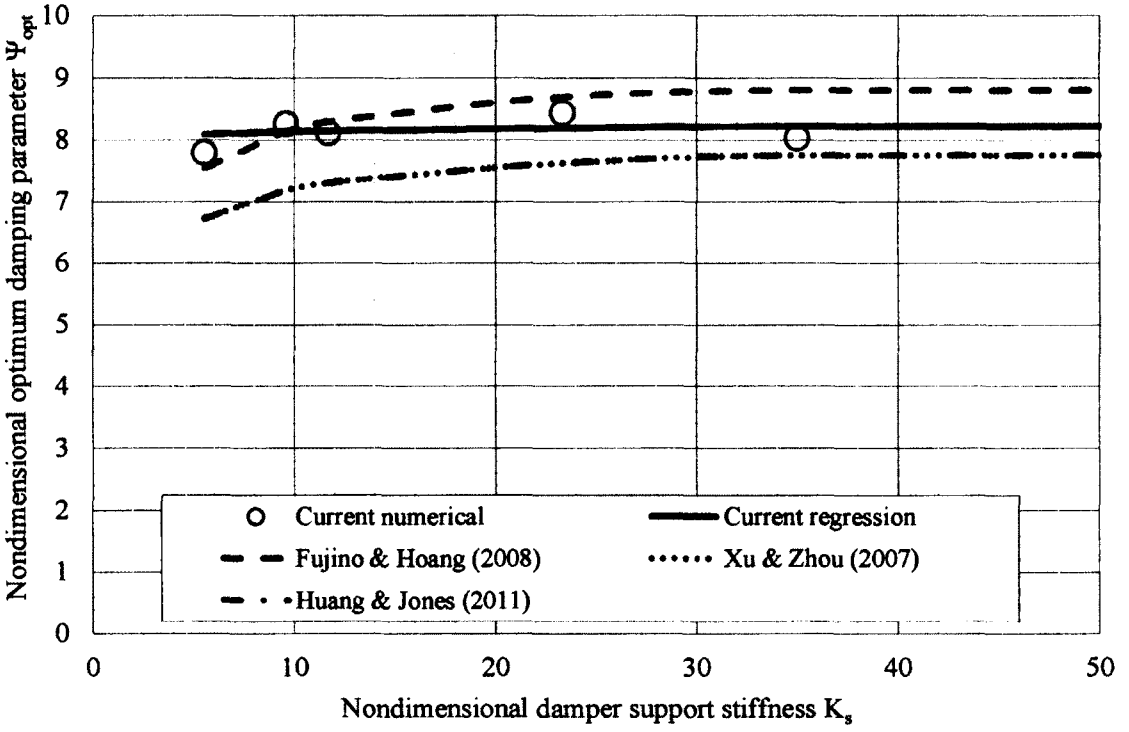

Figure 5-10: $\Gamma_d = 0.04$, $K_d = 0$

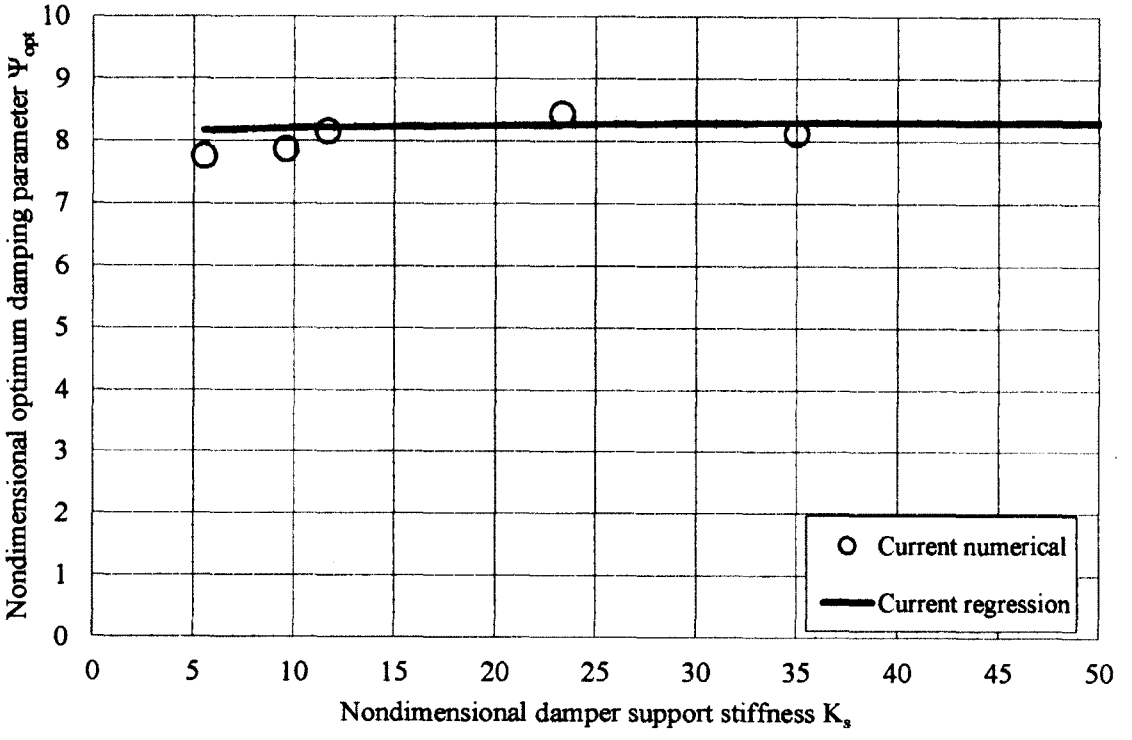

Figure 5-11: $\Gamma_d = 0.04$, $K_d = 0.03$

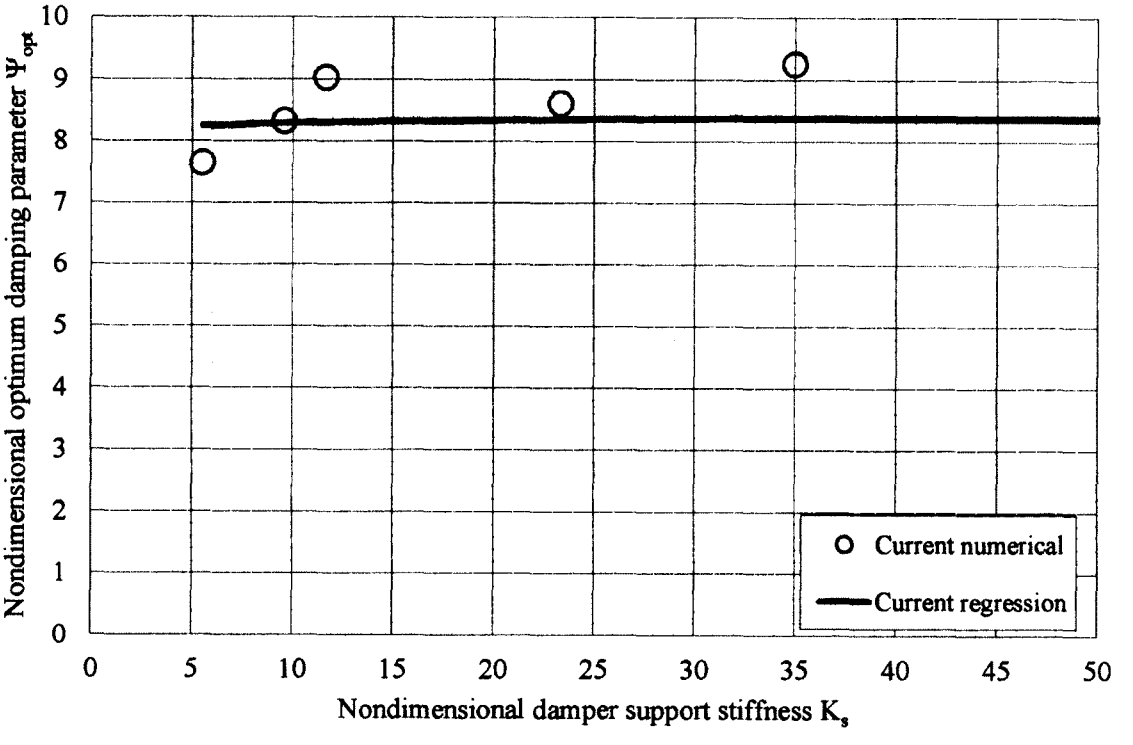

Figure 5-12: $\Gamma_d = 0.04$, $K_d = 0.07$

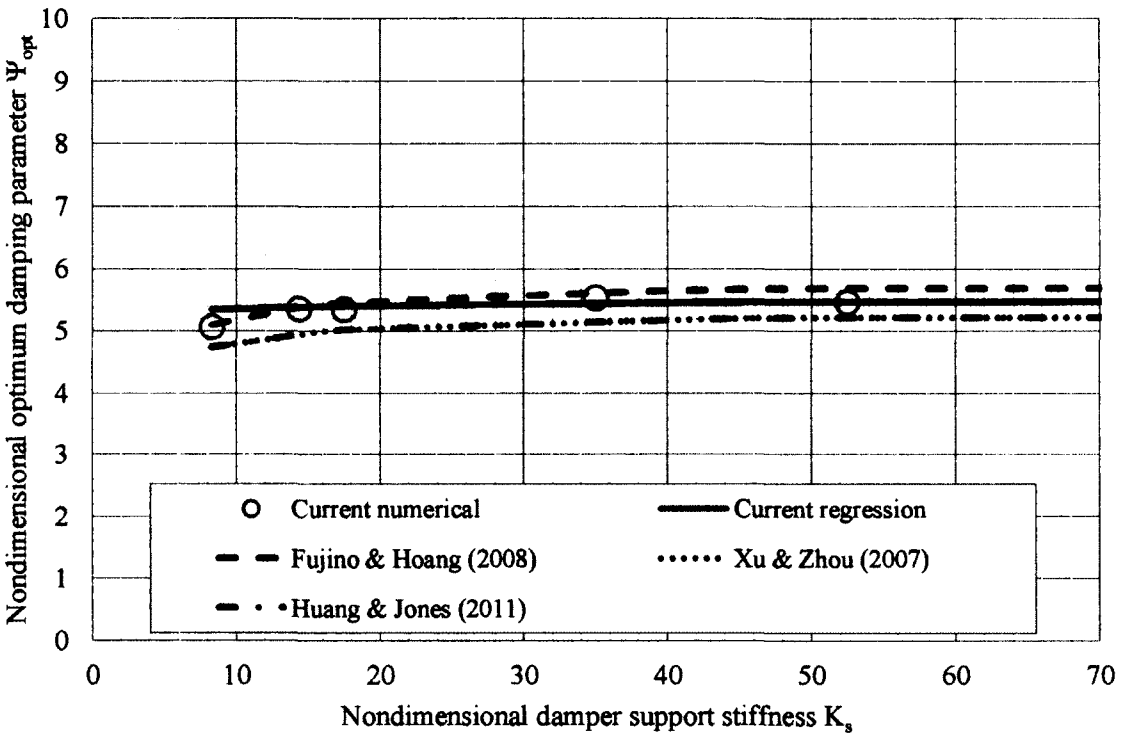

Figure 5-13: $\Gamma_d = 0.06$, $K_d = 0$

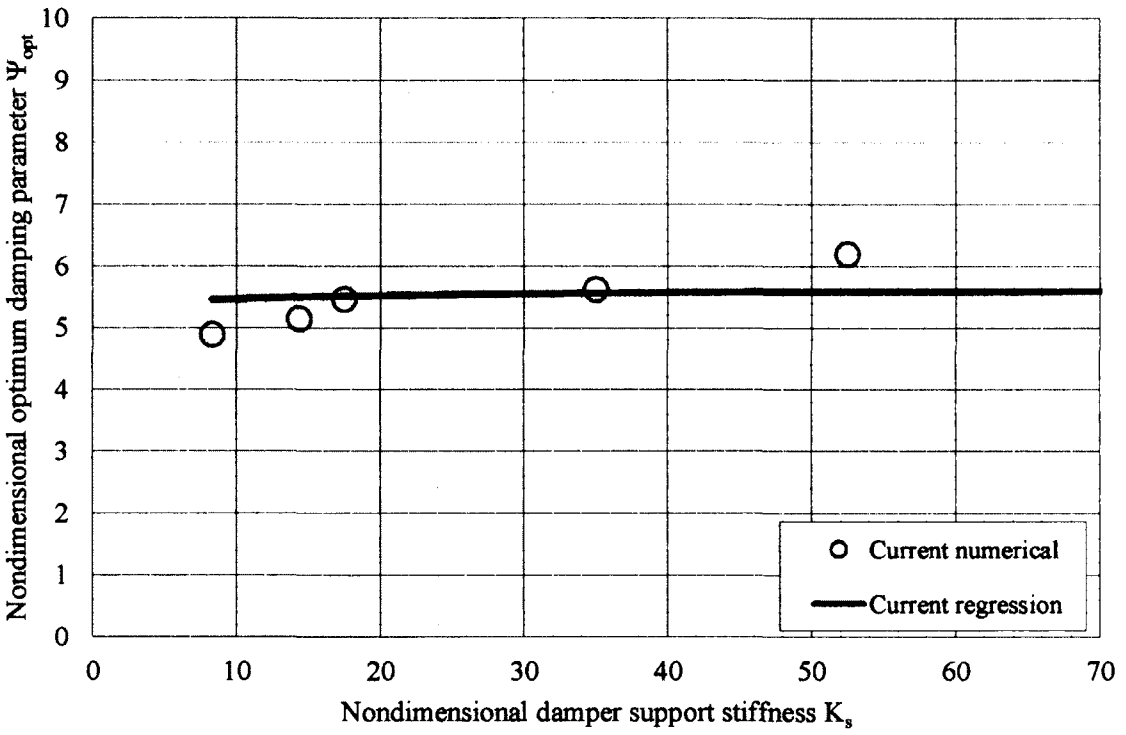

Figure 5-14: $\Gamma_d = 0.06$, $K_d = 0.05$

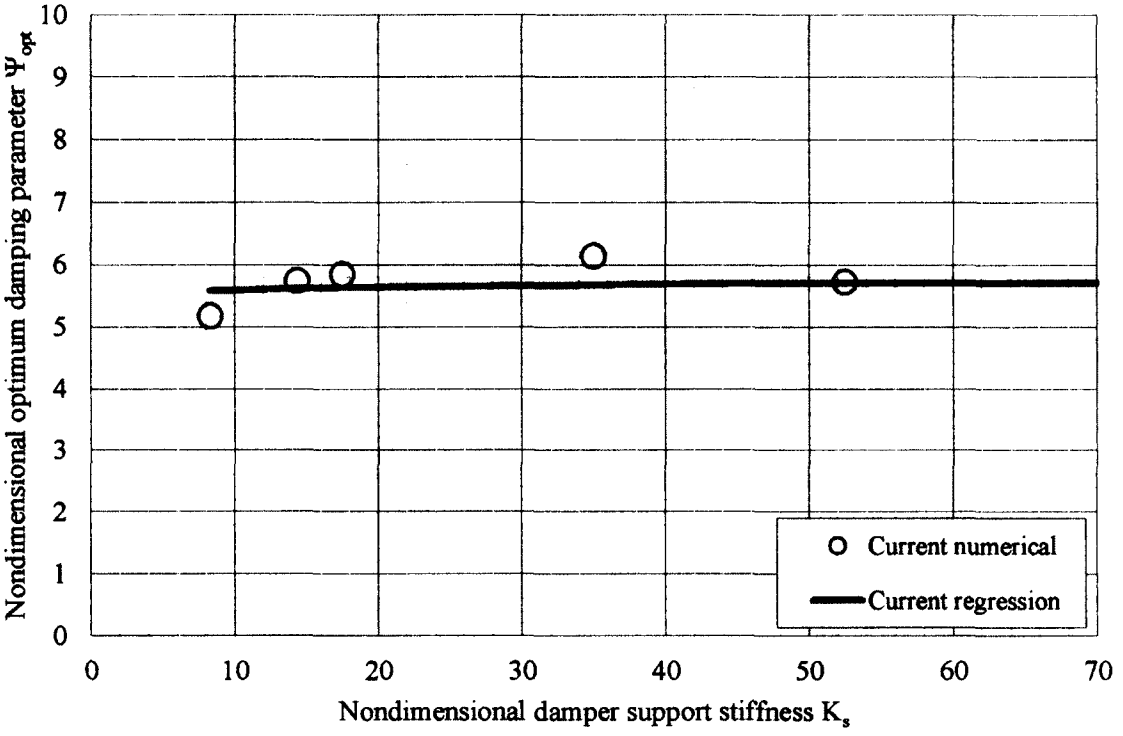

Figure 5-15: $\Gamma_d = 0.06$, $K_d = 0.10$

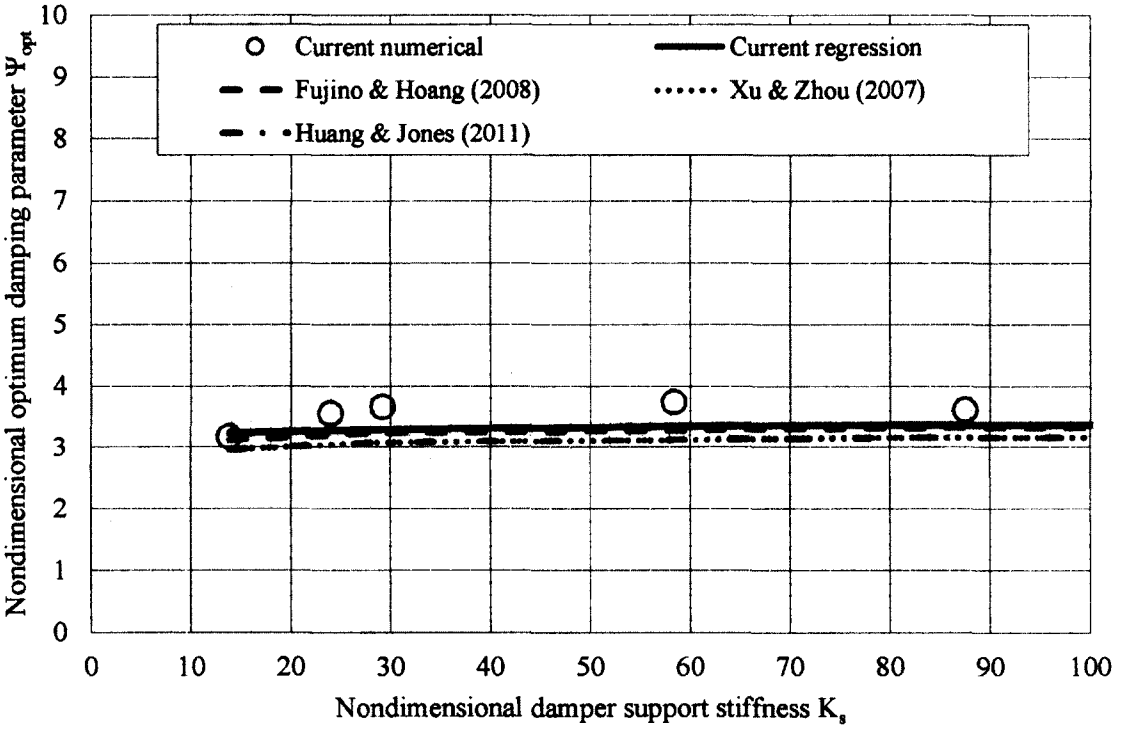

Figure 5-16: $\Gamma_d = 0.10$, $K_d = 0$

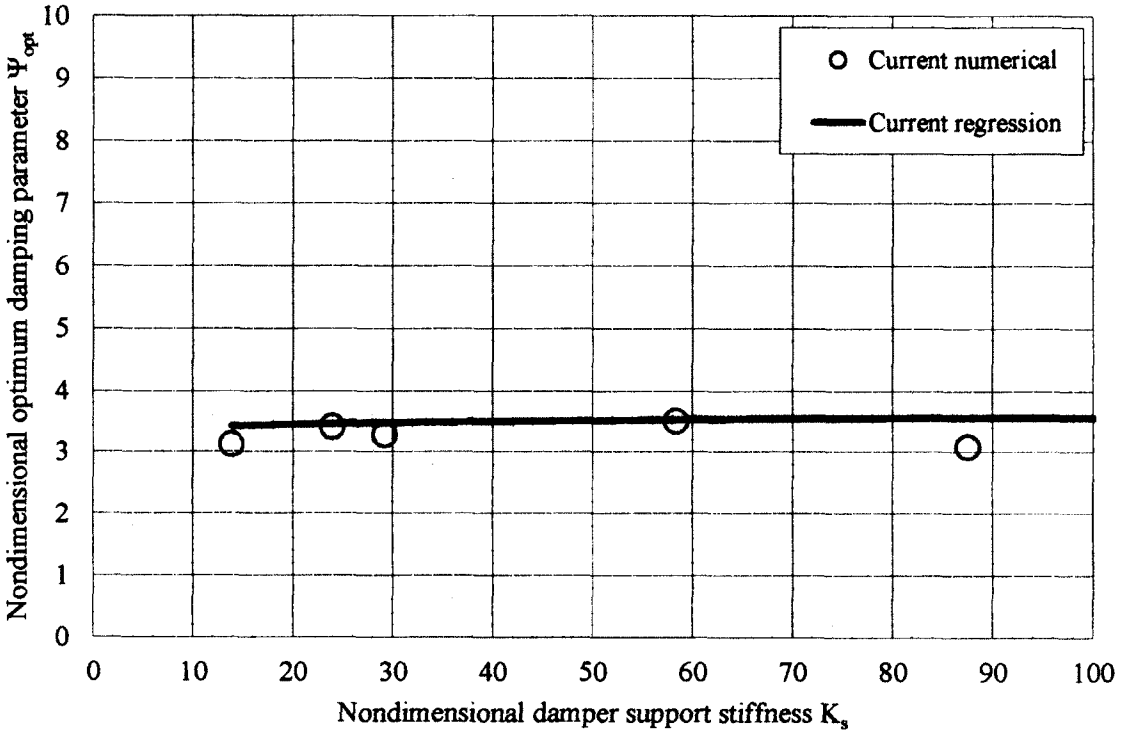

Figure 5-17: $\Gamma_d = 0.10$, $K_d = 0.08$

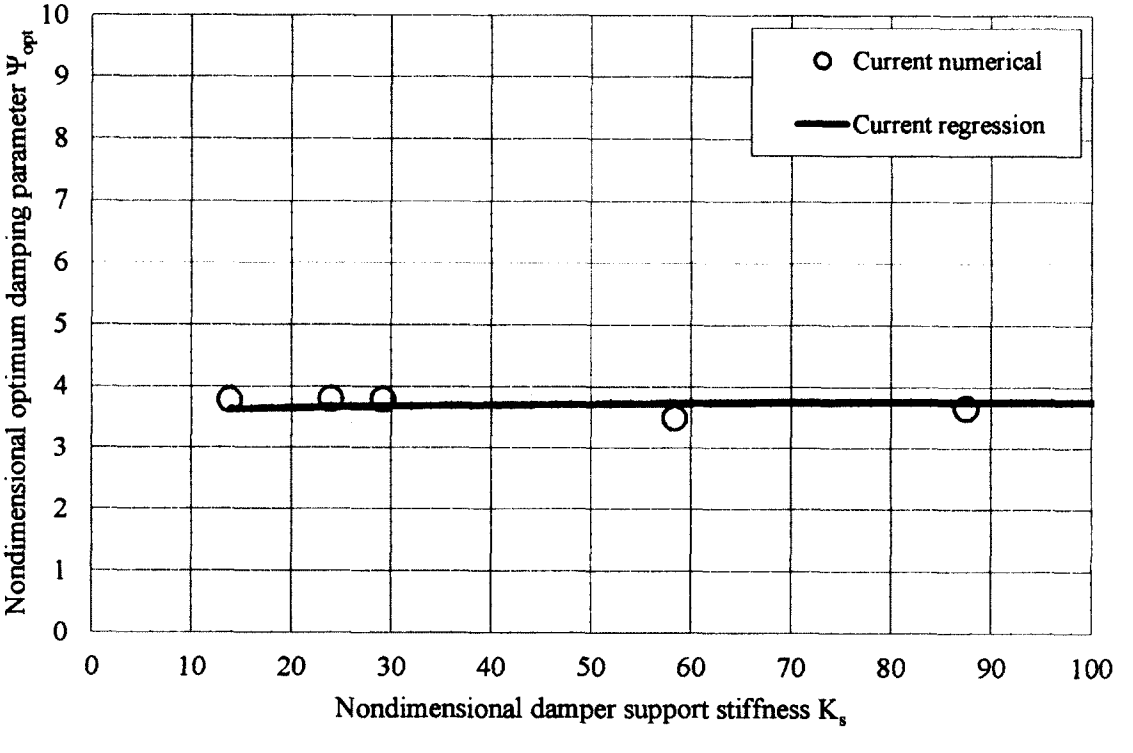

Figure 5-18: $\Gamma_d = 0.10$, $K_d = 0.17$

Zhou (2005) and Sun et al. (2008) each developed an equation to predict the optimum damper size for a given damper location while including the nondimensional damper stiffness. Both of these proposed formulae were based on the taut string assumption and therefore do not include cable bending stiffness and sagging effect. The damper support stiffness was considered to be rigid in both cases. The proposed formula by Zhou (2005) is:

$$c_{opt,i} = \frac{1}{\pi^2} mL\omega_1 \frac{(1+K_d)}{i} \frac{1}{(x_c/L)} \tag{5.3}$$

where m is the mass per unit length of the cable, ω_1 is the undamped circular frequency of a taut cable in the first mode of vibration, and i is the mode of vibration. The one developed by Sun et al. (2008) is:

$$c_{opt} = \frac{A(1+\mu x_c/L)}{(V_a\omega_n)^{\alpha-1} n\pi x_c/L} \tag{5.4}$$

where ω_n is the undamped circular frequency of a taut cable in the n^{th} mode of vibration. Eq. (5.4) allows for a nonlinear damper, where α is the exponent associated with nonlinearity. For a linear damper, as is being considered in the current study, $\alpha = 1$. The term associated with this nonlinear exponent, $V_a\omega_n$, which includes the transverse displacement of the cable at the point of damper attachment, V_a, reduces to 1. The variable μ includes the damper stiffness parameter and can be calculated by $\mu = k_d L/T$. The value of A may be calculated from:

$$A = \frac{\pi}{2\int_0^{\pi} \sin^{\alpha+1}(x)dx} \tag{5.5}$$

In the case of the current study, $\alpha = 1$ because a linear damper is being considered and the value of A simplifies to 1.

In both formulations, the optimum damper size is predicted to increase as the damper stiffness increases. This is the same trend as in the regression approximation, Eq. (5.1), developed in the current study. These formulations are used to compare with the approximation of the optimum nondimensional damping parameter, Eq. (5.1), for the combinations of damper location and damper stiffness listed in Table 4-2, and a rigid damper support stiffness. Figure 5-19 displays the comparison between the current regression approximation, Eq. (5.1), the current numerical results, and the formulae developed by Zhou (2005) and Sun et al (2008) for the rigid damper support condition.

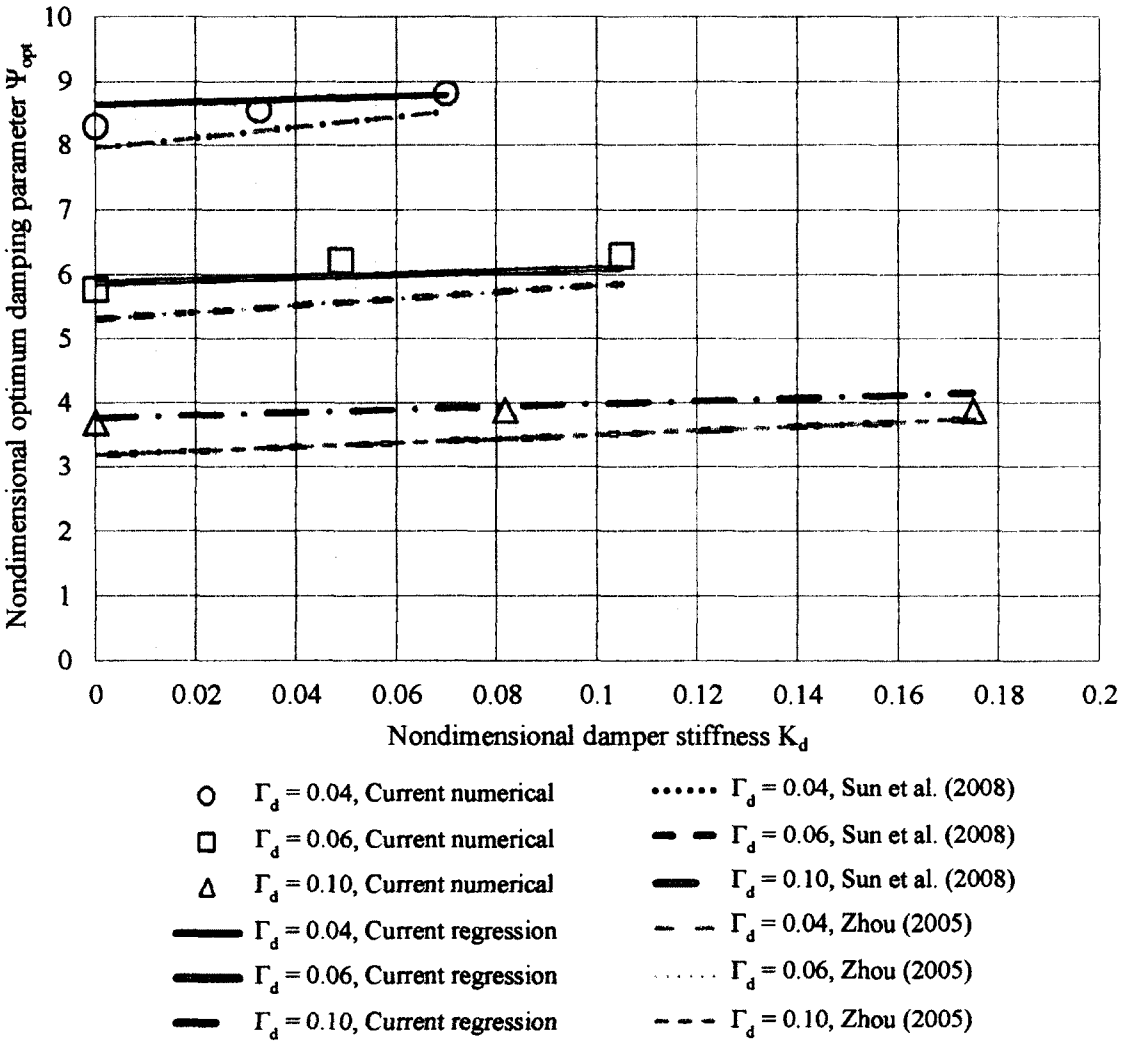

Figure 5-19: Rigid damper support stiffness

Several comments may be made about the results shown in Figure 5-19. Firstly, it can be seen that the numerical data points agree well with the regression approximation. In addition, the curves developed from the equations proposed by Zhou (2005) and Sun et al. (2008) overlap at the same damper location. Both of these formulae are shown to underestimate the optimum damper size required at any given damper location. This may be attributed to the taut cable assumption that both of these equations have made.

The approximation for the maximum equivalent first modal damping ratio is plotted in Figure 5-20 for the damper location, damper stiffness, and damper support stiffness combinations listed in Table 4-2. In Eq. (5.2), it can be seen that each of these three parameters affects the maximum attainable structural damping ratio. The damper installation location is linearly proportional to the maximum damping ratio, which increases as the damper is moved closer to the mid-span of the cable. This effect is well documented in literature (e.g. Cheng et al. 2010). Theoretically, a linear viscous damper will perform better when it is installed closer to the cable mid-span, although common practice is to install them within a few percent of the cable length for ease of construction and aesthetics.

The damper support stiffness will also affect the maximum achievable damping ratio. The modal damping ratio is linearly proportional to the natural logarithm of the damper support stiffness in Eq. (5.2). Therefore, a weaker support may cause a linear viscous damper to exhibit a damping ratio lower than would be predicted without considering this parameter.

In addition, Eq. (5.2) implies that the maximum modal damping ratio is negatively correlated to the damper stiffness. A simplified explanation for this correlation may be suggested by examining the behaviour of a viscously damped freely vibrating system. The damping ratio of such a system may be represented by the following:

$$\xi = \frac{c}{2\sqrt{km}} \tag{5.6}$$

In this equation, it is apparent that the damping ratio is inversely proportional to the square-root of the system mass m and stiffness k. Accordingly, an increase in stiffness will result in a corresponding decrease in damping ratio. It is recommended that the stiffness within a linear viscous damper be minimized in order to maximize its attainable modal damping ratio and achieve the optimum cable vibration control.

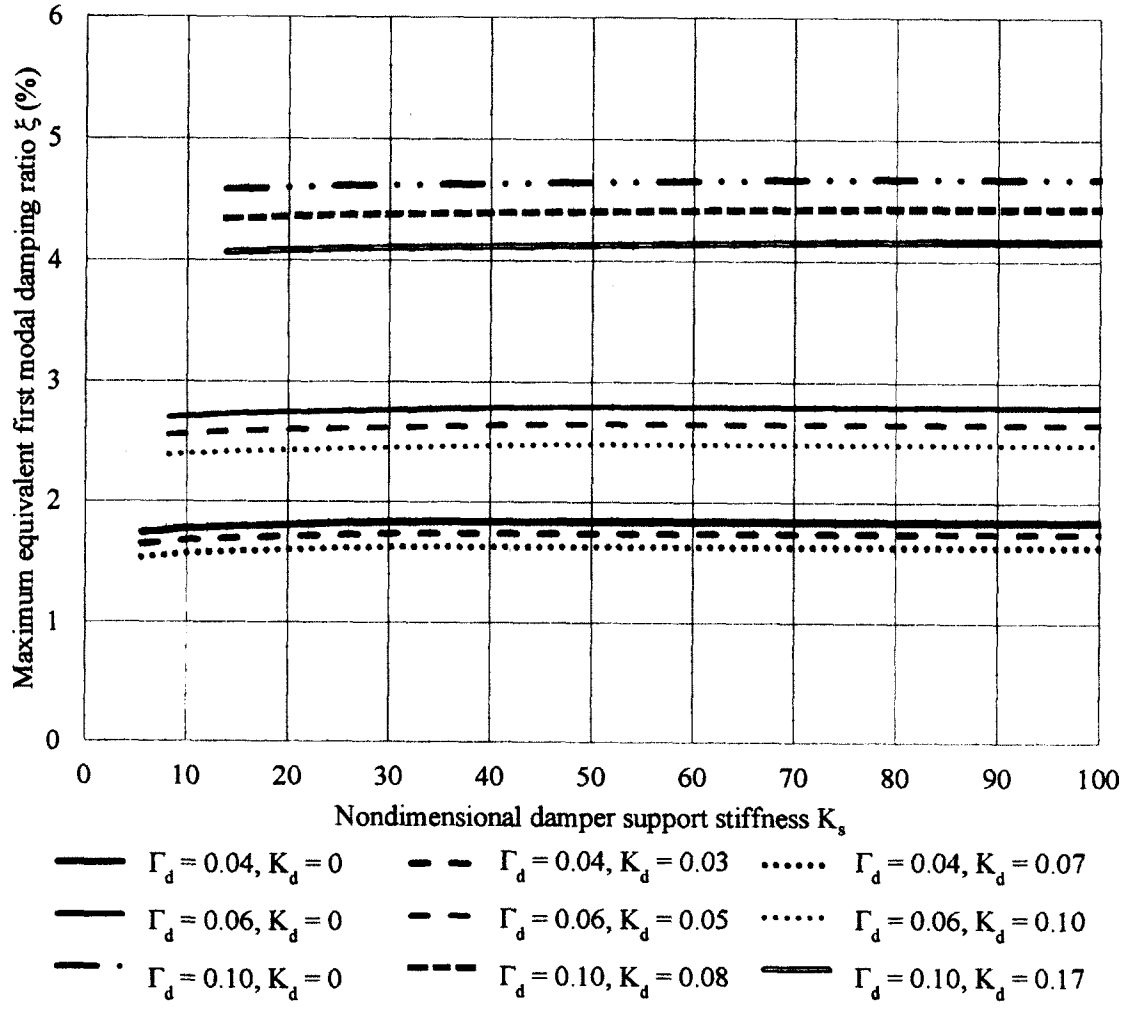

Figure 5-20: Graphical representation of Eq. (5.2)

Figures 5-21 to 5-29 give graphical comparison between the maximum attainable equivalent first modal damping ratio of the studied cable-damper system obtained from the current numerical simulations and the regression approximation equation, Eq. (5.2), for the same combinations of damper location, damper stiffness, and damper support stiffness as listed in Table 4-2. For the convenience of comparison, the predictions from the equations developed by Xu and Zhou (2007), Fujino and Hoang (2008), and Huang and Jones (2011) are also displayed (refer to Section 3.4 for formulae usage details) for the zero damper stiffness conditions in Figures 5-21, 5-24, and 5-27. The curves for the

formulae developed by Xu and Zhou (2007), and Huang and Jones (2011), overlap. The agreement between different sets of results can be readily observed from these figures. The regression approximation is a good representation of the numerical data points, with its coefficient of determination being 0.990.

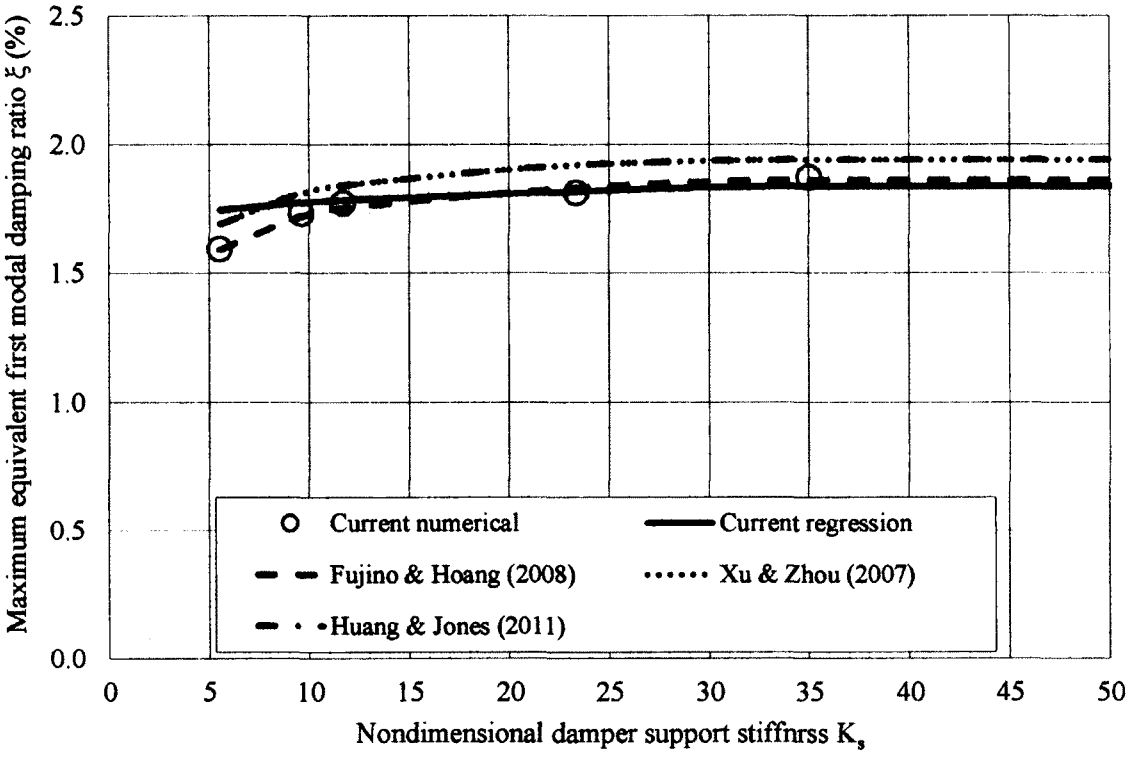

Figure 5-21: $\Gamma_d = 0.04$, $K_d = 0$

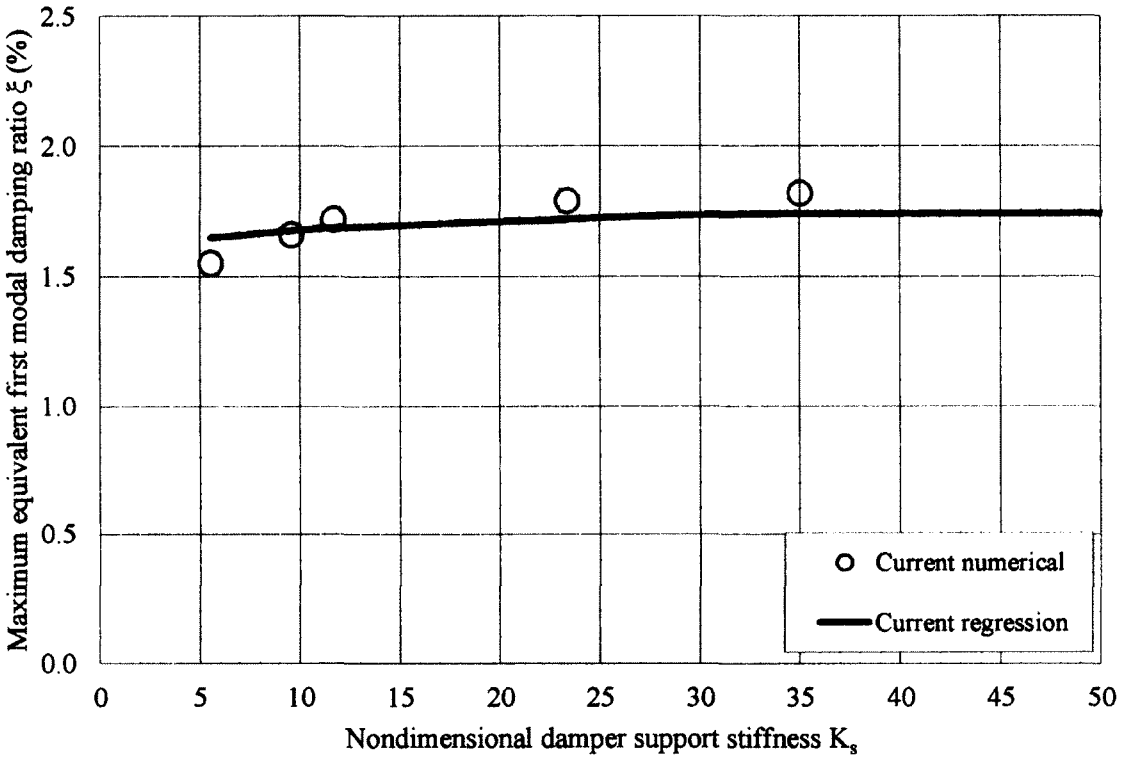

Figure 5-22: $\Gamma_d = 0.04$, $K_d = 0.03$

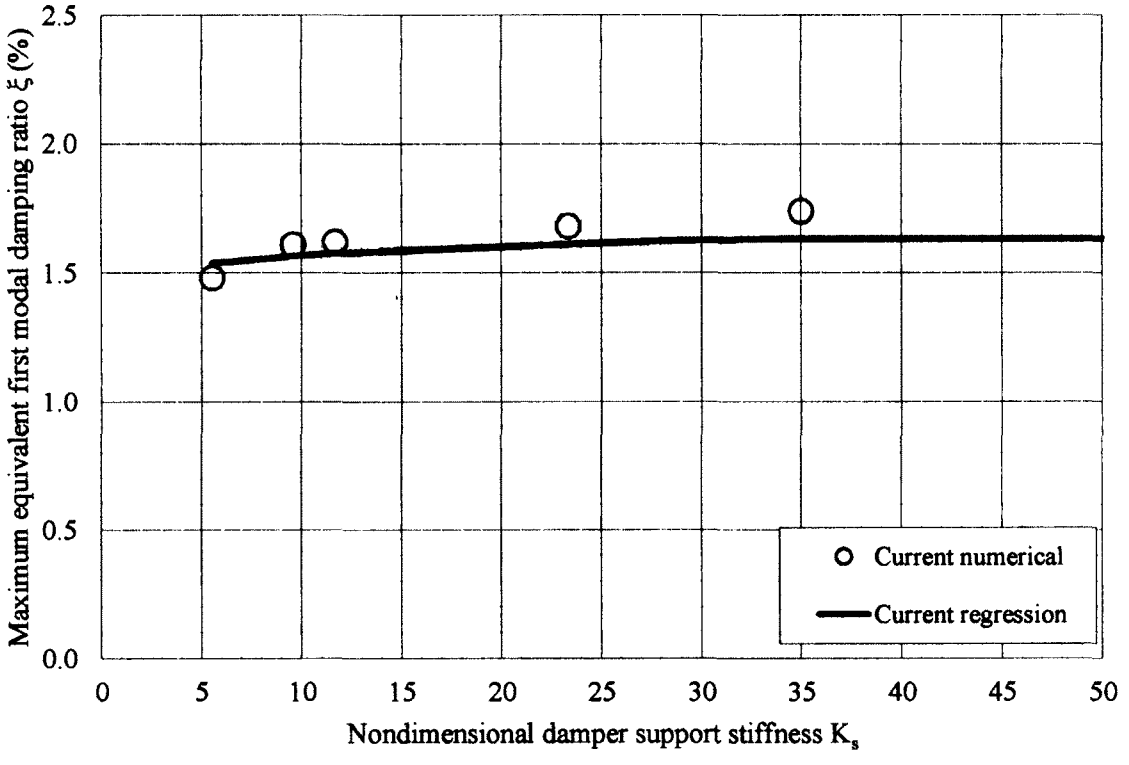

Figure 5-23: $\Gamma_d = 0.04$, $K_d = 0.07$

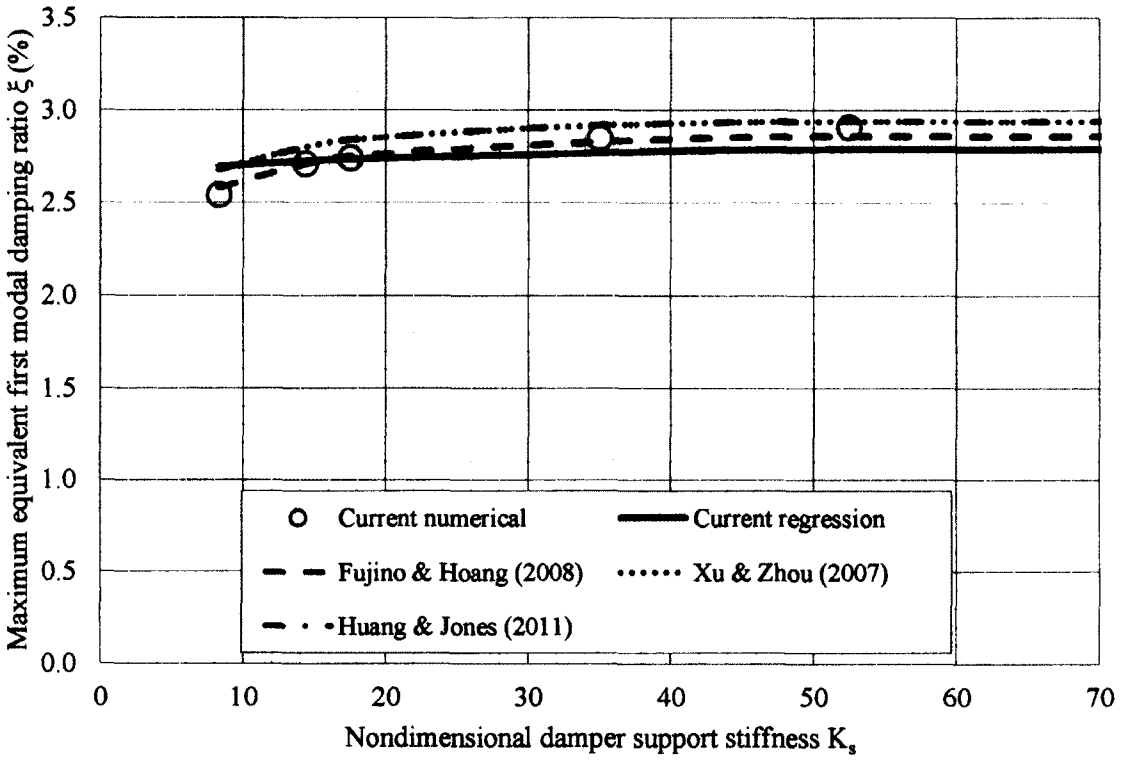

Figure 5-24: $\Gamma_d = 0.06$, $K_d = 0$

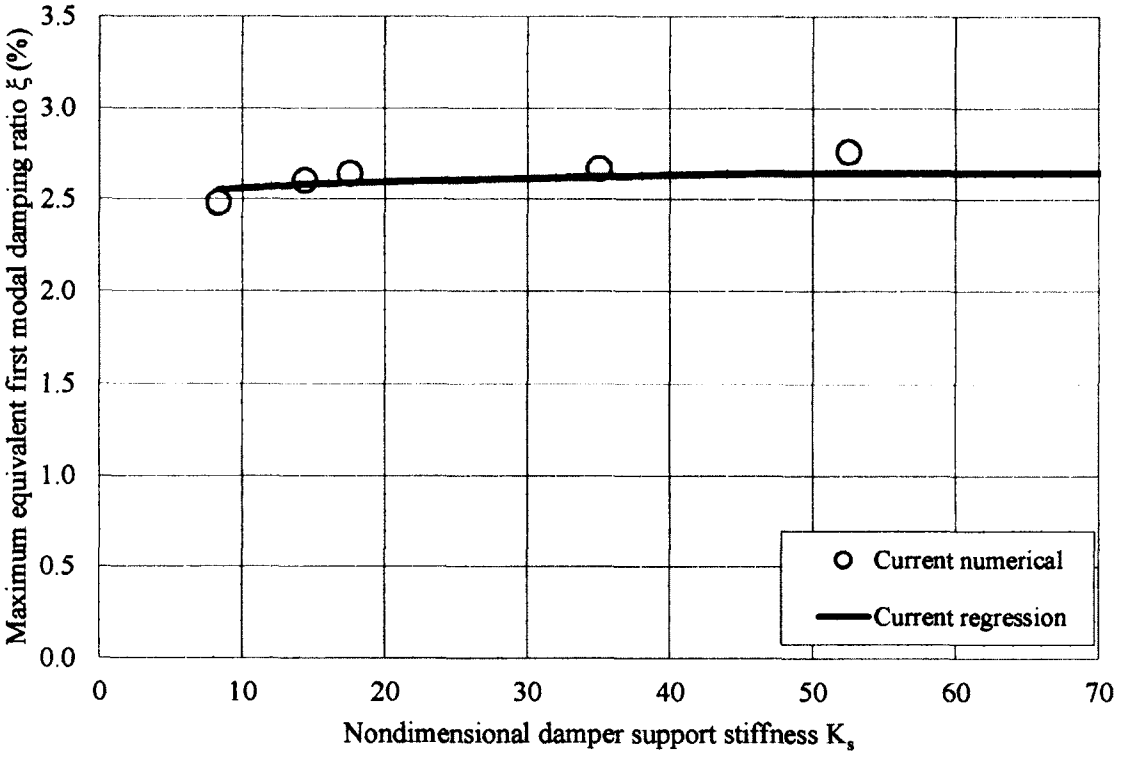

Figure 5-25: $\Gamma_d = 0.06$, $K_d = 0.05$

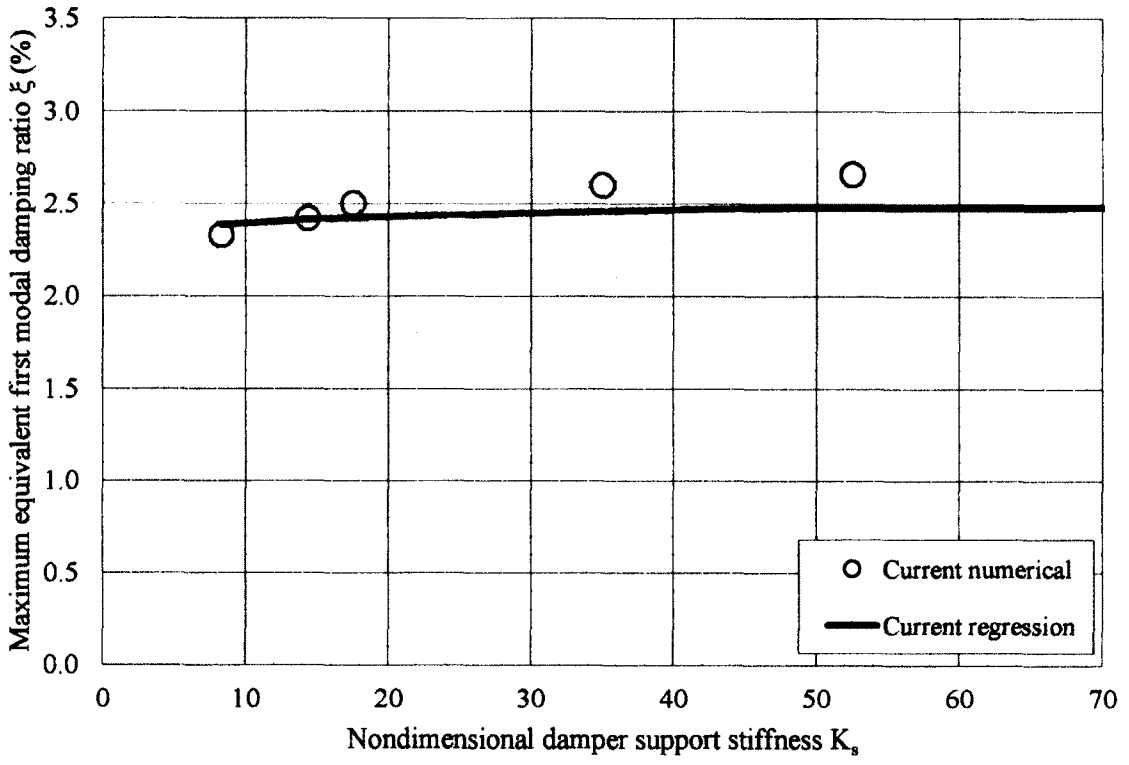

Figure 5-26: $\Gamma_d = 0.06$, $K_d = 0.10$

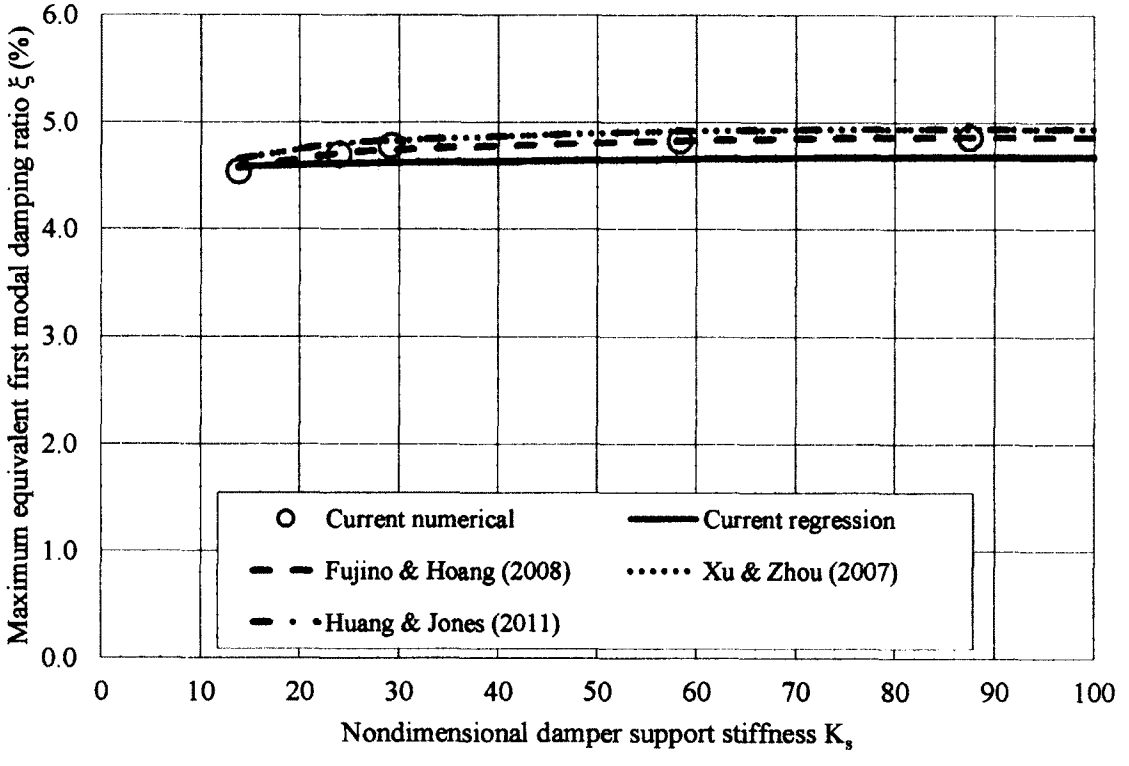

Figure 5-27: $\Gamma_d = 0.10$, $K_d = 0$

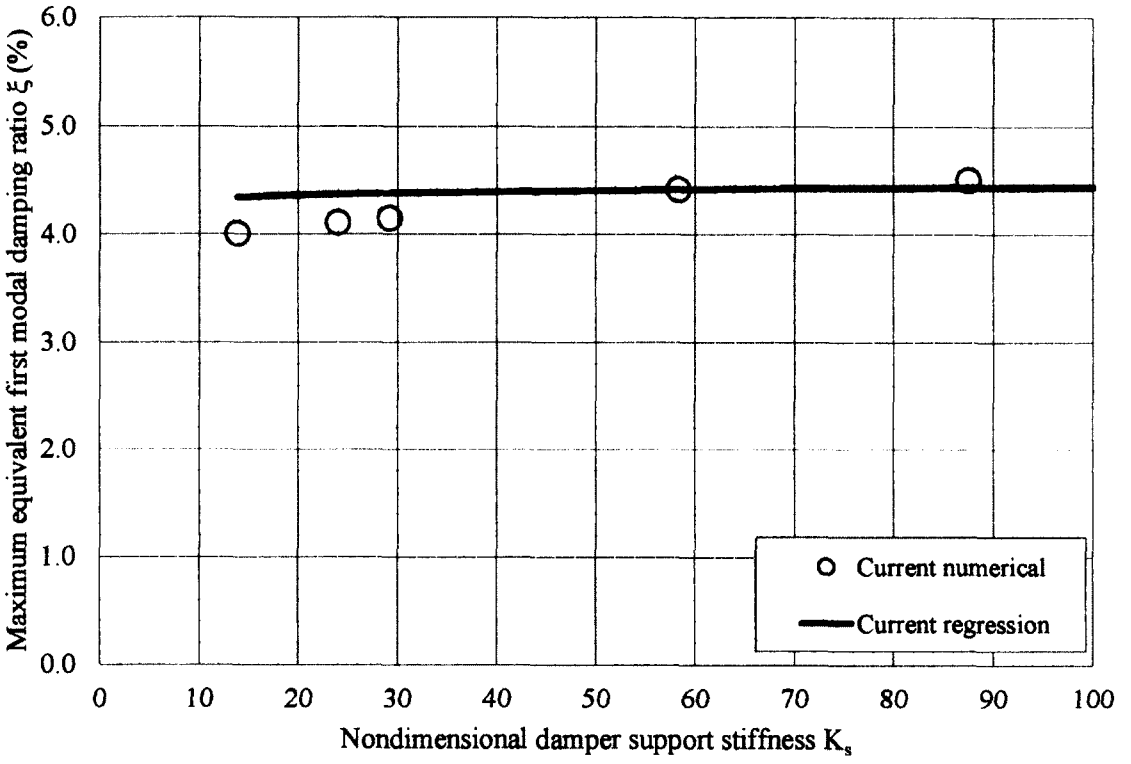

Figure 5-28: $\Gamma_d = 0.10$, $K_d = 0.08$

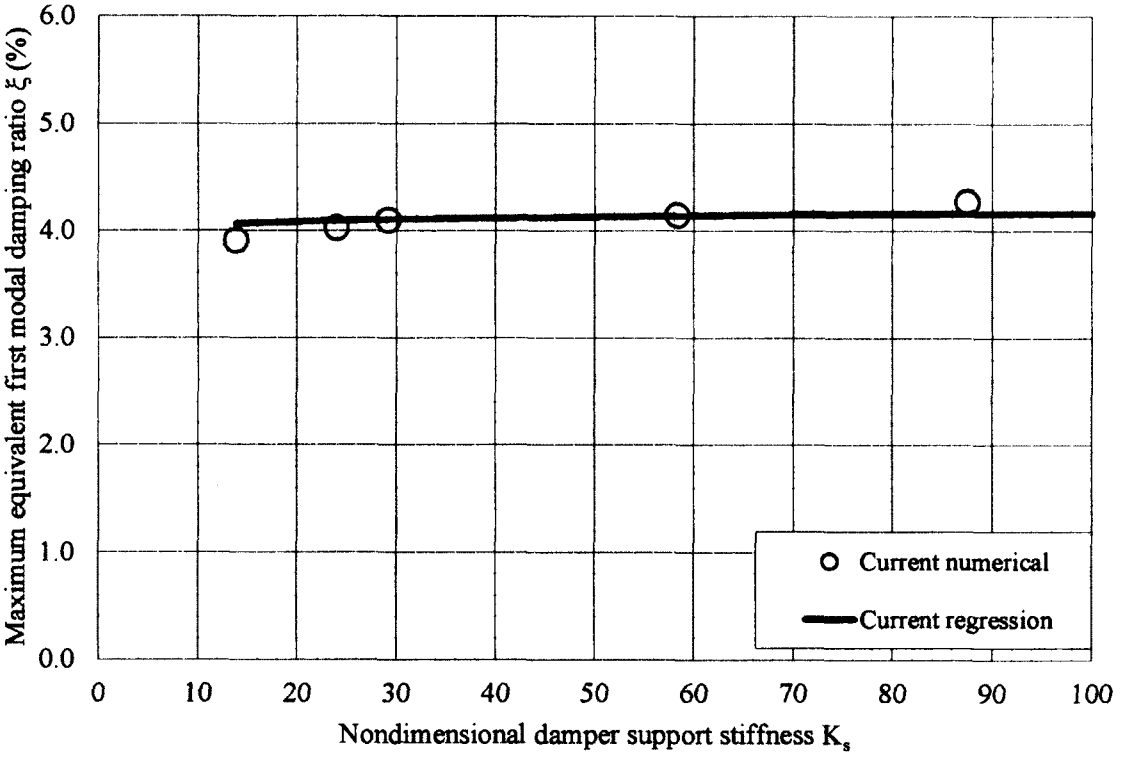

Figure 5-29: $\Gamma_d = 0.10$, $K_d = 0.17$

Sun et al. (2008) developed an equation that predicts the maximum modal damping ratio of a nonlinear viscous damper while including the effects of damper stiffness and assumed the damper support stiffness to be rigid, i.e.

$$\frac{\xi_{n,max}}{x_c/L} = \frac{A|\sin(\omega_n t)|^{\alpha-1}}{(1+\frac{\mu x_c}{L})(1+A|\sin(\omega_n t)|^{\alpha-1})} \tag{5.6}$$

The definitions of parameters in Eq. (5.6) are the same as those in Eq. (5.4). When $\alpha = 1$ is inputted into Eqs. (5.6) and (5.5) for a linear damper case, the latter of which calculates the value of A, the above equation is simplified to the following form:

$$\xi_{n,max} = \frac{x_c/L}{2(1+\frac{\mu x_c}{L})} \tag{5.7}$$

Eq. (5.7) was used to compare with the regression approximation, Eq. (5.2), developed in the current study. This comparison is displayed in Figure 5-30 below. The curves and numerical data points are found to agree well with each other.

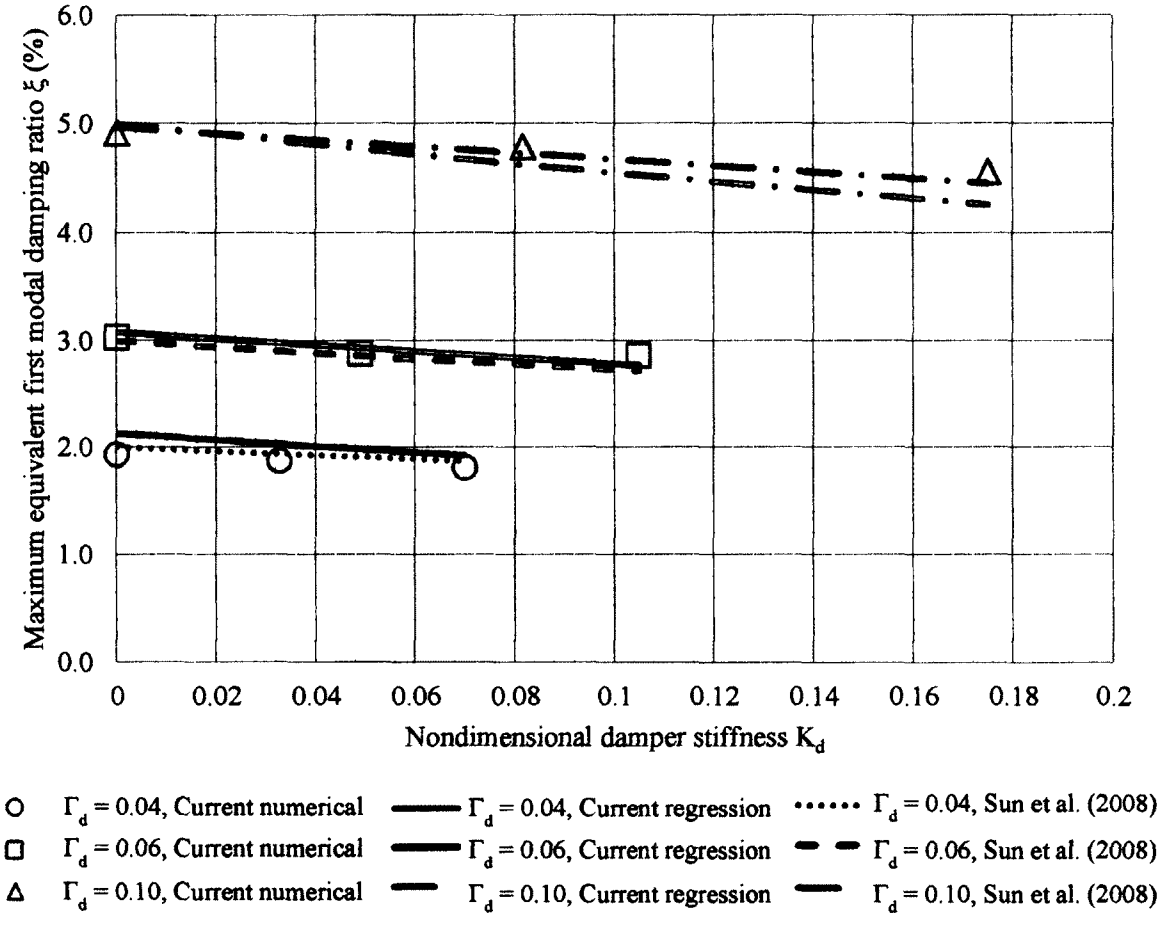

Figure 5-30: Rigid damper support stiffness

Chapter 6: Conclusions and Recommendations

6.1 Conclusions

Cable-stayed bridge is a common bridge type chosen for construction. New structures are being designed to span larger distances than ever. The safe design of cable-stayed bridges is paramount and cable vibration control must be considered in order to maintain the structural integrity of its cables. The stiffness of the damper in use on the bridge, the stiffness of the damper support, and their combined effect will influence the overall performance of the damper in mitigating stay cable vibration. However, there is a lack of study of these stiffness effects and, to the knowledge of the author, even less is to be found on their combined effect. An experimental study was designed and carried out herein using a scaled model of a cable-damper system to measure the effects of damper stiffness, damper support stiffness, and their combined effect during forced vibration tests. A finite element model of the same cable-damper system was developed to simulate the same stiffness effects over a wider range of system parameters. The results from both studies agreed well with the predictions available in literature. As a summary, the following have been completed in this study:

1. Design of a linear viscous damper that includes variable damper stiffness, damper support stiffness, and the ability to combine both stiffness parameters.
2. Design a calibration system for the damper.
3. Conduct cable forced vibration tests to observe the effects of damper stiffness, damper support stiffness and the combined effect of both.
4. Development of a finite element model of a cable-damper system that includes damper stiffness and damper support stiffness.

5. Comparison of numerical and experimental results to each other as well as empirical formulae found in existing literature to observe the effects of the parameters of interest.
6. Develop empirical formulae to predict the optimum damper size and its corresponding maximum attainable first modal damping ratio by considering the effect of damper stiffness and damper support stiffness.

The following can be concluded from the current study:

1. As the damper is moved closer to the cable mid-span, the optimum damper size decreases and the corresponding maximum achievable damping ratio increases.
2. An increase in the damper stiffness results in an increase of the required optimum damper size but a decrease in the maximum achievable damping ratio.
3. An increase in the damper support stiffness results in an increase of the optimum damper size and its corresponding maximum achievable damping ratio.
4. To achieve better effect in cable vibration control, if a linear viscous damper would be used as countermeasure, it is recommended to minimize its own stiffness. Should a damper support be required, it is preferred to choose a more rigid one.

Empirical formulae have been proposed based on the current numerical results, for use in the preliminary design phase of a linear viscous damper for bridge stay cables. The empirical formulae developed in this study are the culmination of extensive study of the effects of damper stiffness and damper support stiffness on the performance of a linear viscous damper for the purpose of mitigating stay cable vibration. They are proposed with the objective to expand the current knowledge base regarding linear viscous damper

design for stay cable vibration control. To the knowledge of the author, these are the first empirical approximations for the optimum damper size and its corresponding maximum attainable first modal damping ratio that include the effects of both damper stiffness and damper support stiffness.

6.2 Future recommendations

It is recommended that future study look towards evaluating various damper supports that may be used on cable-stayed bridges to allow linear viscous dampers to be placed closer to the cable mid-span. In this manner, improved stay cable control may be achieved and empirical formulae such as those proposed in the current study may be used to improve the accuracy in predicting the required optimum damper size and its corresponding maximum attainable first modal damping ratio. An experimental study may also proceed by testing the limits of the effect of damper support stiffness in order to suggest a range of stiffness for the purpose of design.

Bibliography

ANSYS, Inc. (2011). ANSYS 14.0 Documentation.

Cai, C., Wu, W., Shi, X. (2006). Cable Vibration Reduction with a Hung-on TMD System. Part I: Theoretical Study. *Journal of Vibration and Control, 12*(7), 801-814.

Caracoglia, L., Jones, N. (2005). In-plane dynamic behavior of cable networks. Part 2: prototype prediction and validation. *Journal of Sound and Vibration, 279*(3-5), 993-1014.

Caracoglia, L., Jones, N. (2007). Damping of Taut-Cable Systems: Two Dampers on a Single Stay. *Journal of Engineering Mechanics, 133*(10), 1050-1060.

Cheng, S., Darivandi, N., Ghrib, F. (2010). The design of an optimal viscous damper for a bridge stay cable using energy-based approach. *Journal of Sound and Vibration, 329*(22), 4689-704.

Cheng, S., Irwin, P., Tanaka, H. (2008b). Experimental study on the wind-induced vibration of a dry inclined cable - Part II: Proposed mechanisms. *Journal of Wind Engineering and Industrial Aerodynamics, 96*(12), 2254-2272.

Cheng, S., Larose, G., Savage, M., Tanaka, H., Irwin, P. (2008a). Experimental study on the wind-induced vibration of a dry inclined cable - Part I: Phenomena. *Journal of Wind Engineering and Industrial Aerodynamics*, 2231-2253.

Cho, S.-W., Jung, H.-J., Lee, I.-W. (2005). Smart passive system based on magnetorheological damper. *Smart Materials and Structures, 14*(4), 707-714.

Christenson, R., Spencer, B. (2001). Experimental Verification of Semiactive Damping of Stay Cables. *2001 American Control Conference. 6*, pp. 5058-5063. Arlington, VA, United states: Institute of Electrical and Electronics Engineers Inc.

Duan, Y., Ni, Y., Ko, J. (2006). Cable Vibration Control using Magnetorheological Dampers. *Journal of Intelligent Material Systems and Structures, 17*(4), 321-325.

Federal Highway Administration. (2007). *FHWA-RD-05-083 Wind-Induced Vibration of Stay Cables.* U.S. Department of Transportation. McLean, VA: Federal Highway Administration.

Flamand, O. (1995). Rain-wind induced vibration of cables. *Journal of Wind Engineering and Industrial Aerodynamics, 57*(2-3), 353-362.

Fujino, Y., Hoang, N. (2008). Design Formulas for Damping of a Stay Cable with a Damper. *Journal of Structural Engineering, 134*(2), 269-278.

He, Y.-L., Sun, L.-M., Zhou, Y.-G. (2010). Vibration mitigation of stay cables using cross-ties with dampers. *Gongcheng Lixue/Engineering Mechanics*, 259-262.

Hikami, Y., Shiraishi, N. (1988). Rain-wind induced vibrations of cables in cable stayed bridges. *Journal of Wind Engineering and Industrial Aerodynamics, 29 pt 2*(1-3), 409-418.

Hou, N., Wang, X. (2011). Study on parameter vibration of stay cable and resistance measure in consideration of bridge deck vibration. *2011 2nd International Conference on Mechanic Automation and Control Engineering MACE 2011 - Proceedings* (pp. 2593-2597). Inner Mongolia, China: IEEE Computer Society, 445 Hoes Lane - P.O.Box 1331, Piscataway, NJ 08855-1331, United States.

Huang, L. (2011). *Experimental Study on Bridge Stay Cable Vibration Mitigation Using External Viscous Damper* (Master's thesis). University of Windsor, Windsor, ON.

Huang, Z., Jones, N. (2011). Damping of Taut-Cable Systems: Effects of Linear Elastic Spring Support. *Journal of Engineering Mechanics, 137*(7), 512-518.

Hwang, I., Lee, J., Spencer, B. (2009). Isolation System for Vibration Control of Stay Cables. *Journal of Engineering Mechanics, 135*(1), 62-66.

Irvine, H., Caughey, T. (1974). The Linear Theory of Free Vibrations of a Suspended Cable. *Proceedings of the Royal Society of London Series A, 341*, 299-315.

Jia, J., Du, J., Wang, Y., Hua, H. (2008). Design method for fluid viscous dampers. *Archive of Applied Mechanics, 78*(9), 737-746.

Jiang, X. (2006). *A New Energy-Based Method for Evaluating the Damping Properties of Cable-Damper Systems* (Master's thesis). University of Windsor, Windsor, ON.

Johnson, E., Baker, G., Spencer, B., Fujino, Y. (2007). Semiactive Damping of Stay Cables. *Journal of Engineering Mechanics, 133*(1), 1-11.

Kleissl, K., Georgakis, C. (2011). Aerodynamic control of bridge stay cables through shape modification: A preliminary study. *Journal of Fluids and Structures, 27*(7), 1006-1020.

Kovacs, I. (1982). Zur frage der seilschwingungen und der seildampfung. *Bautechnik, 10*, 325-332.

Krenk, S. (2000). Vibrations of a Taut Cable With an External Damper. *Journal of Applied Mechanics, 67*(4), 772-776.

Kumarasena, S., Jones, N., Irwin, P., Taylor, P. (2007). *Wind-Induced Vibration of Stay-Cables.* McLean, VA: Federal Highway Administration, FHWA-RD-05-083.

Macdonald, J., Larose, G. (2006). A unified approach to aerodynamic damping and drag/lift instabilities, and its application to dry inclined cable galloping. *Journal of Fluids and Structures, 22*(2), 229-252.

Main, J., Jones, N. (2001). Evaluation of Viscous Dampers for Stay-Cable Vibration Mitigation. *Journal of Bridge Engineering, 6*(6), 385-397.

Main, J., Jones, N. (2002). Free vibrations of taut cable with attached damper. II: Nonlinear Damper. *Journal of Engineering Mechanics, Vol. 128, No. 10,* 1072-1081.

Matsumoto, M., Yagi, T., Shigemura, Y., Tsushima, D. (2001). Vortex-induced cable vibration of cable-stayed bridges at high reduced wind velocity. *Journal of Wind Engineering and Industrial Aerodynamics, 89*(7-8), 633-647.

Myrvoll, F., Kaynia, A., Hjorth-Hansen, E., Strømmen, E. (2002). Full-Scale Dynamic Performance Testing of the Bridge Structure and the Special Cable Friction Dampers on the Cable-Stayed Uddevalla Bridge. *Proceedings of IMAC-XX: A Conference on Structural Dynamics.* Los Angeles, USA.

Nakamura, A., Kasuga, A., Arai, H. (1998). Effects of mechanical dampers on stay cables with high-damping rubber. *Construction and Building Materials, 12*(2-3), 115-123.

National Cooperative Highway Research Program. (2005). *Inspection and Maintenance of Bridge Stay Cable Systems.* Washington, DC: Transportation Research Board.

Ni, Y., Wang, X., Chen, Z., Ko, J. (2007). Field Observations of rain-wind-induced cable vibration in cable-stayed Dongting Lake Bridge. *Journal of Wind Engineering and Industrial Aerodynamics, 95*(5), 303-328.

Pacheco, B., Fujino, Y., Sulekh, A. (1993). Estimation Curve for Modal Damping in Stay Cables with Viscous Damper. *Journal of Structural Engineering, 119*(6), 1961-1979.

Sun, L., Huang, H., Liang, D. (2008). Studies on Effecting Factors of Damper Efficiency for Long Stay Cables. *Earth & Space 2008: Engineering, Science, Construction, and Operations in Challenging Environments.*

Sun, L., Shi, C., Zhou, H., Cheng, W. (2004). A full-scale experiment on vibration mitigation of stay cable. *IABSE Conference.* Shanghai, China.

Tabatabai, H., Mehrabi, A. B. (2000). Design of Mechanical Viscous Dampers for Stay Cables. *Journal of Bridge Engineering, 5*(2), 114-123.

Tanaka, H., Cheng, S. (2003). Aerodynamics of Cables. *Annual Conference of the Canadian Society for Civil Engineering.* Moncton, New Brunswick, Canada.

Taylor, I., Robertson, A. (2010). Numerical simulation of rivulet dynamics associated with Rain-Wind Induced Vibration. *ASME 2010 3rd Joint US-European Fluids Engineering Summer Meeting, FEDSM 2010 - ASME 2010 7th International Symposium on Fluid-Structure Interactions, Flow-Sound Interactions, and Flow-Induced Vibration and Noise, FSI2 and FIV+N* (pp. 139-148). Montreal, QC, Canada: American Society of Mechanical Engineers, 3 Park Avenue, New York, NY 10016-5990, United States.

Wang, X., Hou, N. (2011). Study on Mechanism Analysis of Rain-Wind-Induced Vibration and Resistance measures. *2nd International Conference on Multimedia Technology, ICMT 2011* (pp. 1239-1243). Hangzhou, China: IEEE Computer Society, 445 Hoes Lane - P.O.Box 1331, Piscataway, NJ 08855-1331, Unit.

Xu, Y., Yu, Z. (1998). Vibration of inclined sag cables with oil dampers in cable-stayed bridges. *Journal of Bridge Engineering, 3*(4), 194-203.

Xu, Y., Zhou, H. (2007). Damping cable vibration for a cable-stayed bridge using adjustable fluid dampers. *Journal of Sound and Vibration, 306*(1-2), 349-360.

Xu, Y., Zhan, S., Ko, J., Yu, Z. (1999). Experimental study of vibration mitigation of bridge stay cables. *Journal of Structural Engineering, 125*(9), 977-986.

Yamaguchi, H., Nagahawatta, H. (1995). Damping effects of cable cross ties in cable-stayed bridges. *Journal of Wind Engineering and Industrial Aerodynamics, 54-55,* 35-43.

Yeo, D., Jones, N. (2011). Computational study on aerodynamic mitigation of wind-induced, large-amplitude vibrations of stay cables with strakes. *Journal of Wind Engineering and Industrial Aerodynamics, 99,* 389-399.

Yi, F., Dyke, S., Caicedo, J., Carlson, J. (2001). Experimental Verification of Multiinput Seismic Control Strategies for Smart Dampers. *Journal of Engineering Mechanics, 127*(11), 1152-1164.

Zhou, H. (2005). *Analytical and experimental studies on vibration control of stay cables* (Ph.D. thesis). Tongji University, Shanghai, China.

Zuo, D., Jones, N., Main, J. (2008). Field observation of vortex- and rain-wind-induced stay-cable vibrations in a three-dimensional environment. *Journal of Wind Engineering and Industrial Aerodynamics, 96*(6-7), 1124-1133.

Appendix A: Matlab m-file

```
% Signal processing using Fourier Transform (Time domain to Frequency domain)
% Find the fundamental frequency
pwelch(b,[],[],2048,1000,'one sided')

% Convert data units to m/s^2
a=b*100.53

% Apply Butterworth filter
Af=filter(Hd,a)

% Convert all filtered data set from time domain to frequency domain
F=fft(Af)

% Convert acceleration to displacement, 7.20 is the fundamental frequency in Hz
Df=F/(2*pi*7.20)^2

% Convert displacement data from frequency to time domain; 100 is meter to centimeter
D=ifft(Df)*100
T=0:1/1000:length(Af)/1000-1/1000

plot(T,D)
xlabel('Time(Second)')
ylabel('Displacement(cm)')
title('Displacement vs Time')
grid on
```

Appendix B: Modal Analysis ANSYS Input File

```
L=9.33                  !Cable length (m)
D=4.65E-3               !Cable diameter (m)
R=2.325E-3              !Cable radius (m)
DELTA=0.10              !Location of damper
T=9.421589879E-4        !Initial strain in axial direction
E1=2E11                 !Elastic Modulus (N/m^2)
DENS1=1.177699E4        !Density (kg/m^3)
!K1=0                   !Stiffness (N/m)
DAM=90                  !Damping coefficient (Nm/s)
L1=L/200                !Element length
/PREP7                  !Enters the model creation preprocessor
MP,EX,1,E1              !Define material
MP,DENS,1,DENS1
MP,PRXY,1,0.3
ET,1,PIPE59,0           !Define PIPE59 element
R,1,D,R                 !Define Real Constants
RMORE,,,,,T
ET,2,COMBIN14,,2        !Define COMBIN14 element
R,2,0,DAM
K,1,
K,2,DELTA*L
K,3,L/2
K,4,L
L,1,2                   !Define a line between two keypoints
L,2,3
L,3,4
TYPE,1                  !Set the element type attribute pointer
MAT,1                   !Set the element material attribute pointer
REAL,1                  !Set the element real constant set attribute pointer
LESIZE,ALL,L1           !Specify the divisions and spacing ratio on unmeshed
                        lines
LMESH,1,3               !Generate nodes and line elements along lines
```

```
NUM1=NODE(DELTA*L,0,0)
*GET,NUM2,NODE,,NUM,MAX     !Retrieve value and store it as a scalar parameter or part of an array parameter
N,NUM2+1,DELTA*L            !Define node
TYPE,2
REAL,2
E,NUM1,NUM2+1               !Define element by node connectivity
D,NUM2+1,ALL,0              !Define degree-of-freedom constraints at node
NNODE=NODE(L/2,0,0)
NSEL,,LOC,X,-0.001,0.001    !Select a subset of nodes
D,ALL,ALL,0
NSEL,,LOC,X,L-0.001,L+0.001
D,ALL,ALL,0
ALLSEL,ALL                  !Select all entities
D,ALL,UZ,0                  !Model defined to be a 2D model in the X-Y plane
ALLSEL,ALL
FINISH
/SOLU                       !Enter the solution processor
ANTYPE,STATIC               !Specify the analysis type as static and restart status
SSTIF,ON                    !Activate stress stiffness effects in a nonlinear analysis
NLGEOM,ON                   !Include large-deflection effects in a static or full transient analysis
ACEL,,9.80                  !Specify the linear acceleration of the global Cartesian reference frame for the analysis
AUTOTS,ON                   !Specify to use automatic time stepping
TIME,1                      !Set the time for a load step
DELTIM,15,5,25              !Specify the time step sizes to be used for this load step
SOLVE
FINISH
/SOLU
ANTYPE,MODAL                !Perform a modal analysis
MODOPT,DAMP,12,,,,1         !Specify modal analysis options; damped system
UPCOORD,1.0,ON
PSTRES,ON                   !Specify that prestress effects are included
MXPAND,12                   !Specify the number of modes to expand
```

```
EMATWRITE,YES
PSOLVE,TRIANG
PSOLVE,EIGDAMP
!PSOLVE,EIGFULL
FINISH
/SOLU                    !Additional solution step for expansion
EXPASS,ON
PSOLVE,EIGEXP            !Required to review mode shapes in the postprocessor
FINISH
/POST1                   !Enter the database results postprocessor (general
                         postprocessor)
/DSCALE,,1
SET,NEXT
PLDISP,1
SET,LIST
```

Appendix C: Time-History Analysis ANSYS Input File

```
L=9.33                  !Cable length (m)
D=4.65E-3               !Cable diameter (m)
R=2.325E-3              !Cable radius (m)
DELTA=0.1               !Location of damper
T=9.421589879E-4        !Initial strain in axial direction
E1=2E11                 !Elastic Modulus (N/m^2)
DENS1=1.177699E4        !Density (kg/m^3)
KD=0                    !Stiffness (N/m)
KS=200000               !Damper support stiffness (N/m)
DAM=90                  !Damping coefficient (Nm/s)
L1=L/200                !Element length is
/CONFIG,NRES,9999
/PREP7                  !Enter the model creation preprocessor
MP,EX,1,E1              !Define a linear material property
MP,DENS,1,DENS1
MP,PRXY,1,0.3
ET,1,PIPE59,0           !Define element type
R,1,D,R                 !Define the element real constants
RMORE,,,,,T             !Add real constants to set
ET,2,COMBIN14,,2
R,2,KD,DAM              !Real constant defining damper stiffness and damper
                        coefficient
R,3,KS,0                !Real constant defining damper support stiffness and
                        zero damper stiffness
K,1,                    !Define keypoint
K,2,DELTA*L
K,3,L/2
K,4,L
L,1,2                   !Define line between two keypoints
L,2,3
L,3,4
TYPE,1                  !Set the element type attribute pointer
```

```
MAT,1                          !Set the element material attribute pointer
REAL,1                         !Set the element real constant set attribute pointer
LESIZE,ALL,L1
LMESH,1,3                      !Generate nodes and line elements along lines
NUM1=NODE(DELTA*L,0,0)
*GET,NUM2,NODE,,NUM,MAX
N,NUM2+1,DELTA*L               !Define a node
TYPE,2
REAL,2
E,NUM1,NUM2+1                  !Define an element by node connectivity

N,NUM2+2,DELTA*L               !Create node for base of support spring
TYPE,2                         !Activate local element 2 (COMBIN14)
REAL,3                         !Activate real constant 3 (support stiffness)
E,NUM2+1,NUM2+2                !Create node between damper base node and spring
                               base node
D,NUM2+2,ALL,0                 !All degrees-of-freedom fixed at base of support spring
                               (ground)
NNODE=NODE(L/2,0,0)
NSEL,,LOC,X,-0.001,0.001       !Select a subset of nodes
D,ALL,ALL,0
NSEL,,LOC,X,L-0.001,L+0.001
D,ALL,ALL,0
ALLSEL,ALL                     !Select all entities
D,ALL,UZ,0                     !Model defined to be a 2D model in the X-Y plane
ALLSEL,ALL
FINISH
/SOLU                          !Enter the solution processor
ANTYPE,TRANS                   !Specify the analysis type as transient analysis
TRNOPT,FULL
OUTRES,,ALL
OUTRES,NSOL,ALL
OUTRES,V,ALL
OUTPR,NSOL,ALL
```

```
OUTPR,V,ALL
TIMINT,OFF                    !Turn off transient effects
SSTIF,ON
NLGEOM,ON
TIME,1E-10
LSWRITE,1
SSTIF,ON
NNODE=NODE(L/2,0,0)
D,NNODE,UY,-0.30
NSUBST,2                      !Specify the number of substeps to be taken this load
                              step
KBC,1
TIME,0.001                    !Set the time for a load step
LSWRITE,2
TIMINT,ON                     !Include transient effects
TINTP,,0.25,0.5
CNVTOL,M,-1
SSTIF,ON
DDELE,NNODE,UY
KBC,1
AUTOTS,ON
TIME,1.5                      !Set the time for a load step
DELTIM,0.4E-3,0.1E-3,0.6E-3   !Specify the time step sizes to be used for this load step
LSWRITE,3
LSSOLVE,1,3,1                 !Read and solve multiple load steps
FINISH
/POST26                       !Enter the time-history results postprocessor
NSOL,3,NNODE,V,Y,VY
NSOL,4,NNODE,U,Y,UY
LINE,3000
/AXLAB,X,TIME (S)             !Axis labels
/AXLAB,Y,DISPLACEMENT (M)
PLVAR,4
```

```
*GET,TSIZE,VARI,,NSETS
*DIM,TIME,ARRAY,TSIZE
VGET,TIME(1),1
FINISH
/POST1
*GET,NSBSTP1,ACTIVE,,SET,N
SET,FIRST,3
*GET,NSBSTP2,ACTIVE,,SET,N
SET,LAST,3
NSBSTP=NSBSTP2-NSBSTP1+1
*DIM,E_KENE,ARRAY,NSBSTP
2
ESEL,,TYPE,,1
SET,1,1
ETABLE,KENE,KENE
SSUM
ESEL,,TYPE,,1
*GET,ST_KE,SSUM,,ITEM,KEN
E
E_KENE(1)=ST_KE
*DO,I,1,2
SET,2,I
ETABLE,KENE,KENE
SSUM
ESEL,,TYPE,,1
*GET,ST_KE,SSUM,,ITEM,KEN
E
E_KENE(I+1)=ST_KE
*ENDDO
*DO,I,1,NSBSTP
SET,3,I
ETABLE,KENE,KENE
SSUM
*GET,ST_KE,SSUM,,ITEM,KEN
E
E_KENE(I+3)=ST_KE
*ENDDO
```

```
/AXLAB,X,TIME (S)
/AXLAB,Y,KINETIC ENERGY
(J)
*VPLOT,TIME(1),E_KENE(1)
/OUT,KINETIC,TXT                !Output file (kinetic.txt)
*VWRITE,TIME(1),E_KENE(1)
(1X,'  ',F17.10,'    ',F17.10)
/OUT
FINISH
```

Appendix D: Numerical Simulation Results (4%L and 10%L)

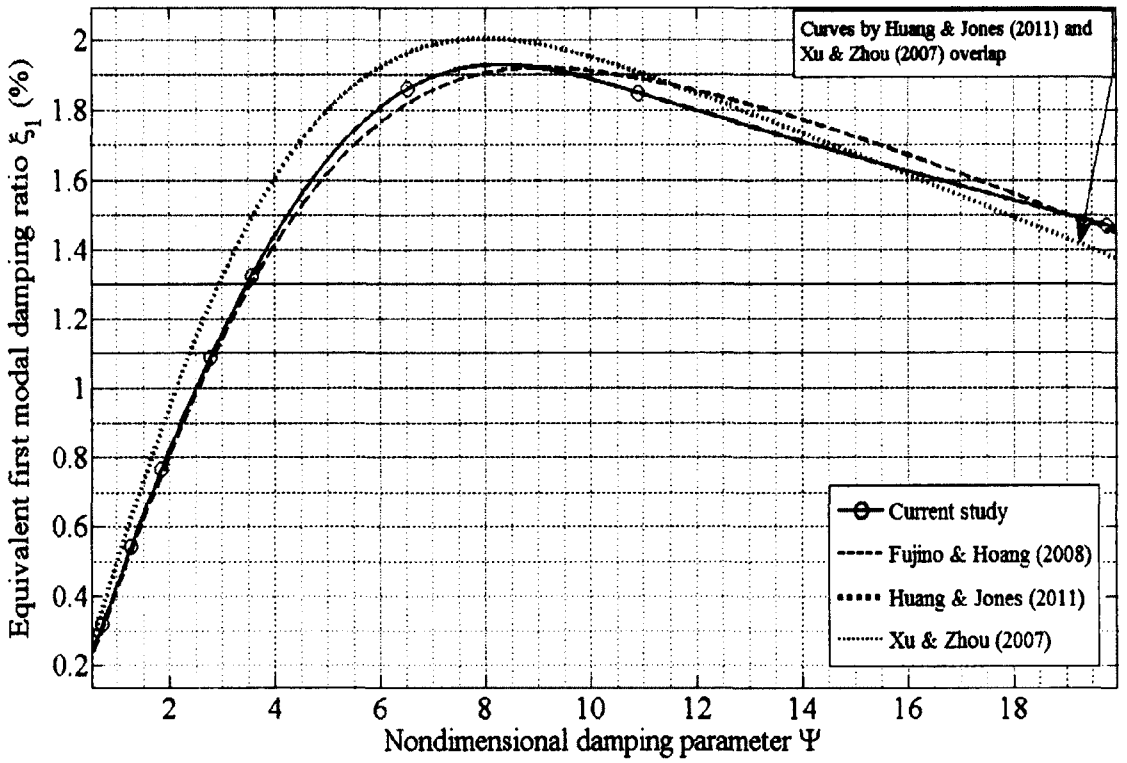

Figure D-1: Relation between equivalent first modal damping ratio and damper size at $\Gamma_d = 0.04$ (Rigid damper support and no damper stiffness)

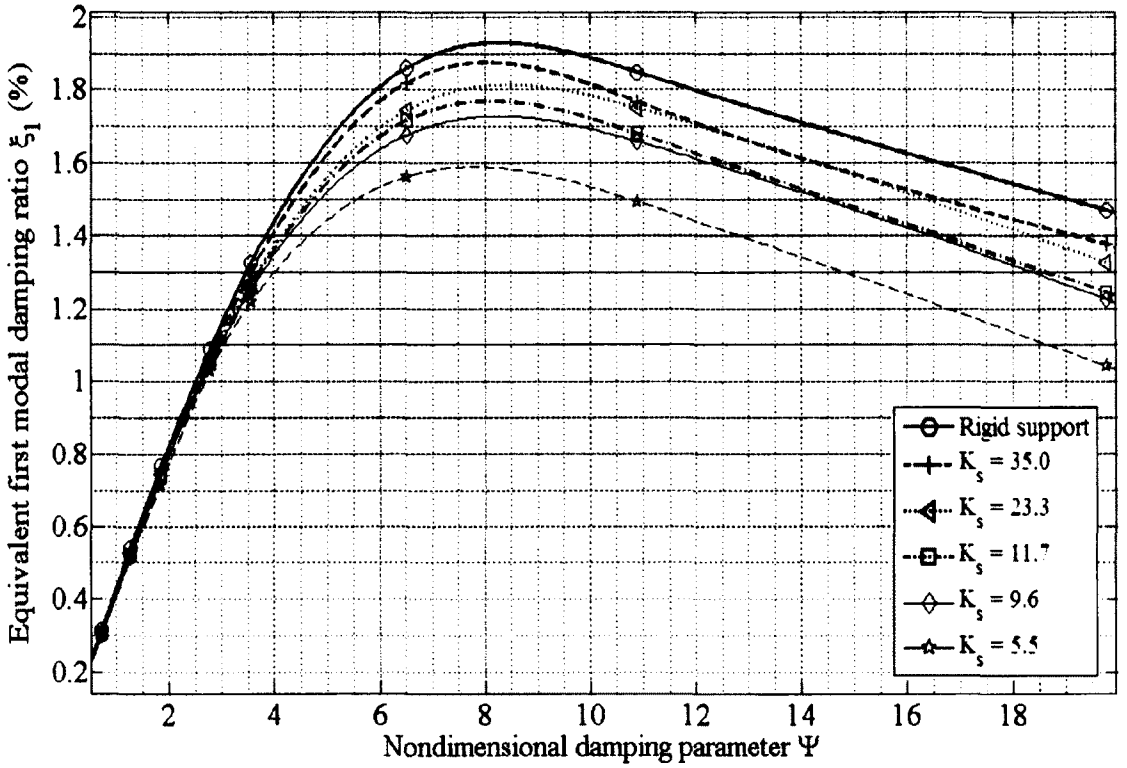

Figure D-2: Effect of damper support stiffness ($\Gamma_d = 0.04$)

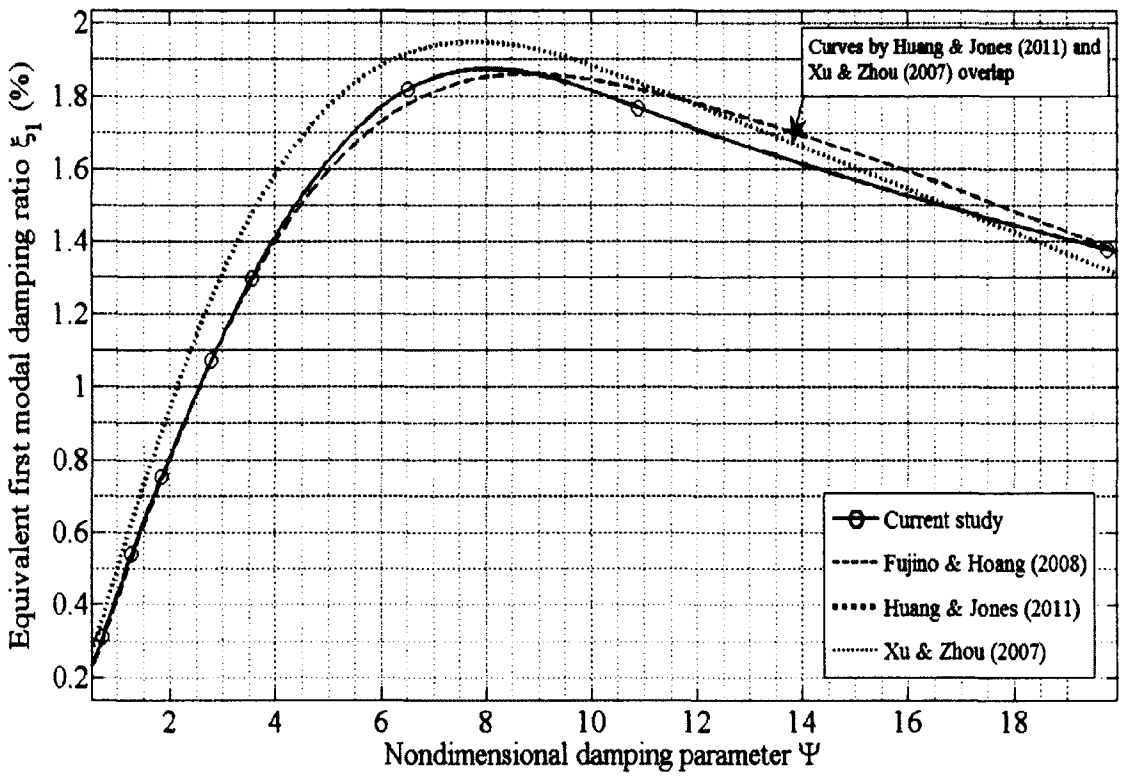

Figure D-3: Effect of damper support stiffness ($K_s = 35.0$, $\Gamma_d = 0.04$)

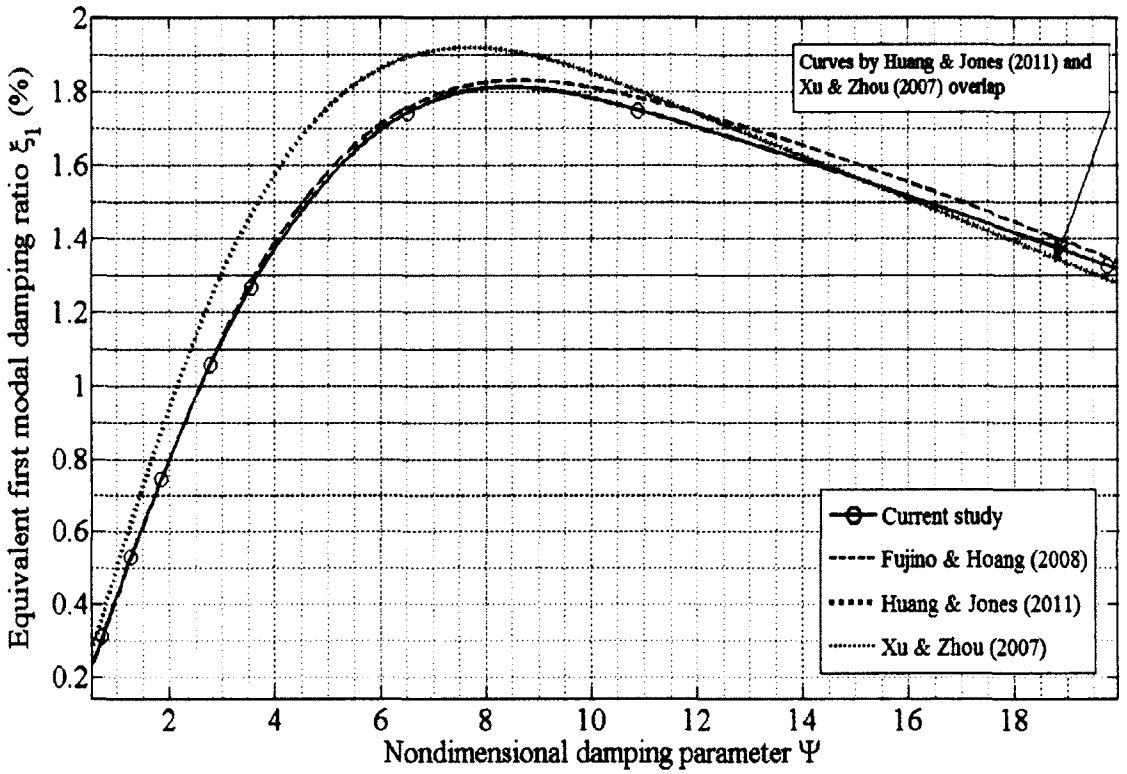

Figure D-4: Effect of damper support stiffness (K_s = 23.3, Γ_d = 0.04)

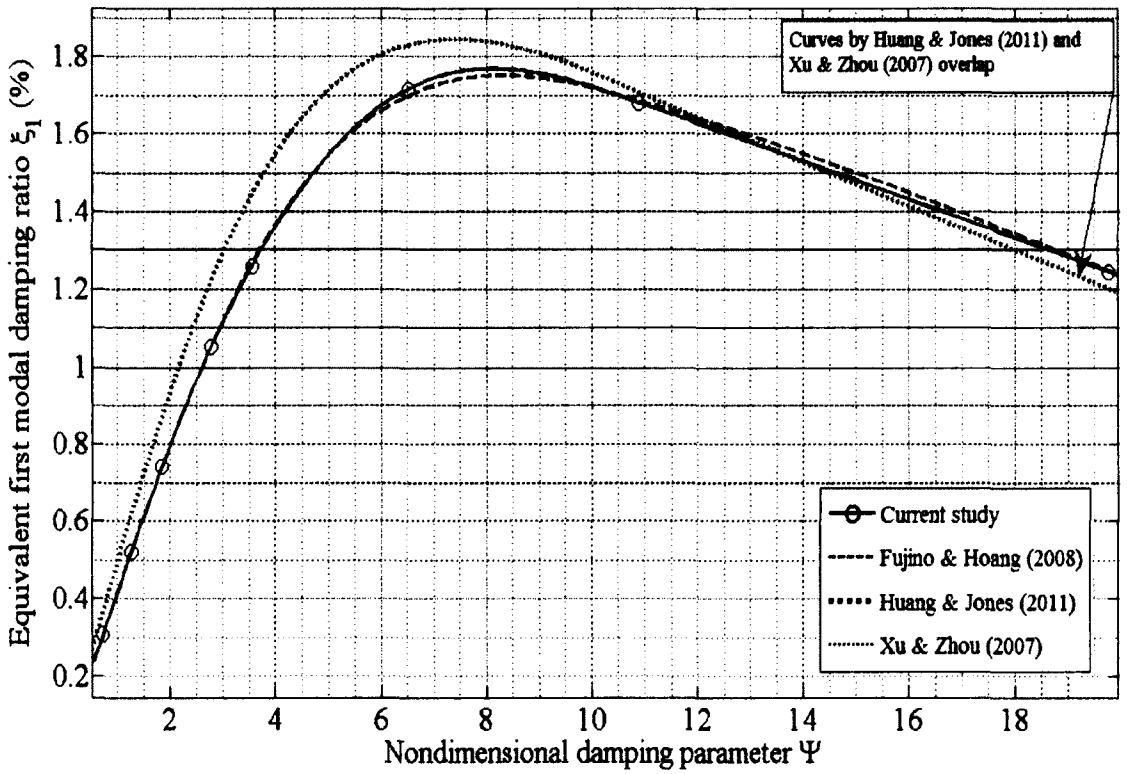

Figure D-5: Effect of damper support stiffness (K_s = 11.7, Γ_d = 0.04)

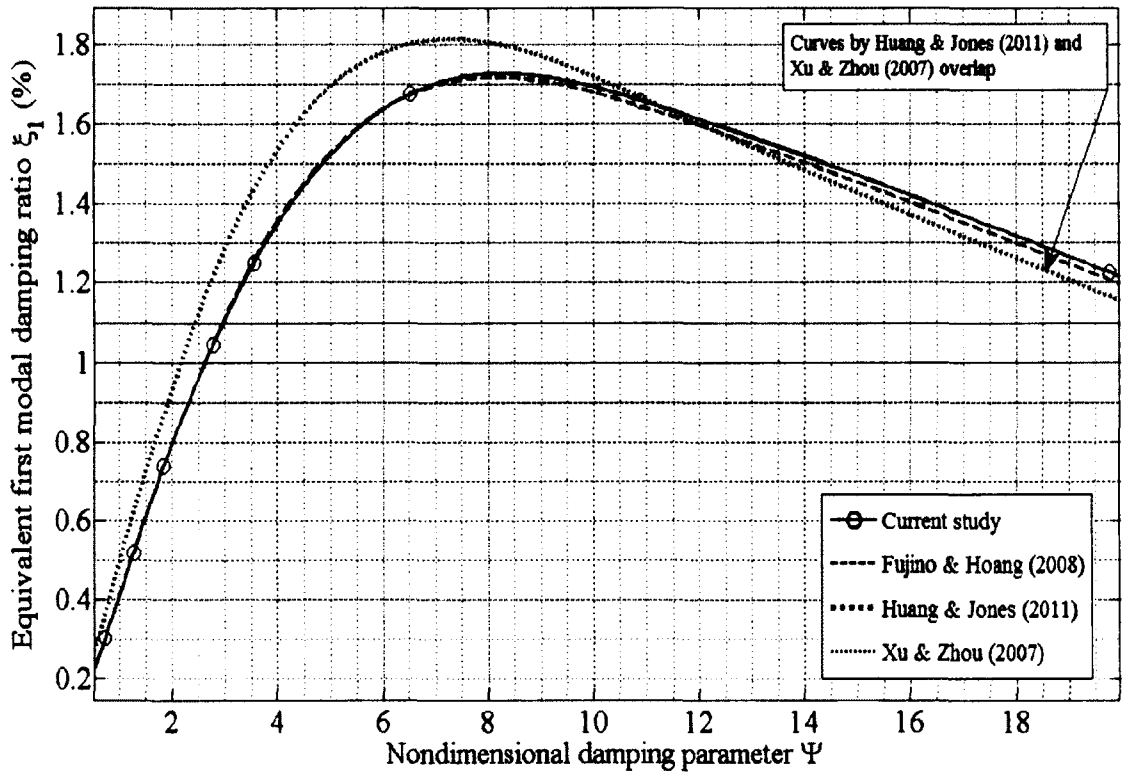

Figure D-6: Effect of damper support stiffness ($K_s = 9.6$, $\Gamma_d = 0.04$)

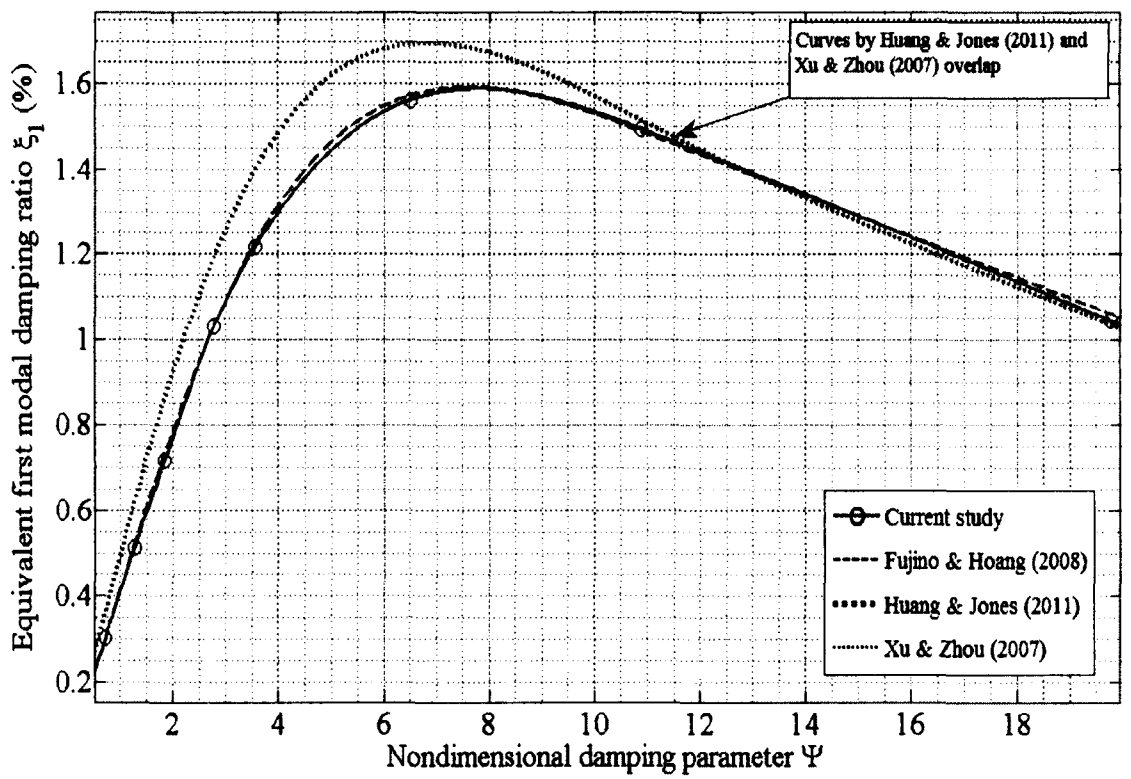

Figure D-7: Effect of damper support stiffness ($K_s = 5.5$, $\Gamma_d = 0.04$)

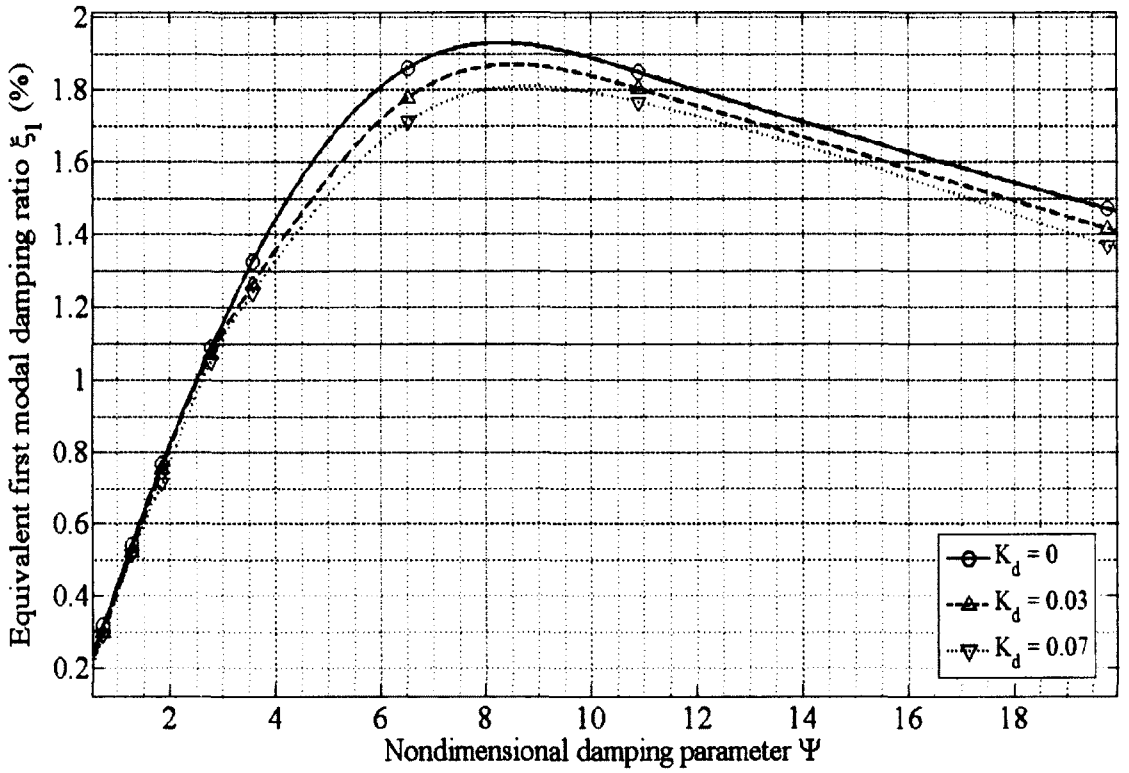

Figure D-8: Effect of damper stiffness ($\Gamma_d = 0.04$)

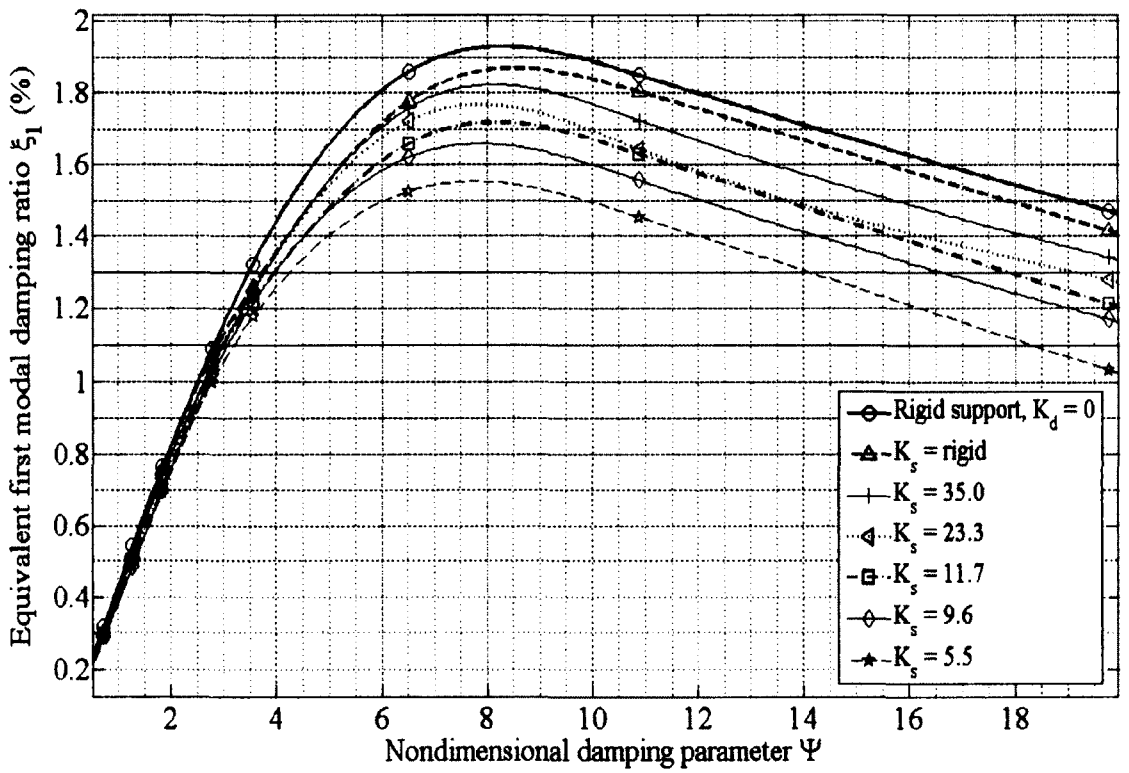

Figure D-9: Combined effect of damper stiffness and damper support stiffness ($K_d = 0.03$, $\Gamma_d = 0.04$)

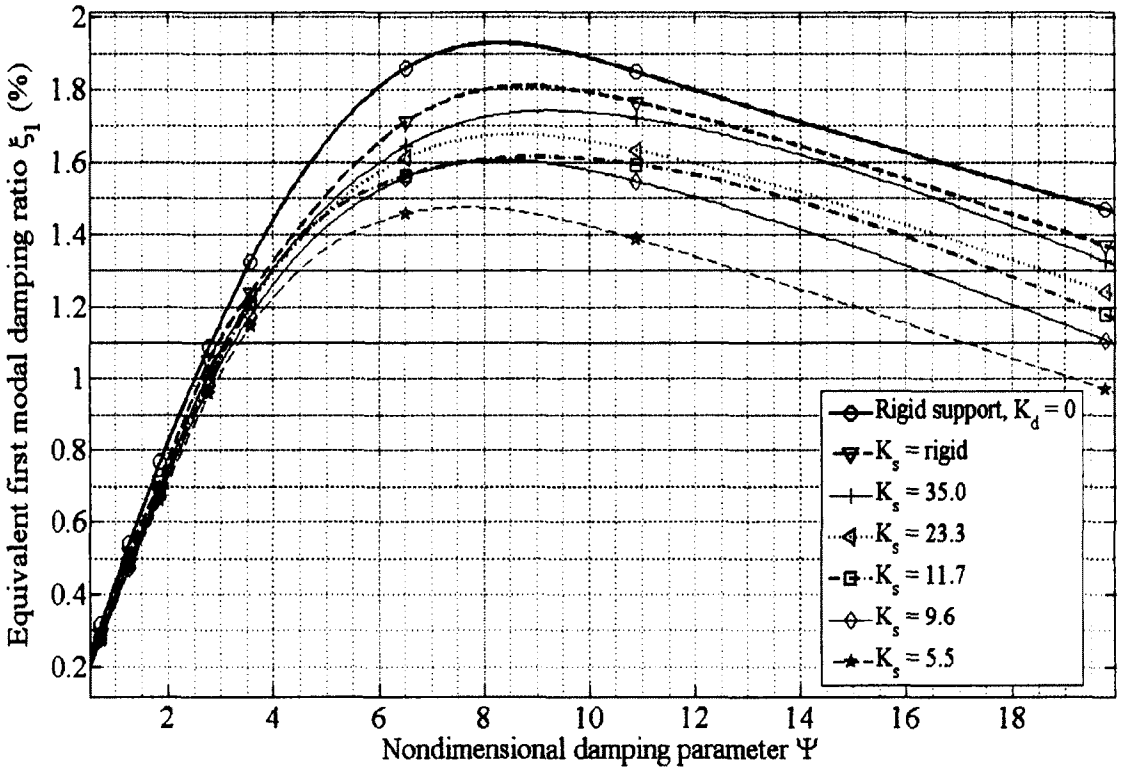

Figure D-10: Combined effect of damper stiffness and damper support stiffness ($K_d = 0.07$, $\Gamma_d = 0.04$)

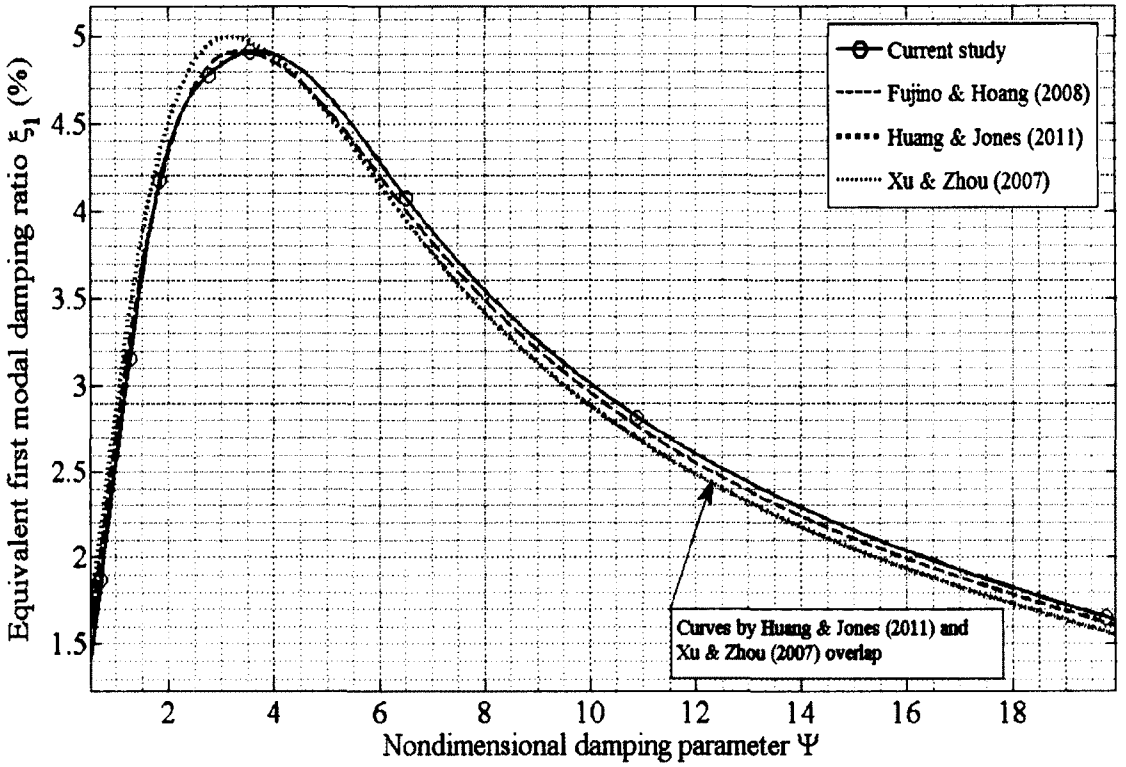

Figure D-11: Relation between equivalent first modal damping ratio and damper size at $\Gamma_d = 0.10$ (Rigid damper support and no damper stiffness)

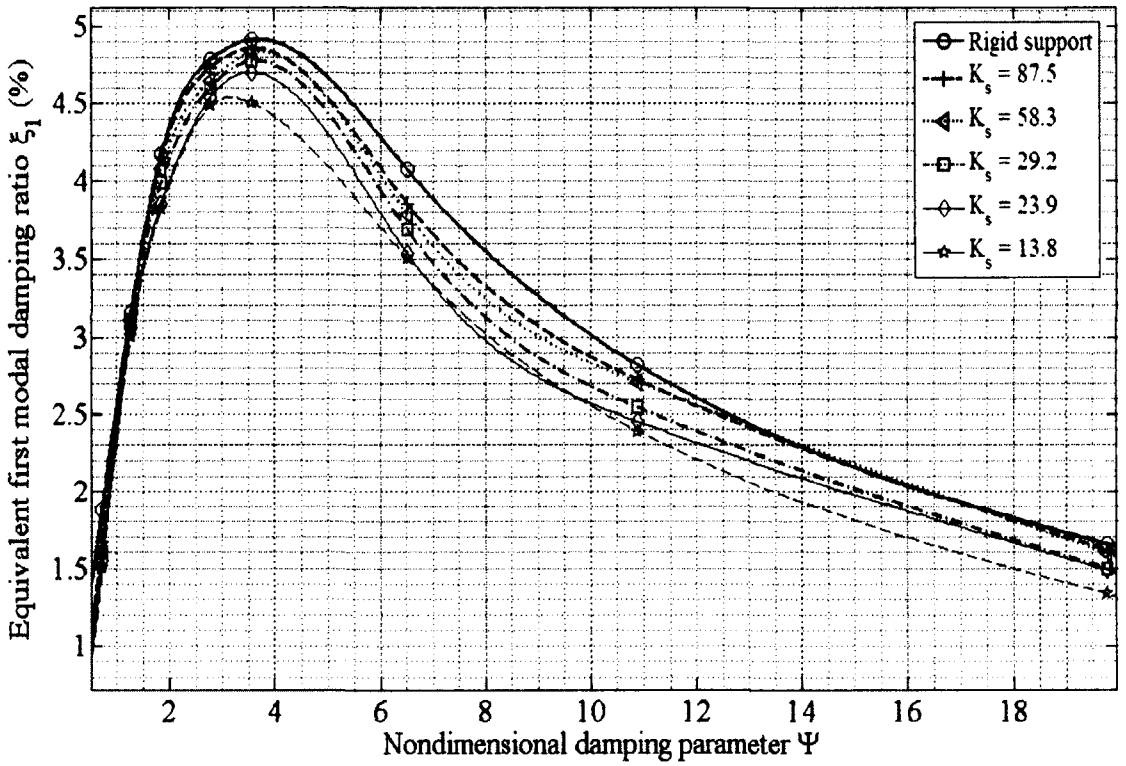

Figure D-12: Effect of damper support stiffness ($\Gamma_d = 0.10$)

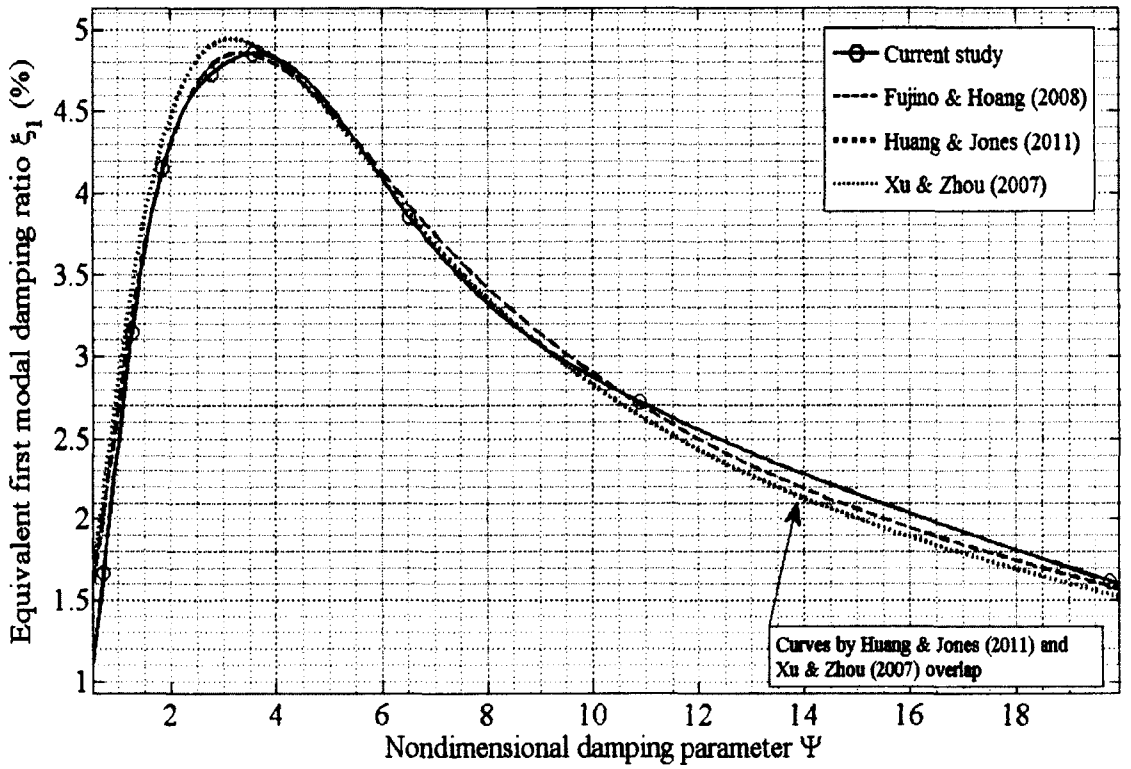

Figure D-13: Effect of damper support stiffness ($K_s = 87.5$ $\Gamma_d = 0.10$)

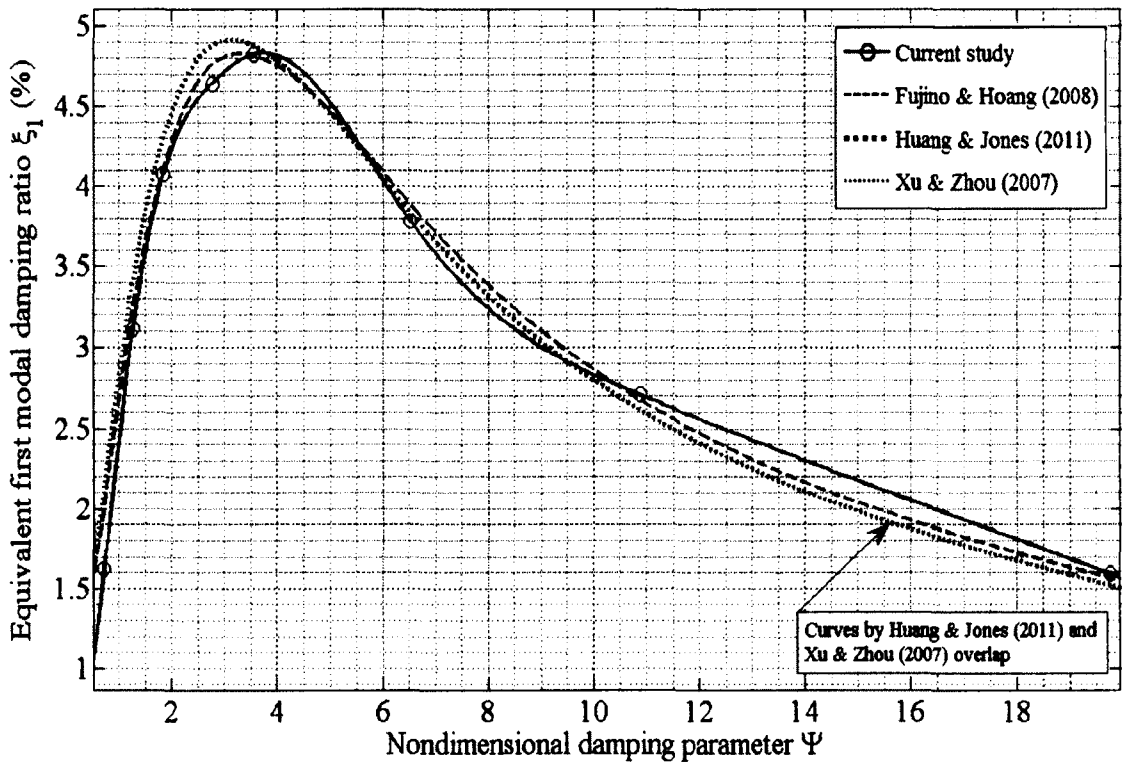

Figure D-14: Effect of damper support stiffness ($K_s = 58.3$, $\Gamma_d = 0.10$)

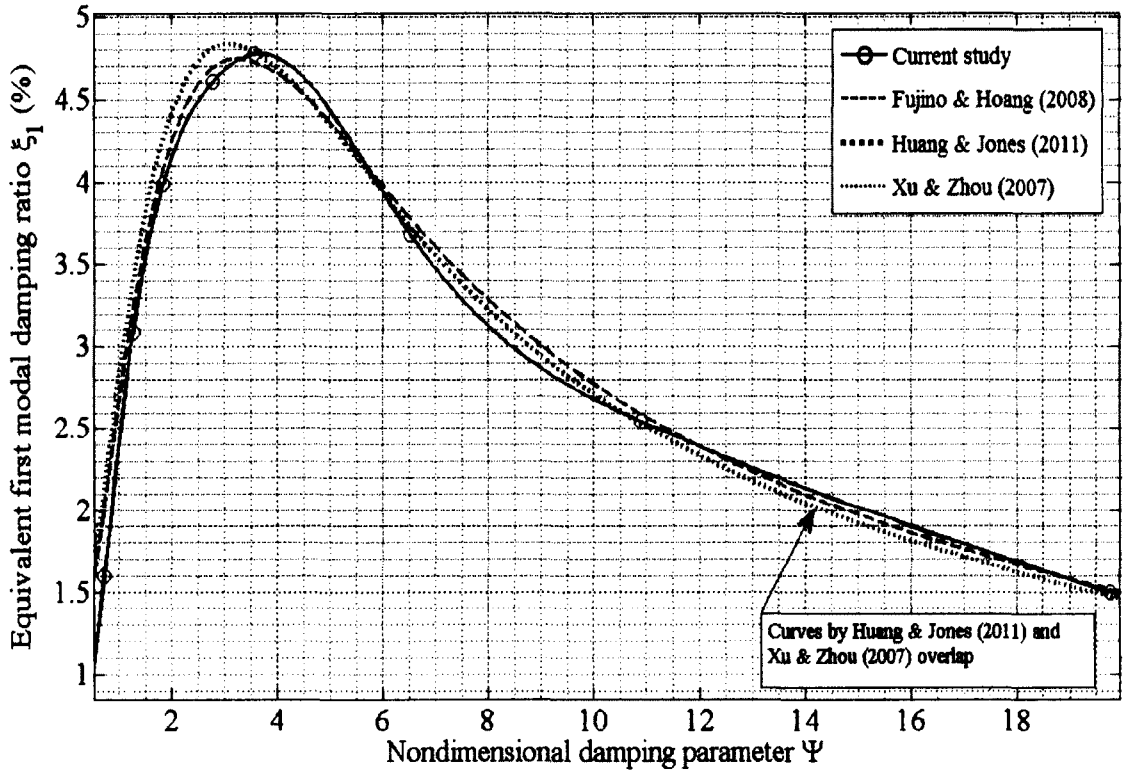

Figure D-15: Effect of damper support stiffness ($K_s = 29.2$, $\Gamma_d = 0.10$)

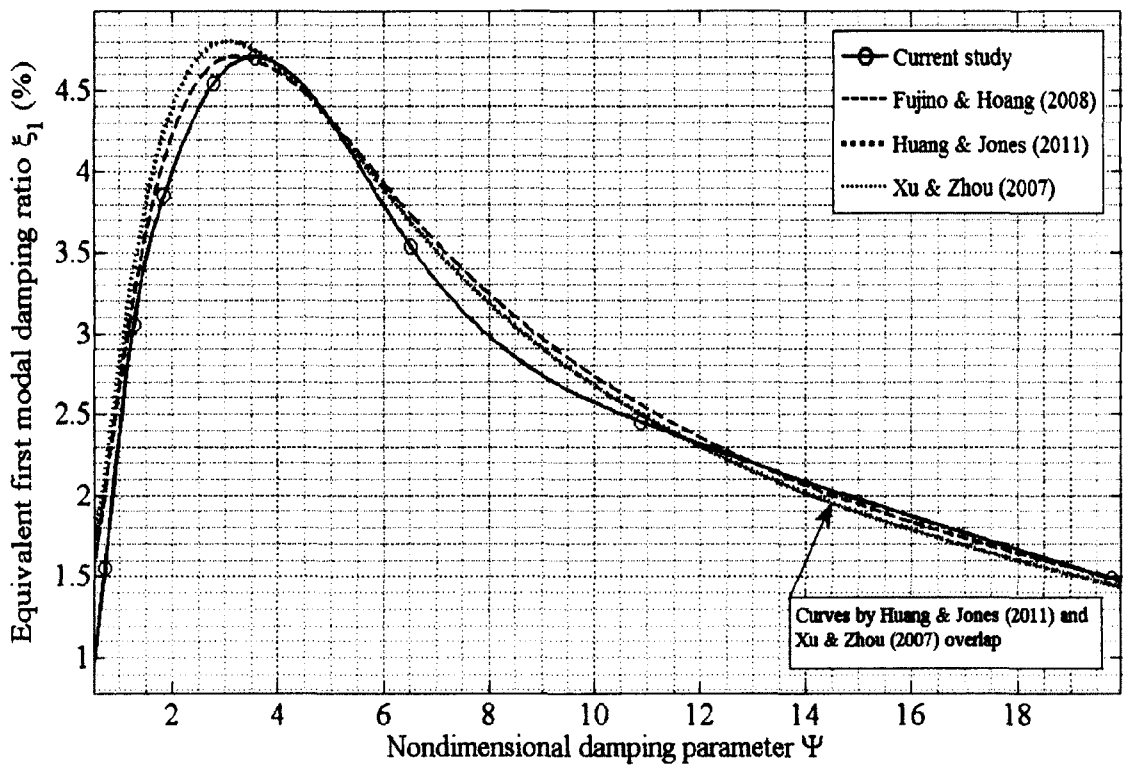

Figure D-16: Effect of damper support stiffness ($K_s = 23.9$, $\Gamma_d = 0.10$)

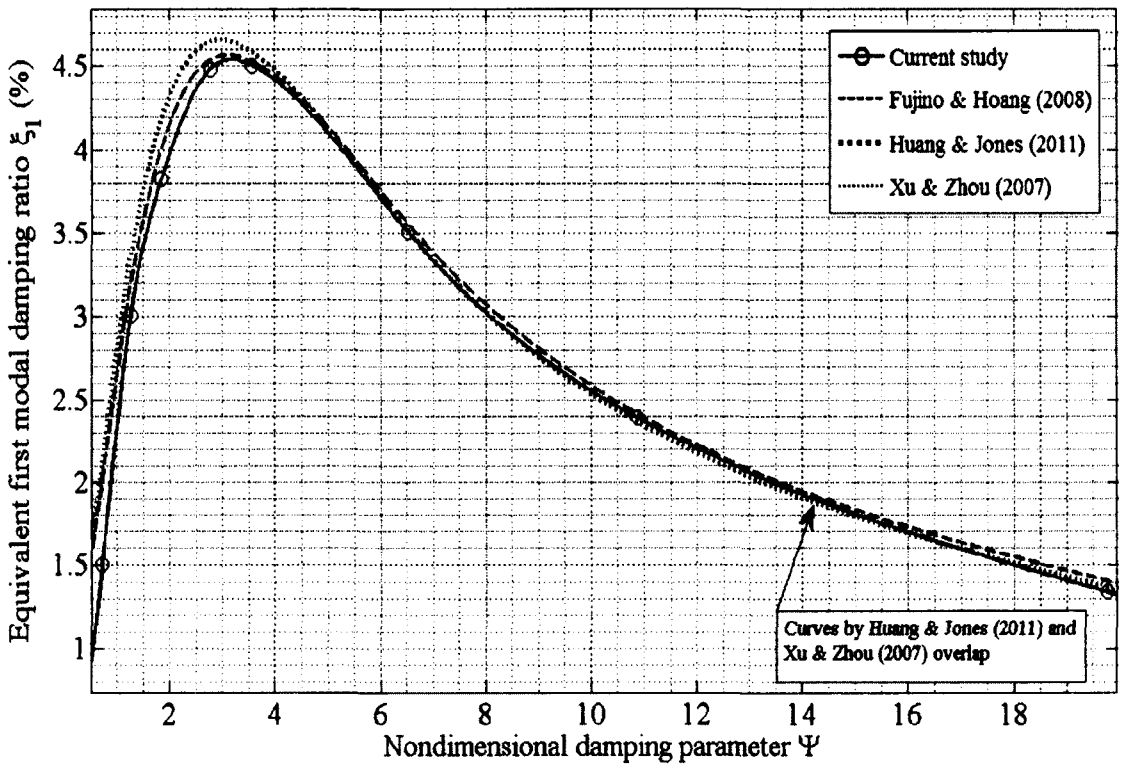

Figure D-17: Effect of damper support stiffness ($K_s = 13.8$, $\Gamma_d = 0.10$)

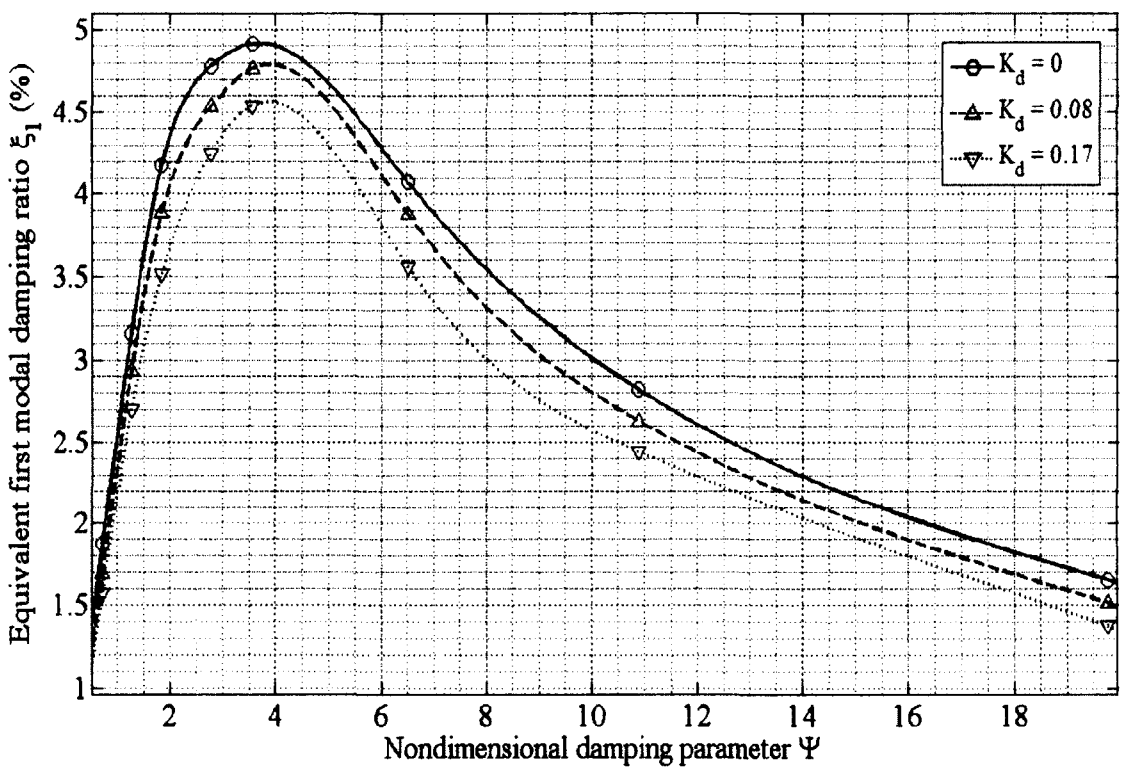

Figure D-18: Effect of damper stiffness ($\Gamma_d = 0.10$)

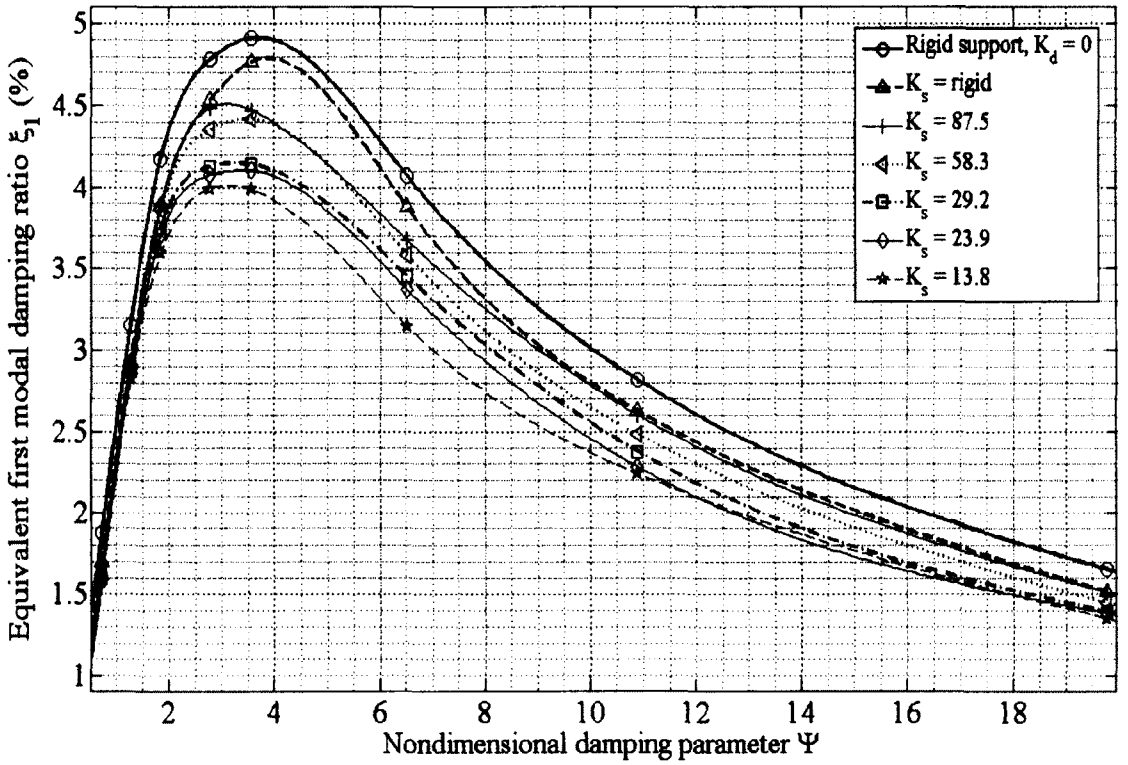

Figure D-19: Combined effect of damper stiffness and damper support stiffness ($K_d = 0.08, \Gamma_d = 0.10$)

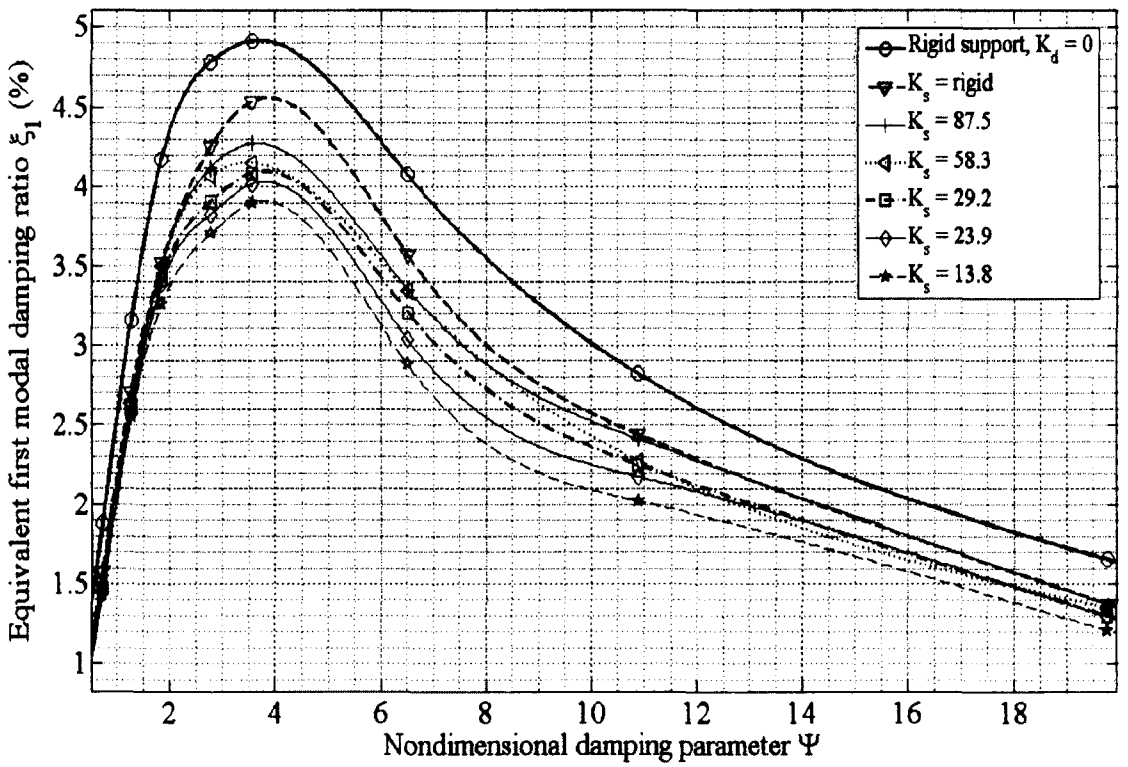

Figure D-20: Combined effect of damper stiffness and damper support stiffness ($K_d = 0.17, \Gamma_d = 0.10$)

Vita Auctoris

NAME	Jennifer Anne Fournier
PLACE OF BIRTH	Windsor, Ontario
YEAR OF BIRTH	1988
EDUCATION	University of Windsor, Windsor, Ontario 2006 – 2010 B.A.Sc.
	University of Windsor, Windsor, Ontario 2010 – 2012 M.A.Sc.